

CHARACTERIZATION OF INJECTABLE
LIQUID EMBOLIC PARTICLES

by

Trevor Robert Cotter

A Thesis Submitted in Partial Fulfillment

of the Requirements for the Degree

Master of Science in Applied Physics

Northern Arizona University

May 2018

Approved:

Timothy A Becker, Ph.D., Chair

Christopher J Mann, Ph.D.

Robert S Kellar, Ph.D.

ABSTRACT

Cerebral aneurysms can be found in over 2% of the American population, and their rupture into hemorrhagic stroke carries a 40% mortality rate. This makes their treatment important to clinicians trying to prevent this from happening to millions of people. A novel polymer, poly(propylene glycol) diacrylate and pentaerythritol tetrakis (3-mercaptopropionate) (PPODA-QT), has been developed in order to successfully embolize these aneurysms. It is injected through a catheter into the aneurysm, where it cures and the aneurysm can heal itself, eliminating the risk of rupture and stroke. This thesis focuses on the embolic risks presented during the injection and curing of PPODA-QT.

The first aim of this project was to build an endovascular flow model that could accurately mimic conditions found in the human body. This was used to practice procedures and evaluate embolic risk. In the second aim, multiple microscopy methods were used to capture and analyze particles shed downstream during the procedure to ensure that the injection would be safe for use in living models. In the final aim, rabbit aneurysm models were used to confirm that no negative embolic effects were observed.

A model was built that could control pressure, temperature, and pressure. The model was designed with customizable inserts that could be changed to model various anatomies.

Differential interference contrast (DIC) microscopy was used to analyze filters that captured downstream particles produced during the procedure. Feasibility of inline digital holography was also performed. Finally, a rabbit aneurysm model was developed in order to treat different aneurysm morphologies. This thesis presents a series of methods that can be used to study of the embolic risks of a novel aneurysm treatment with the potential to impact millions of lives.

ACKNOWLEDGEMENTS

I would like to thank everyone that assisted over the course of this project. In addition to my committee, I would also like to thank William Merritt, Connor Gonzalez, Sharna Beahm, and April Huckleberry for all their help in the Bioengineering Devices Lab (BDL). The microscopy work was completed with the help of Aubrey Funke in the Imaging and Histology Core Facility, and the animal work was guided by Scott Nichols and Leslie Hempleman.

Two engineering capstone groups also assisted with this work. William Merritt, Connor Gonzalez, Anne Marie Holter, Amy Swartz, and Kayla Goodrich assisted with the *in vitro* model, and Kevin LoGrande, Mohammad Almutairi, and Saleh Aldhufairi assisted with the digital holography and MATLAB and ImageJ analysis. Chris Settanni helped with *in vitro* model work, and Richard Gaughan assisted with holography details. The Statistical Consulting Lab also gave guidance on the statistical analysis. The NAU Graduate Student Government gave financial assistance for conference travel and attendance.

Finally, I would like to thank the groups outside of NAU that lended a hand in this project.

Andrew Ducruet and Bill Bachard offered their surgical expertise from Barrow Neurological Institute in Phoenix, AZ. Anevas Technologies, Inc. sponsored parts of this project. A National Institutes of Health STTR grant (1-R41 NS097069-01 A1) funded the vast majority of the work, the SEM was paid for with a National Science Foundation award (DBI:1229740), and funding pooled between the Departments of Biological Sciences, Chemistry and Biochemistry, Communication Sciences and Disorders, the Colleges of Health and Human Services, Engineering, Forestry, and Natural Sciences, and the office of the Vice President for Research of NAU were combined for the purchase of the confocal microscope used for DIC microscopy.

TABLE OF CONTENTS

ABSTRACT.....	ii
ACKNOWLEDGEMENTS.....	iii
TABLE OF CONTENTS.....	iv
TABLE OF TABLES.....	vii
TABLE OF FIGURES.....	viii
CHAPTER 1.....	1
BACKGROUND.....	1
STROKE DISEASE STATE.....	1
CURRENT NEUROINTERVENTIONAL TREATMENTS.....	3
PPODA-QT – A NOVEL LIQUID EMBOLIC MATERIAL.....	8
RESEARCH QUESTIONS, HYPOTHESES, AND AIMS.....	11
CHAPTER 2.....	13
AIM 1 - IN VITRO MODEL DEVELOPMENT.....	13
BACKGROUND.....	13
IN VITRO MODEL SYSTEM KEY REQUIREMENTS.....	14
MATERIALS, SENSING, AND PARTICLE CAPTURE.....	15
LABVIEW INTERFACE.....	24
DISCUSSION.....	28
CHAPTER 3.....	31

AIM 2 - PARTICLE COUNTING AND CHARACTERIZATION	31
BACKGROUND	31
METHODS	33
RESULTS	37
DISCUSSION.....	43
CONCLUSION.....	45
CHAPTER 4	47
AIM 3 - IN VIVO MODEL.....	47
INTRODUCTION	47
MATERIALS AND METHODS.....	49
RESULTS	51
DISCUSSION.....	55
CONCLUSION.....	57
CHAPTER 5	58
CONCLUSIONS.....	58
AIM 1 - DEVELOP AN IN VITRO MODEL THAT MIMICS HUMAN PHYSIOLOGICAL AND ANATOMICAL CONDITIONS	58
AIM 2 - USE THE AFOREMENTIONED IN VITRO MODEL AND DIFFERENT MICROSCOPY TECHNIQUES TO CHARACTERIZE THE SHAPE AND NUMBER OF LIQUID EMBOLIC PARTICLES RELEASED DURING ANEURYSM EMBOLIZATION	59

AIM 3 - DEVELOP AN IN VIVO RABBIT ANEURYSM MODEL THAT CAN EVENTUALLY BE USED TO EVALUATE LIQUID EMBOLIC EFFICACY AND SAFETY	60
HYPOTHESIS 1 - AN IN VITRO SYSTEM THAT MIMICS HUMAN PHYSIOLOGICAL AND ANATOMICAL CONDITIONS CAN BE BUILT TO TEST LIQUID EMBOLIC CONFORMATION TO THE USP <788>	60
HYPOTHESIS 2 - AN IN VIVO ANEURYSM MODEL CAN BE DEVELOPED TO EVALUATE LIQUID EMBOLIC WITHOUT OBSERVED NEGATIVE EMBOLIC EFFECTS	61
LIMITATIONS AND FURTHER RESEARCH.....	61
FINAL FLOW LOOP DESIGN AND PARTICLE COUNTING APPROACH	61
REFERENCES	63
APPENDICES	68
APPENDIX A.....	68
IN VITRO MODEL DIAGRAMS.....	68
APPENDIX B	80
IMAGEJ AND MATLAB COUNTING PROGRAM.....	80
APPENDIX C	92
RABBIT PROCEDURE MATERIALS	92

TABLE OF TABLES

Table 1 Aneurysm Dimensional Classifications.....	5
Table 2 USP <788> Requirements	11
Table 3 Specifications for the in vitro model.....	14
Table 4 Parameters recorded during particle control test. Data was taken before the test and after 20 minutes of flow. 2 trials were used for each microsphere injection, and 3 were used for the PPODA-QT tests.....	27
Table 5 The number of injected sphere standards and PPODA-QT injected into the model and the number of particles counted by the automated counting program. The 3000 Sphere Trial 2 was ignored as an outlier because it at least one orders of magnitude different than the other trials. More explanation below.	41
Table 6 Summary of the rabbit embolization surgeries	55

TABLE OF FIGURES

Figure 1 Two types of aneurysms classified by shape (bafound.org).....	1
Figure 2 A spherical pressure vessel and its associated size, pressure, and stress labels (unl.edu).3	
Figure 3 Diagram showing the process of filling an intracranial aneurysm with metal coils (hopkinsmedicine.org)	4
Figure 4 Saccular aneurysm dimensional schematic	5
Figure 5 A liquid embolic being injected into an aneurysm via microcatheter with a balloon occluding the neck to prevent downstream migration of the embolic agent.	6
Figure 6 Pipeline Flow Diverter (left) and WEB Flow Disruptor (right) (Jiang et. al 2016)	7
Figure 7 (A) PPODA (Mw≈900), (B) QT (Mw≈488), (C) Michael-type addition reaction mechanism (Brennecka et. al 2012).....	9
Figure 8 PPODA-QT visualized by SEM at 418x (McLemore et. al 2009).....	9
Figure 9 PPODA-QT (A–C), Coil and PPODA-QT (D–F), and Coil Only (G–I) explanted canine aneurysms. The Coil Only group shows the least amount of tissue growth and healing (Brennecka et. al 2013).....	10
Figure 10 A schematic of the in vitro flow loop complete with all the necessary physical components.	15
Figure 11 Utah Medical DPT-100 Pressure Transducer with accessories (utahmed.com)	16
Figure 12 Example of a K-type wire thermocouple (thermocoupleinfo.com).....	16
Figure 13 Omega FTB-421 Pressure Transducer. Flow goes through the clear part at the top, and the output signal comes from the black opening in the bottom (omega.com).....	17
Figure 14 A plot showing the linear relationship between flow rate and digital frequency	17

Figure 15 Output showing the change in flow meter digital frequency over the course of 0.75 seconds. The flow meter can operate on a range from 100-2500mL/min.	17
Figure 16 An overview of the Signal Amplification Box.....	18
Figure 17 Stenner 170DM5 Infusion Pump (lockewell.com).....	19
Figure 18 Sterlitech 25mm filter holder (L) and an example close-up of pores on an EMD Millipore Sigma Filter Membrane (R) (emdmillipore.com).....	20
Figure 19 Example CAD drawing of the model core (L), actual model with three aneurysms (C), simplified model with only one aneurysm and no branching (R).....	21
Figure 20 Schematic of the in-line digital holography setup (top), and a photo of the actual setup (bottom).....	23
Figure 21 Philips BV Pulsera (L) (labx.com) and an image of the simple aneurysm model filled with contrast. The model is held together with steel clamps that appear black (R)	24
Figure 22 Total in vitro flow loop physical setup.....	24
Figure 23 Simplified version of the Flow Loop Monitor VI that tracks the physiological parameters in the in vitro flow loop	26
Figure 24 The pressure on both sides of the filter after injecting DI water containing 0 particles.	27
Figure 25 The pressure change from proximal to distal the filter for all trial configurations.	28
Figure 26 The change in flow rate across each filter for each trial configuration.	28
Figure 27 Syringe-Fitting configuration for PPODA-QT mixing	33
Figure 28 Example of the x-y grid of pictures taken (L), and an example of a sphere taken at various focus depths to illustrate the use of a z stack (R) (Northwestern University)	36

Figure 29 Example of a filter analyzed under normal bright field (BF) light microscopy (L) and Differential Interference (DIC) microscopy (R) 36

Figure 30 Flow chart illustrating the process of the coupled Matlab and ImageJ automated particle counting analysis..... 37

Figure 31 SEM image taken of various PPODA-QT morphologies. On the left is a 500x image with multiple particles of PPODA-QT. This sample was generated with little concern for contamination (such as the bubble and large flake on the left), but still shows multiple types of PPODA-QT shapes. In the center is a ~10 μ m PPODA-QT sphere, and smaller PPODA-QT spheres are scattered throughout the image. In the top right, expanded in the image on the right, are different small particles, including spherical and jagged PPODA-QT. 38

Figure 32 A 418x image of the surface of PPODA-QT when formed in DI water. 38

Figure 33 Images showing the edges of air bubbles as well as small particles and their associated diffraction patterns (L) as well as an image showing the base diffraction pattern of the CMOS camera detector cover (R)..... 39

Figure 34 The various stages of particle counting via DIC microscopy, MATLAB, and ImageJ. a) shows the most in focus image in a given z-stack. b) shows the same location, but with each pixel corresponding to the minimum intensity across the 5 image z-stack (10.0 μ m spacing). c) shows this image once it has been converted to black and white and the intensity threshold was increased to remove many of the pores and small objects. d) shows the 2 particles detected, as well as the output of their area and major and minor diameter. 40

Figure 35 Particles counted by the automated particle counting method vs the number of particles put into the system. 42

Figure 36 Image showing a mock catheter with PPODA-QT stuck to the tip (L), the explanted PPODA-QT embolic (C), and a 3mL syringe for reference (R)..... 42

Figure 37 Diagram showing the initial creation procedure and progression of the rabbit elastase aneurysm model (Brinjikji et. al 2016). 48

Figure 38 The full surgical vessel area (top) and the sealed RCC during the elastase incubation under fluoroscopy (bottom). 52

Figure 39 Aneurysm filling procedure. Left shows the aneurysm in white. A microcatheter sits inside it, and a balloon filled with contrast occludes the neck. Right shows the vessel after the procedure with the aneurysm fully occluded and therefore not visible. 53

Figure 40 Rabbit 9073. The images show the vessel before excision (L) and PPODA-QT visible at the neck of the aneurysm (R) 54

Figure 41 Image of PPODA-QT that has been ejected from the aneurysm and would disrupt the RS blood flow. 54

CHAPTER 1

BACKGROUND

Stroke Disease State

Stroke is the fifth leading cause of death in the United States, claiming the lives of approximately 140,000 people per year.¹ Strokes can come in two forms: ischemic and hemorrhagic. Ischemic strokes occur when clots or foreign particles block vessels and cause ischemia, or an insufficient blood supply to regions of the body. Hemorrhagic strokes occur when blood vessels rupture and cause internal bleeding and ischemia in downstream tissues. These can be caused by burst arteriovenous malformations (AVMs), fistulas, or lesions that expand into aneurysms. Cerebral aneurysms, or aneurysms found in the circulatory system of the brain, are especially dangerous. There are two main cerebral aneurysm shapes: saccular and fusiform (**Figure 1**).² They are found in 2% of the US population, and 30,000 of them rupture each year, causing hemorrhagic stroke. Of these, 40% are fatal and the remaining 2/3 cause permanent neurological damage.³ The enormous consequences of aneurysm rupture makes it a high priority for preventative treatment, but unfortunately there are few symptoms of stroke formation until it is too late.

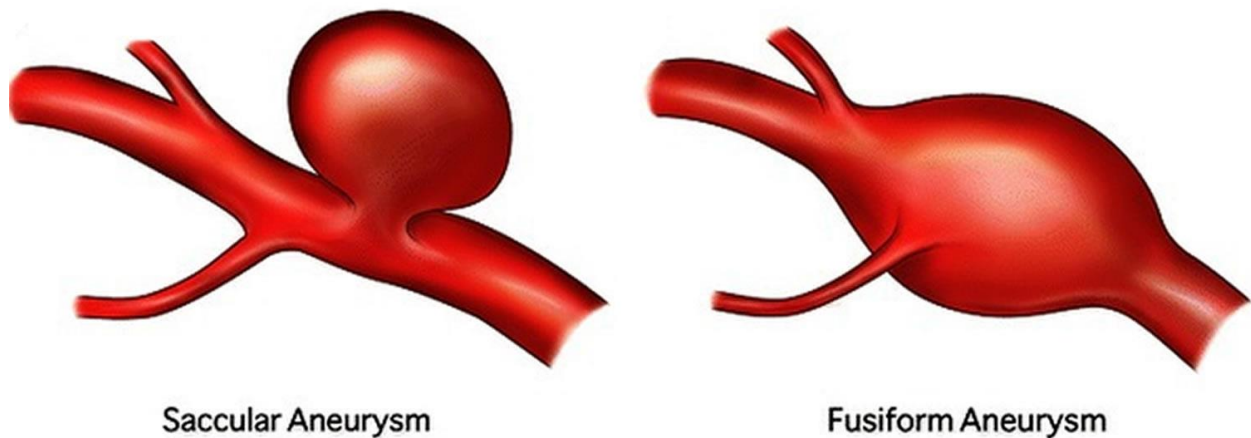


Figure 1 Two types of aneurysms classified by shape (bafound.org)

Various genetic and lifestyle factors can increase the likelihood of stroke. Age is a significant factor in stroke susceptibility (66% of stroke patients are over 65), but strokes do occur in people of all ages.¹ Lifestyles and resulting comorbidities can also affect stroke susceptibility, with high blood pressure, high cholesterol, smoking, obesity, and diabetes all increasing the likelihood of stroke.¹ Even though these relationships are well-established, the actual detection of the aneurysms that precede hemorrhagic stroke is a difficult proposition. Identification of aneurysms requires an angiogram, a medical imaging technique performed by injecting a radiopaque contrast agent into the bloodstream so that the blood vessel anatomy can be observed with a fluoroscope or X-ray. This surgery is expensive, time-consuming, and highly specialized; thus it is not performed as a routine diagnostic procedure. Most aneurysms are discovered when performing other procedures and are then treated.

A saccular aneurysm can be modeled as a simple spherical pressure vessel as shown in **Figure 2**.⁴ In this model, stress σ (Newtons/meter²) in the aneurysm wall is proportional to pressure p (Pascal or Newton/meter²), radius r (meter), and inversely proportional to wall thickness t (meters) via **Equation (1)**.⁴ While neither the blood pressure nor maximum vessel wall stress change drastically or significantly in the human body, the radius of the aneurysm does increase over time. According to **Equation (1)**, as either pressure or radius increase (or as the wall thins out), the wall stress must increase.⁴ When the radius increases past the aneurysm wall's max stress, the vessel will burst, causing hemorrhagic stroke. To prevent this, the maximum wall stress capabilities could be increased, the pressure and radius can be decreased, or the wall thickness can be increased. Since increasing the aneurysm wall's natural maximum stress is an impossible task, steps are taken to modify the blood pressure and radius of the aneurysm. Initial passive techniques include medication, reduced exercise, and dietary restrictions to lower blood

pressure. However, surgical intervention is often needed to prevent further aneurysm development. A variety of devices and products have been developed to reduce pressure in the aneurysm or shrink the total wall exposed to the endovascular blood pressure in order to prevent aneurysm rupture.

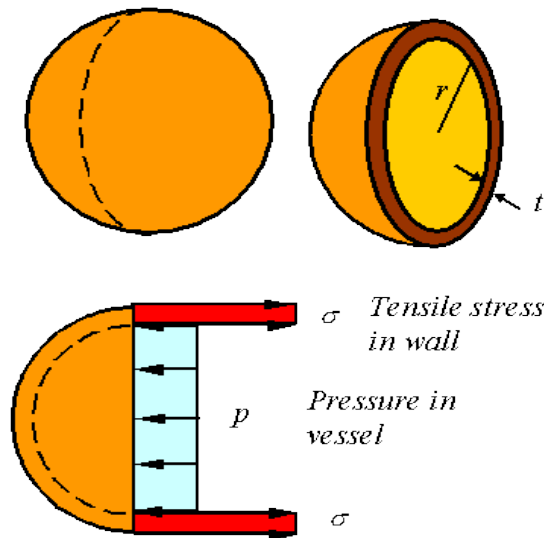


Figure 2 A spherical pressure vessel and its associated size, pressure, and stress labels (unl.edu).

$$\sigma = \frac{pr}{2t} \quad (1)$$

Current Neurointerventional Treatments

Metal Embolic Coils

The current gold standard in minimally-invasive aneurysm treatment is the use of metal embolic coils. These coils are pushed straight through a microcatheter into the aneurysm. The coils then curl as they are exposed beyond the tip of the microcatheter. Once inside the aneurysm, they ball up and the surgeon fills it with as many coils as possible as shown in **Figure 3**.⁵ This disrupts

blood flow and promotes clotting inside the aneurysm so that it can heal rather than continue to expand.

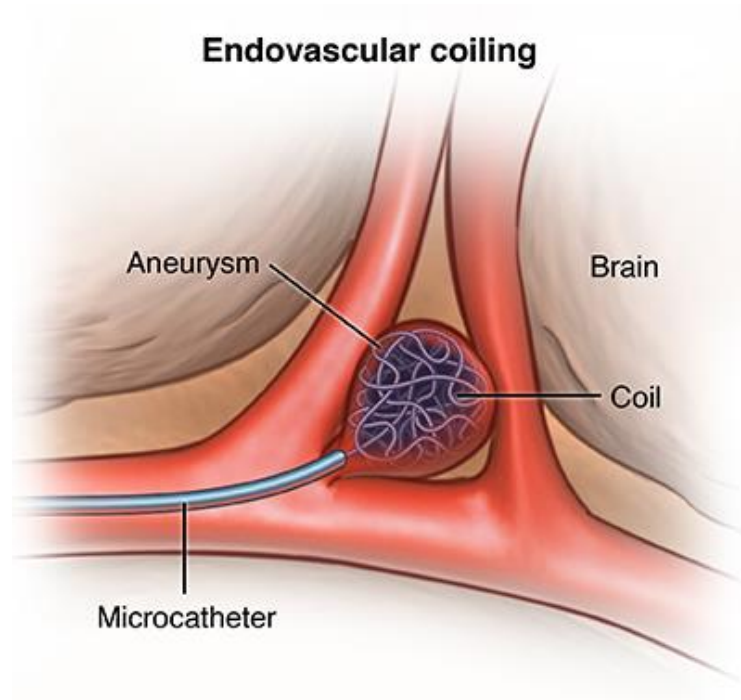


Figure 3 Diagram showing the process of filling an intracranial aneurysm with metal coils (hopkinsmedicine.org)

Metal coils do have some significant disadvantages. For one, metal coils are unable to fill more than 30% of aneurysm volume. In addition, even the softest metal coils are orders of magnitude stiffer than the surrounding tissue, leading to stress mismatches and uneven force transfer at the tissue-coil interface. This can lead to recanalization and then further expansion of the aneurysms. Recanalization increase is related to aneurysm dome and neck size (**Figure 4** and **Table 1**), with 15-35% recanalization in all medium aneurysms, and 25-50% in medium wide-necked aneurysms; large and giant wide-necked aneurysms are even more difficult options for coil treatment, with 35-70% recanalization rates.⁶⁻¹⁷

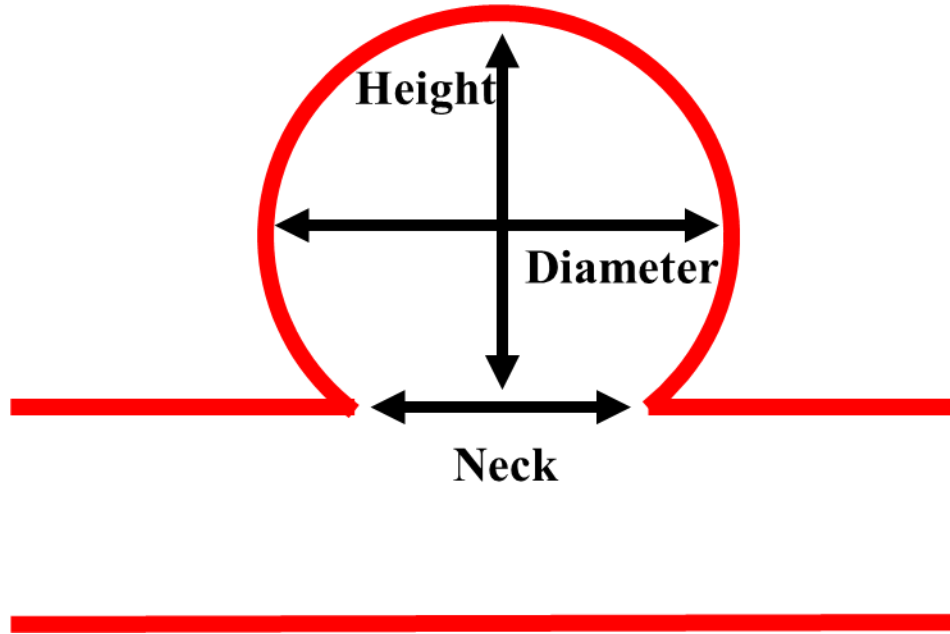


Figure 4 Saccular aneurysm dimensional schematic

Table 1 Aneurysm Dimensional Classifications

Aneurysm Size Classification	Medium	Large	Giant
Dome Height (mm)	5-15	16-25	25+
Neck Size Classification	Small	Medium	Wide
Dome-Neck Ratio ¹⁸	>2:1	2:1 to 1.33:1	<1.33:1

Another limiting factor of metal embolic coils is cost. One very common product, Stryker Neurovascular’s Target 360 platinum-tungsten coil, costs \$700-\$1,500 per coil. Assuming an average use of 8-10 coils per aneurysm, the total cost of embolization agent per procedure is approximately \$10,000. For larger, aneurysms, this number can balloon to over \$100,000.^{19,20} This is only the cost of the embolic agent, meaning that the total surgical cost is much greater.

Liquid Embolics

Liquid embolics, sometimes called “liquid coils,” have been developed more recently to address some of the primary concerns with metal coils: recanalization, difficulty filling larger aneurysms,

and cost. These products consist of some sort of liquid that can be injected through a microcatheter and cure into a solid to fill the aneurysm (**Figure 5**). These devices are advantageous in that they can conform to any shape, including wider-necked aneurysms that are difficult to treat with coils. In addition, liquid embolics distinguish themselves from coils and other products in that they can completely fill aneurysms without any dead volume, a condition that often leads to long-term complications and repair failure.^{7,8,10,12,13,15,16} They can be sold as a single application capable of treating any aneurysm size, which drastically reduces both cost and procedure time. They also have the advantage that they can be used in conjunction with the current coil standard to fill gaps left between coils to minimize the potential for recanalization.

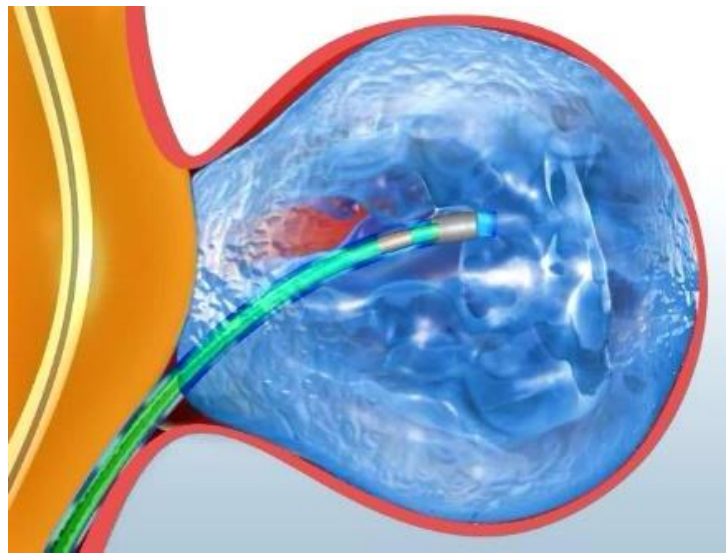


Figure 5 A liquid embolic being injected into an aneurysm via microcatheter with a balloon occluding the neck to prevent downstream migration of the embolic agent.

Only one liquid embolic has become popular in clinical use: Onyx (Onyx HD-500[®]) by Medtronic. It is composed of ethylene co-vinyl alcohol (EVOH) dissolved in dimethyl sulfoxide (DMSO). After Onyx is injected, the DMSO solvent dissipates into the bloodstream. In order to reduce cytotoxicity and vasospasm caused by acute DMSO exposure, Onyx must be injected

slowly, which leads to long procedures and additional complications.^{21–30} In addition, Onyx must be used with specific catheters that are chemically compatible with its components. The combination of these factors has prevented Onyx from becoming clinically standard.

Other Treatment Options

The final category of endovascular surgical aneurysm treatments consists of flow-modification devices, namely flow diverters and flow disruptors (**Figure 6**).³¹ Flow diverters, such as the Pipeline Embolization Device (PED) (Medtronic), promote flow through the blood vessel rather than the aneurysm. Graft-stents, which consist of flexible fabric or sheet of material surrounding a stent, can also be used to direct blood flow.³² Flow disruptors, such as the Woven EndoBridge (WEB) device (Sequent Medical), fill the aneurysm to minimize flow inside it. Unfortunately, both of these devices are metal and therefore have limited biocompatibility. In addition, they are unable to conform to irregular anatomies and cannot effectively promote healing in medium- and wide-neck aneurysms.^{33–37}

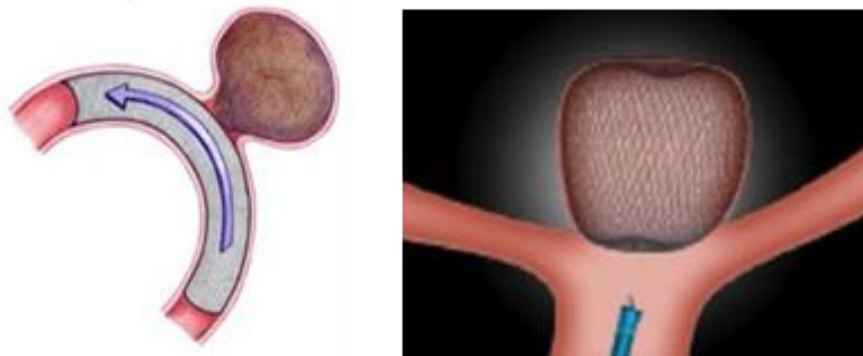


Figure 6 Pipeline Flow Diverter (left) and WEB Flow Disruptor (right) (Jiang et. al 2016)

PPODA-QT – a Novel Liquid Embolic Material

One material, PPODA-QT, has already shown promise as a new type of liquid embolic that can be used to treat aneurysms. It has been developed in collaboration between Arizona State University (ASU), Northern Arizona University (NAU), and Aneuvast Technologies (ATI, Flagstaff, Arizona).

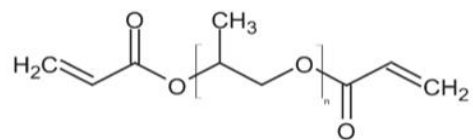
Chemistry

PPODA-QT is a 3 part polymer that can be made quickly and cheaply, and is also compatible with all existing catheter technologies. It consists of polypropylene glycol (PPODA), pentaerythritol tetrakis (3-mercapto-propionate) (QT), which crosslink independently, without the need for additional agents (**Figure 7**).³⁸ A basic aqueous activator accelerates this process from hours to under 5 minutes, making this reaction amenable to endovascular surgeries, where longer balloon protection times have been linked to ischemia.^{25,39} This solution is made of iohalamate meglumine (Conray[®] 60) brought to 11.00pH by 5.0N NaOH. Conray[®] is used because it is radiopaque, meaning it is visible during the procedure under fluoroscopic imaging. This enables it to be used in minimally-invasive endovascular procedures.

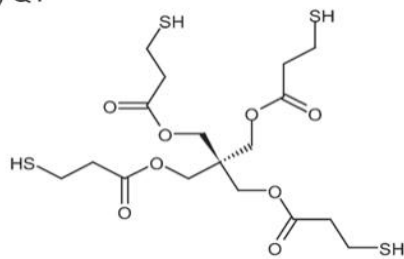
Previous Studies

PPODA-QT has already been used in *in vivo* and *in vitro* studies. Surface analysis of PPODA-QT has been performed (**Figure 8**), but in-depth particulate characterization has not yet been performed.⁴⁰ It has been found to be non-adhesive (to the surrounding tissue), self-aggregating, biocompatible, and allow blood vessel healing in canine models (**Figure 9**).⁴¹ One of the goals of the BDL at NAU is to use a new rabbit model that uses a less traumatic model creation surgery to further demonstrate PPODA-QT's biocompatibility.

A) PPODA



B) QT



C) Michael-type Addition

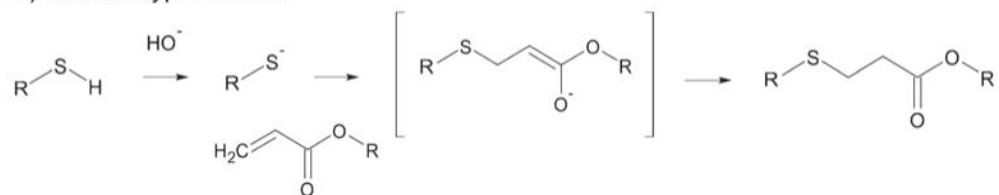


Figure 7 (A) PPODA ($M_w \approx 900$), (B) QT ($M_w \approx 488$), (C) Michael-type addition reaction mechanism (Brennecke et. al 2012)

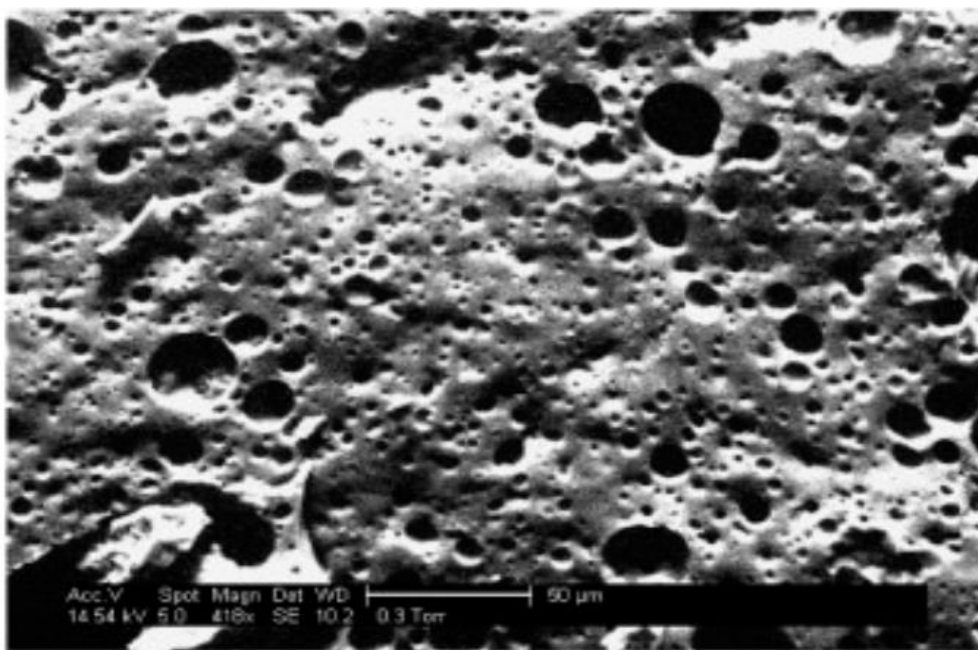


Figure 8 PPODA-QT visualized by SEM at 418x (McLemore et. al 2009)

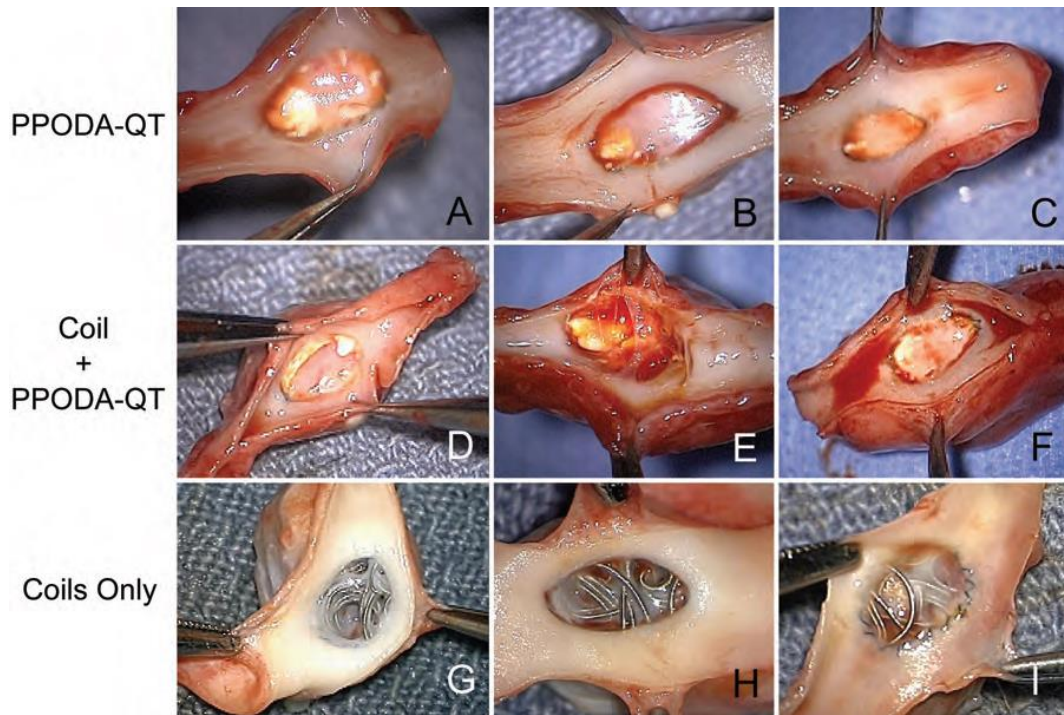


Figure 9 PPODA-QT (A–C), Coil and PPODA-QT (D–F), and Coil Only (G–I) explanted canine aneurysms. The Coil Only group shows the least amount of tissue growth and healing (Brennecke et. al 2013)

Risks

While all medical procedures involve risks, endovascular neurosurgery is exceptionally hazardous due to surgical proximity to essential tissues. In order to minimize the chance of harm to patients, a number of standards have been developed to ensure devices are adequately safe for use. These include requirements that devices will conform to stiffness, foreign, and visibility standards so that they can be used by different surgeons with the same results. In the case of liquid embolics such as PPODA-QT, potential downstream migration of the device during and after curing is a major concern and must be understood completely. The United States Pharmacopia (USP) is a collection of standards and drug information that is used regulate medical devices.

USP <788>

The USP <788> Standard focuses on the safety of injectable liquids in terms of their embolic risk. It sets limits on the number of particles of different sizes released during an injection of a given material in order to minimize downstream embolisms. It outlines two methods for analyzing the number of particles released: in-line particle counting and filter-based microscopic analysis. This project focuses on the latter. Particles smaller than 10 μ m in diameter, are considered too small to be of concern, those from 10-25 μ m are of moderate concern, and those \geq 25 μ m are of high concern (**Table 2**).⁴²

Table 2 USP <788> Requirements

USP <788> Particulate Matter in Injections	
Particle Size	Allowable Particles Per Injection
\leq 10 μ m	NA
\geq 10 μ m	\leq 3000
\geq 25 μ m	\leq 300

Research Questions, Hypotheses, and Aims

Within the context embolic risk, two questions must be answered when developing injectable biomaterials (such as PPODA-QT) for medical use:

Research Question 1 – Can the liquid embolic meet the USP <788> requirements of particulate matter released during injection?

Research Question 2 – Regardless of conformation to USP <788>, can the liquid embolic be successfully used to treat aneurysms without downstream embolic consequences?

To answer these questions, the following hypotheses are proposed:

Hypothesis 1 – An *in vitro* system that mimics human physiological and anatomical conditions can be built to test liquid embolic conformation to the USP <788>

Hypothesis 2 – An *in vivo* aneurysm model can be developed to evaluate liquid embolic without observed negative embolic effects

The subsequent chapters explore the three specific aims that were used to confirm the hypotheses. They are:

Aim 1 – Develop an *in vitro* model that mimics human physiological and anatomical conditions

Aim 2 – Use the aforementioned *in vitro* model and different microscopy techniques to characterize the shape and number of liquid embolic particles released during aneurysm embolization

Aim 3 – Develop an *in vivo* rabbit aneurysm model that can eventually be used to evaluate liquid embolic efficacy and safety

CHAPTER 2

AIM 1 - IN VITRO MODEL DEVELOPMENT

Background

Before their use in humans, medical devices must be tested in a variety of scenarios to prove that they will be safe. A variety of models can be used to simulate different physiological conditions. These can be classified into two types: *in vivo* and *in vitro* models. *In vivo* models are living organisms. Common *in vivo* models for neuroendovascular procedures are pigs and dogs.^{6,18} They can be used to mimic physical characteristics of the eventual human patient, such as the Reference papers with both size and shape of a bone implant, or they can be used to assess biologic compatibility, such as the effectiveness of drugs in disrupting physiological processes. *In vitro* models take place outside of the organism in both biological and non-biological systems. These models can be used to assess material degradation, device mechanical properties, or other parameters. *In vivo* and *in vitro* models are often used in conjunction to fully evaluate the safety and efficacy of devices.

The goal of this section of the project is to develop an *in vitro* model that can accurately mimic the human neurovascular system in various disease states. This will allow for the testing of devices in this simulated condition so that they can be evaluated before human and animal use.

The development of this *in vitro* model is Aim 1 in the pursuit of answering Hypothesis 1:

Hypothesis 1 – An *in vitro* system that mimics human physiological and anatomical conditions can be built to test liquid embolic conformation to the USP <788>.

Aim 1 – Develop an *in vitro* model that mimics human physiological and anatomical conditions.

In Vitro Model System Key Requirements

Using anatomical and physiological literature review of neuroendovascular systems as well as basic ease-of-use and device design constraints, the following requirements were identified:

- Body Temperature
- Physiological Pressures
- Physiological Blood Flow
- Physiological Fluid Viscosity
- Relevant Aneurysm Anatomy
- Accessible via Endovascular Techniques
- Accommodates USP <788>

The specifications associated with each of these requirements are tabulated in **Table 3**.

Table 3 Specifications for the in vitro model

In Vitro Model Specifications	
Fluid Temperature	37±3°C
Pulsatile Pressure Mean	100mmHg ⁴³
Flow Rate	100-250mL/min ⁴³
Fluid Viscosity	.003-0.004 Pa·s ⁴⁴
Aneurysm Size	Medium to Giant ^{18,45,46}
Aneurysm Neck Size	Small to Large ^{18,45,46}
Endovascular Technique Accessibility	Visible and Fluoroscopically Transparent
Catheter Accessibility	Access Port with Hemostatic Valve
Accommodates USP <788>	Downstream Filters to Capture Particles >10µm

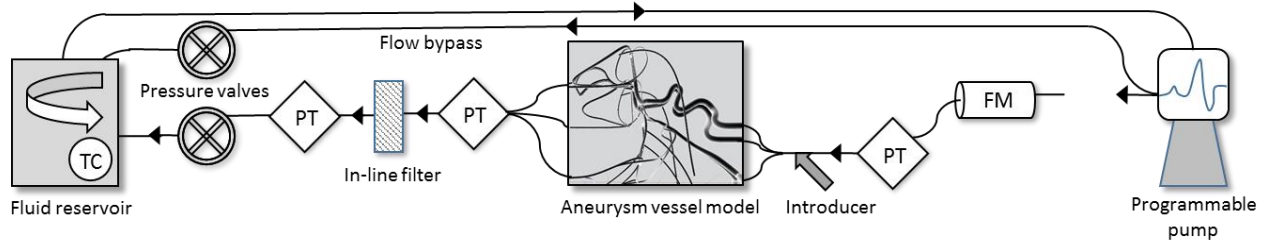


Figure 10 A schematic of the in vitro flow loop complete with all the necessary physical components.

Materials, Sensing, and Particle Capture

Each physiological parameter must be monitored with appropriate sensors to ensure that it meets the conditions found in the human body. The build and sensors are outlined here:

Fluid

The blood was simulated with DI water, but other fluids that would mimic other parameters such as viscosity can be substituted into the model. For initial testing, water was sufficient to confirm the model could mimic flow rates, pressures, and temperatures during a procedure. All components of the model were connected with silicone tubing.

Pressure Transducers (PT)

Utah Medical DPT-100 pressure transducers were identified as ideal candidates for this project (**Figure 11**).⁴⁷ They have a documented connection schematic so that they can be incorporated into various electrical designs. A full specification table is shown in **APPENDIX A**. They consist of a four inputs and outputs: ground, +5V power, PT+ Out, and PT- Out. This signal was amplified with an LM741CN operational amplifier (Op-amp) with input and feedback resistors of 220 Ω and 10k Ω , respectively, in an inverting configuration, giving a gain of -45 (schematic in **APPENDIX A**) was observed to be sufficient to amplify for the data acquisition system (DAQ).



Figure 11 Utah Medical DPT-100 Pressure Transducer with accessories (utahmed.com)

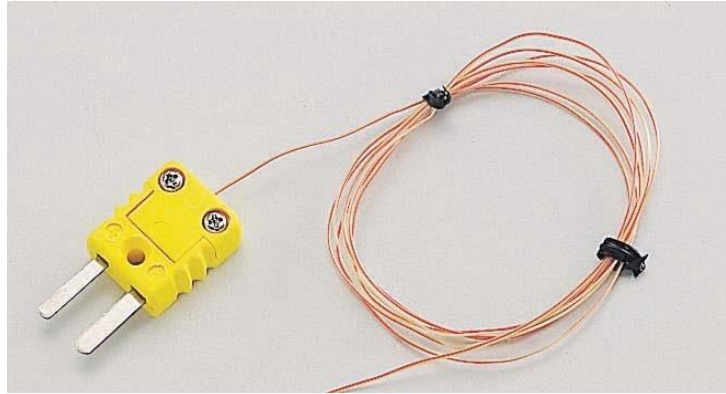


Figure 12 Example of a K-type wire thermocouple (thermocoupleinfo.com)

Thermocouples (TC)

K-type (nickel-chromium/nickel-alumel) thermocouples were chosen for their ubiquity and simplicity, as well as their ability to operate over large temperature ranges (**Figure 12**).⁴⁸ They operate on the principle of unequal electrical conductivity, which generates a miniscule potential across the junction of the two metals. Because the voltage is so small, the signal had to be amplified by 2 sequential Op-amps in the same configuration as the circuit outlined above (**APPENDIX A**).

Flow Meters (FM)

An Omega FTB-421 low flow plastic turbine was chosen for this model because it was capable of monitoring a large range of flow rates under 2.5L/min, well above the necessary range (**Figure 13** and **APPENDIX A**).⁴⁹ The output square wave frequency varies as a linear function of flow rate, so sampling frequency was chosen to obey the Nyquist frequency, in order to avoid aliasing. In addition, pressure changes due to the pulsatile nature of the pump mean that sample

times must be very short to avoid frequency change issues that would create averaging concerns (**Figure 14**). When the sampling frequency is increased to 1kHz and the sampling time dropped to 0.1 seconds (100 cycles), a clear linear trend can be calibrated (**Figure 15**). The flow meter is fed with a +12V input and a 10kΩ pull-up resistor, and then the output voltage is split between two 100kΩ resistors (**APPENDIX A**). Its operating range is 100-2500mL/min, covering the entire range of the chosen neurovasculature.⁴³



Figure 13 Omega FTB-421 Pressure Transducer. Flow goes through the clear part at the top, and the output signal comes from the black opening in the bottom (omega.com)

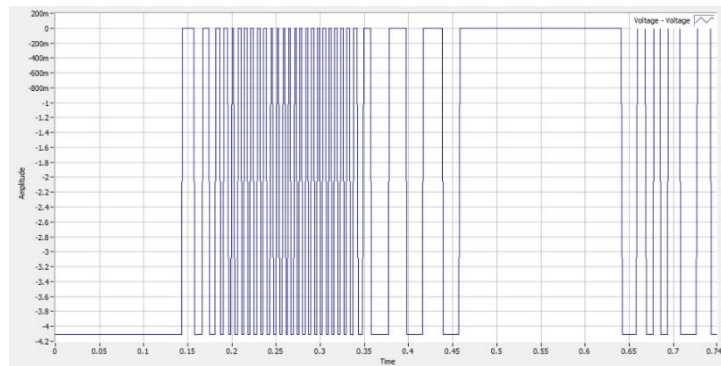


Figure 14 A plot showing the linear relationship between flow rate and digital frequency

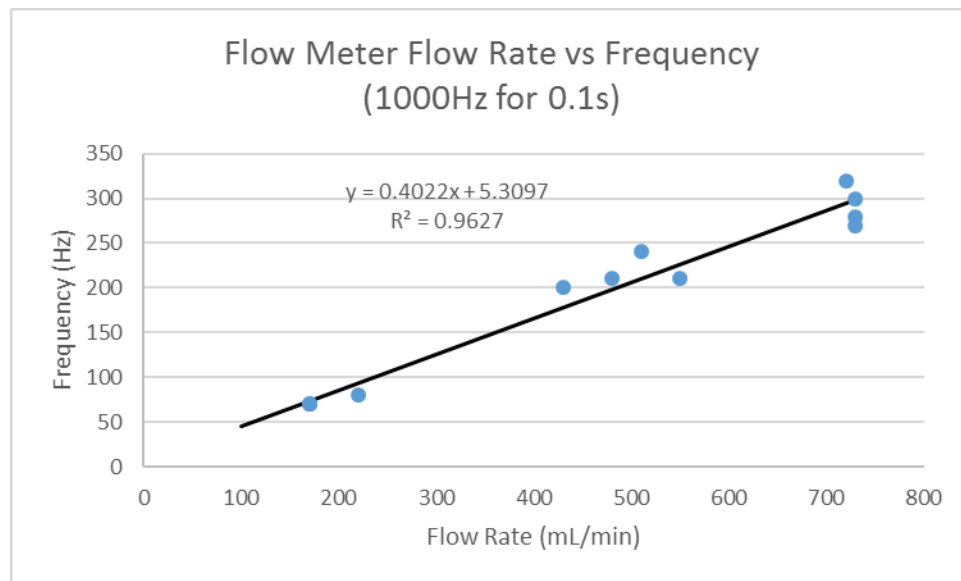


Figure 15 Output showing the change in flow meter digital frequency over the course of 0.75 seconds. The flow meter can operate on a range from 100-2500mL/min.

Signal Amplification Box

In order to house all of the amplification circuits, a custom box was design in SolidWorks and 3D-printed out of polylactic acid (PLA) plastic at the Cline Library MakerLab on a MakerBotReplicator (5th Gen). The circuits described above and detailed in **APPENDIX A** were housed inside this box (**Figure 16**). It is capable of amplifying 4 pressure transducers, 2 thermocouples, and 2 flow meters. This box is powered by an Agilent E3630A power supply set to outputs of +/-12V (op-amp power and FM signal), +5V (PT power), 0V (ground). These signals output to a National Instruments USB-6009 DAQ, which is connected to the computer.

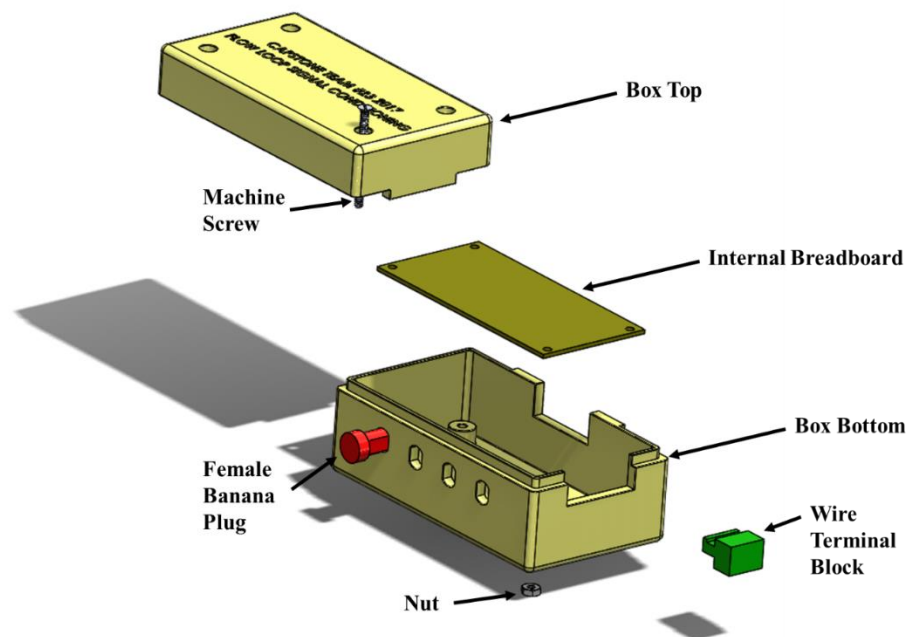


Figure 16 An overview of the Signal Amplification Box

Pump

A Stenner 170DM5 infusion pump was chosen for its robustness, tunability, and ability to run for long periods of time. It can pump at rates of 1-450mL/min, and the multiple adjustable pumping heads allow the user to approximate a physiologically-relevant cyclical pattern (**Figure 17**).⁵⁰

Immediately distal to the pump, a 10x2.5” cartridge filter was installed with a polypropylene 1 μ m filter to ensure that the fluid being delivered to the model is clean. Because the water is pre-filtered, the downstream particle capture device will only be capturing particles generated during the procedure from the embolic device and delivery tools, rather than debris from the reservoir, pump, and other sources.



Figure 17 Stenner 170DM5 Infusion Pump (lockwell.com)

Particle Capture Filter

Next, a system to capture downstream particles needed to be designed. A Sterlitech 25mm polypropylene filter holder was integrated into the flow so that any 25mm filter membranes could be used (**Figure 18**).⁵¹ Filter membranes were chosen because they can easily be analyzed via microscopy. Millipore Sigma Isopore 25mm filter membranes were used. After experimenting with pore sizes ranging from 0.4-8.0 μ m, 5.0 μ m pore membranes (TMTP02500) were chosen because they allow for significant image analysis differentiation between the pores and the 10+ μ m particles mandated by USP <788> while still enabling physiologically-relevant

flow rates of up to 1250mL/min (**Figure 18**).⁵² Physiological conditions in the human vessels are 113-367mL/min (internal/external carotid and vertebral arteries for healthy patients) and pressures are 78-149mmHg (internal carotid for elderly patients).^{43,53}

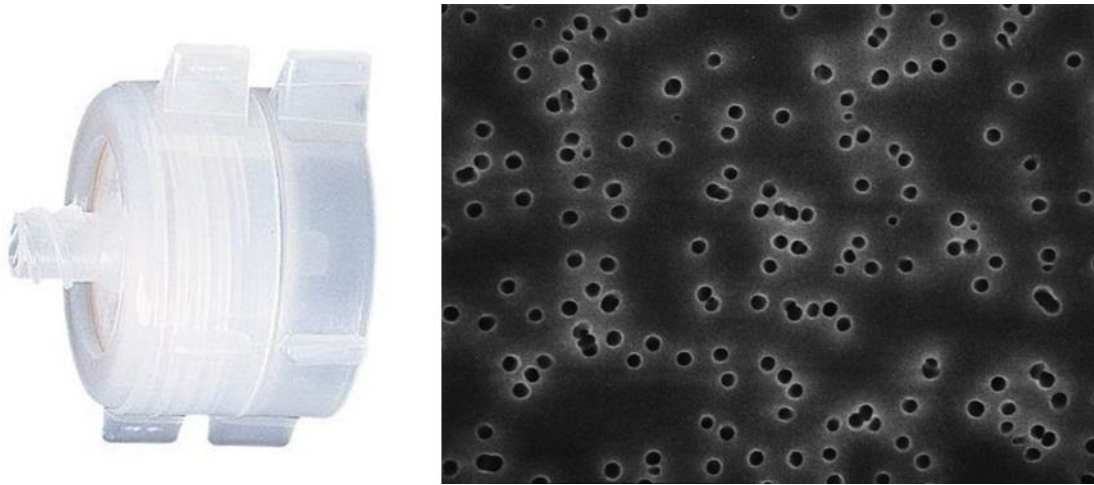


Figure 18 Sterlitech 25mm filter holder (L) and an example close-up of pores on an EMD Millipore Sigma Filter Membrane (R) (emdmillipore.com)

Anatomical Model and Catheter Access

In order to test endovascular devices accurately *in vitro*, a model had to be developed. This model was created for surgical access simplicity and accurate aneurysm neck sizes and volumes, rather than full anatomical accuracy. This makes it an effective model for rapid testing of aneurysm treatments. The two-part model was created with a cast polymer resin and plastic core. A core was designed in SolidWorks and 3D-printed in PLA. It meets the dimensions of various cerebral blood vessels (internal carotid – ICA, anterior communicator – ACA, middle cerebral – MCA) as shown in **Figure 19**, with aneurysm of sizes (height x width x neck) of 12x12x6mm (medium size, medium neck), 19x15x8mm (large size, small neck), and 10x8x4mm (medium size, small neck), respectively. The simplified model has an aneurysm of 10x8x4mm (medium size, small neck), which are incompletely occluded long-term in 21% of cases.⁷ These models

can be modified to meet the sizes and shapes of various aneurysm distinctions as outlined in **CHAPTER 1**, enabling the model to be used for a wide variety of disease states. The core ends were capped with silicone tubing that is permanently left in the model. The model itself was made of Smooth-On Clear Flex™ 50, a clear, soft urethane resin.⁵⁴ This material was chosen not for its specific stiffness or trackability properties (it is stiffer than native vasculature), but because it is clear both optically and fluoroscopically, which makes the model more user-friendly than opaque materials. It was mixed and put under vacuum to remove bubbles. A base was poured into a mold and allowed to cure for two hours. Then the core was placed on top and the mold was filled halfway up the core with another layer of Clear Flex and allowed to cure overnight. The next day, the mold was completely filled and allowed to cure overnight. The next day, the two halves were split so the core could be removed. Then connectors were inserted into the model to connect it to the flow loop. Multiple model shapes and sizes were used over the course of this project (**Figure 19**).

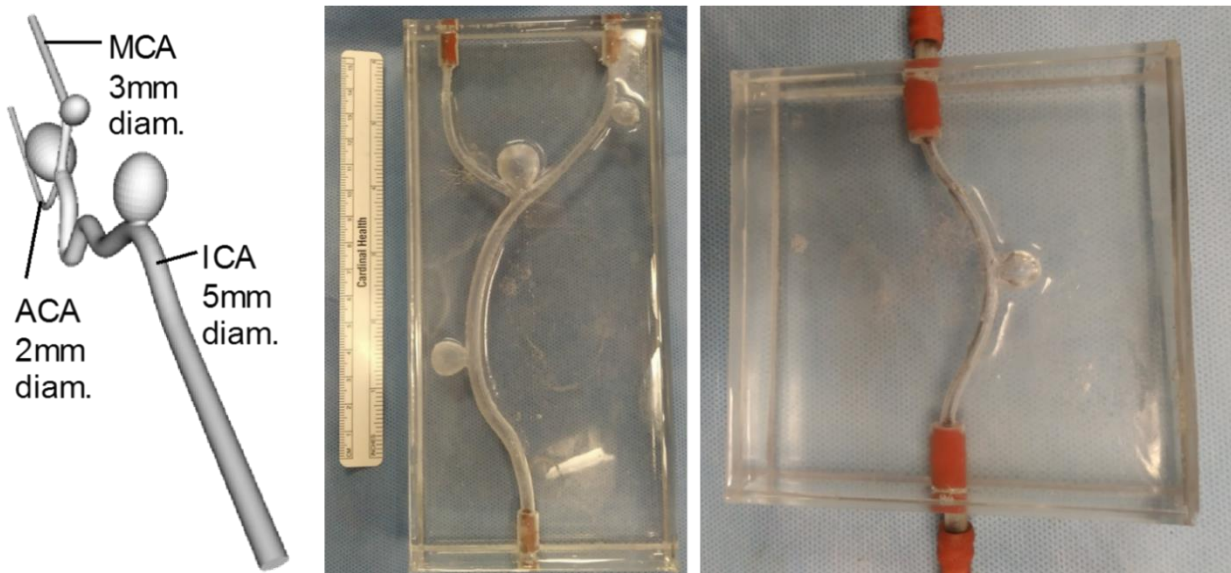


Figure 19 Example CAD drawing of the model core (L), actual model with three aneurysms (C), simplified model with only one aneurysm and no branching (R).

Digital In-Line Holography

As an alternative to filter-based particle counting, an in-line holography system was designed to be added if desired. This non-invasive system can be added where the inline filters currently are positioned. The complicated system of filter insertion, removal, and analysis is susceptible to contamination, clogging, and damage, and therefore can be greatly simplified by using holography. The system consists of a Helium-Neon laser, which passes through a 40x objective, 25 μ m spatial filter, and 26mm diameter x 106mm focal length lens (Edmund Optics 32-246) to focus and bring it to the correct size. It then passes through the flowing sample and onto a CMOS camera (Basler Ace acA2440-35um) (**Figure 20**). Then the image can be analyzed to count the particles present, as well as their shape and internal structure at any focus depth in the sample.⁵⁵ Furthermore, the holography setup can count particles as small as 1 μ m, drastically increasing the resolution of the counting system. While more expensive to set up, it has minimal operating costs and doesn't require consumables such as new filters. In addition, the analysis can be done in real-time and without affecting any of the physiological parameters essential to the flow loop. It can be used for both acute and long-term procedures with equal ease, offering a drastic improvement over the filter technique.

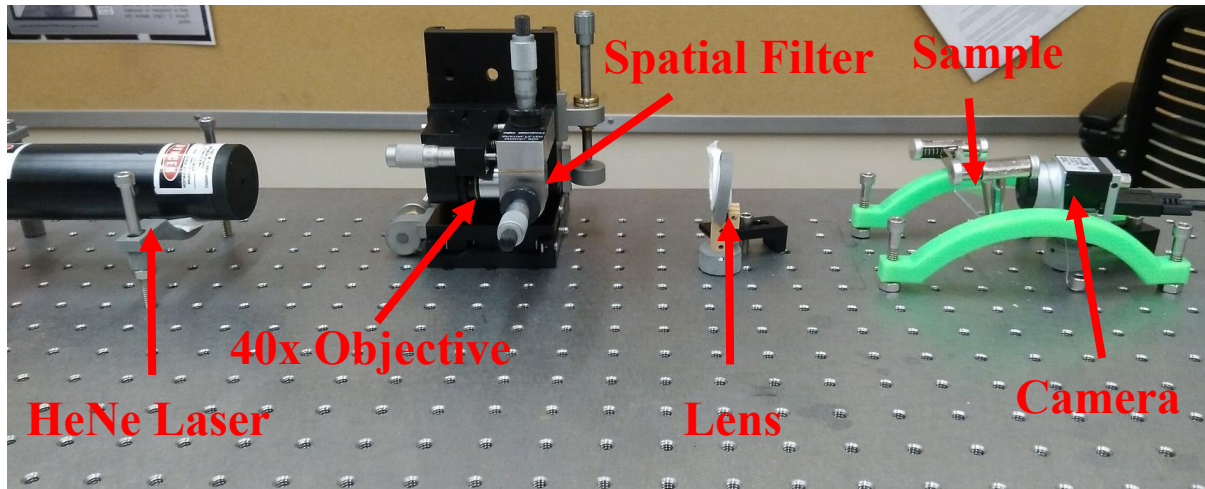
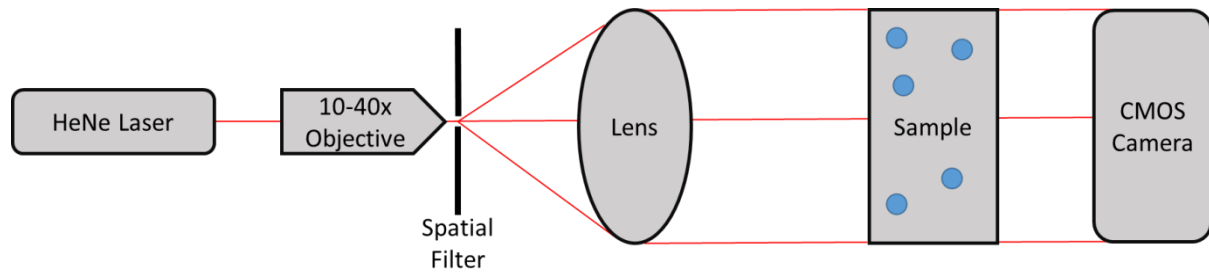


Figure 20 Schematic of the in-line digital holography setup (top), and a photo of the actual setup (bottom)

Fluoroscopy

This system was designed to be used with endovascular imaging techniques to make it a realistic model. In endovascular surgery, a fluoroscope is used for visualization. A fluoroscope continuously emits and collects X-rays that are passed through the surgical site. These X-rays are absorbed preferentially by different materials. Materials that are dense (both anatomically and molecularly) absorb the X-rays. Less dense materials allow the X-rays to pass more easily. Contrast media, such as Conray[®] outlined in **CHAPTER 1**, appears dark on the fluoroscopy screen. Contrast is used to illuminate the blood vessels and help endovascular surgeons follow them to surgical sites. **Figure 21** shows the lab's Philips BV Pulsera Fluoroscope and an image taken of the simple anatomic model from **Figure 21 (R)**.⁵⁶



Figure 21 Philips BV Pulsera (L) (labx.com) and an image of the simple aneurysm model filled with contrast. The model is held together with steel clamps that appear black (R)

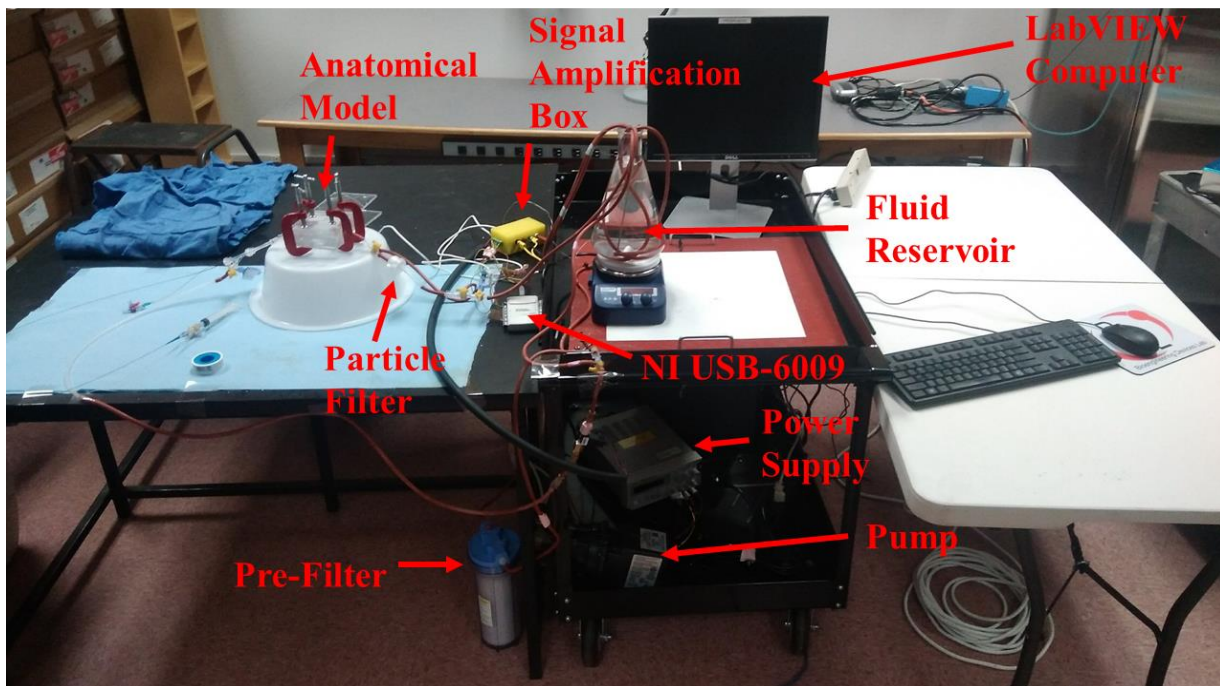


Figure 22 Total in vitro flow loop physical setup

LabVIEW Interface

A National Instruments (NI) virtual instrument (VI) was developed in order to monitor the flow loop and ensure that all physiological parameters are met. The signals are read from the NI USB-

6009 DAQ, converted into arrays, and then analyzed. The user selects a specific sampling frequency and number of samples to export. For example, a sampling frequency of 1000Hz and 100 samples would output an array of 100 data points every 0.1 seconds. This data is then averaged and fed into a calibration structure. Under “Automatic Calibration,” the user selects a minimum and maximum value for each sensor and clicks a switch when the sensor is subject to that condition. Once two data points have been recorded, a linear fit is computed so that all other values can be interpolated. The pressure transducers, thermocouples, and flow meters are calibrated with a blood pressure cuff, room and body temperature solutions, and a volumetric flask, respectively. The pressures and temperatures were calibrated at ranges of 50-180mmHg and 23-37°C, respectively. Due to issues with recording data at a high sampling frequency and the necessity of a high frequency to analyze the digital flow meter, flow rates were measured manually with a 200mL volumetric flask. The calibration values can then be brought over to the “Manual Calibration” setting, where the user can adjust and save the values. The values are also averaged for easier real-time visualization and plotted. The data for all sensors can also be recorded to a timestamped .csv file for further analysis. **Figure 23** shows the front panel of a streamlined version of the VI (block diagram can be found in **APPENDIX A**).

8 Tests with 0-4500 suspended 10µm polypropylene particles (2 trials at each number)) were performed, as well as 3 trials with PPODA-QT (outlined in **CHAPTER 3**). The particles were injected into the aneurysm, and flow was maintained for 20 minutes. “Before” was defined as before the injection was performed, and “after” was defined as after the 20 minutes of flow. The pressures, flow rates (calculated manually with 200mL volumetric flask), and temperatures (from water bath with stir plate thermometer) shown in **Table 4** (all data in **APPENDIX A**) are taken before, during, and after this whole process at a frequency of 50Hz and 5 samples read at a time,

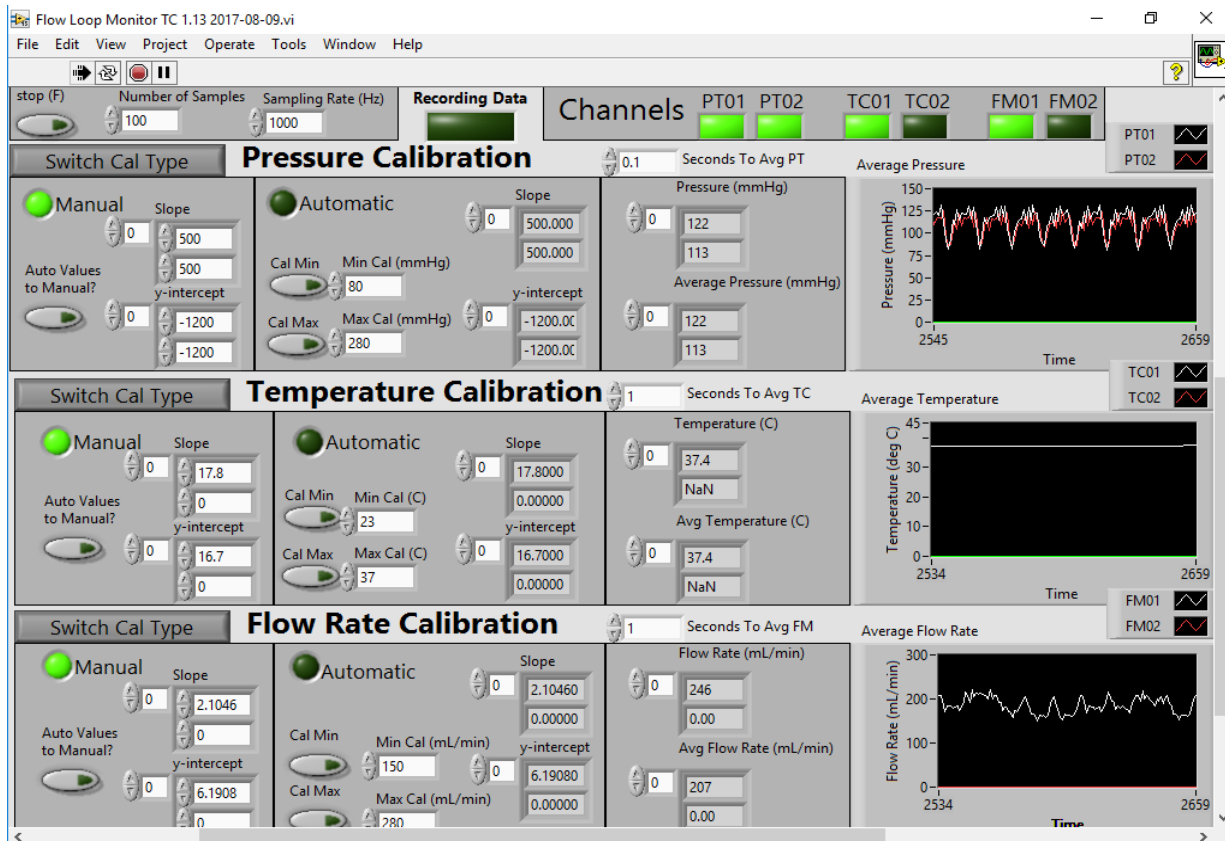


Figure 23 Simplified version of the Flow Loop Monitor VI that tracks the physiological parameters in the in vitro flow loop

and results were found to be similar to those found in the literature.⁴³ Proximal refers to the pressure gauge at the inlet of the model, and distal refers to the gauge immediately downstream from the filter. The data is also summarized by comparing the pressure drop across the filter at the beginning and end of the 0 sphere trial (**Figure 24**), the average pressure drop for all trials over the course of the experiment (**Figure 24**), and the drop in flow rate in all filters over the course of all trials (**Figure 26**). The deviations given for each trial is the difference between the mean and the max/min of the oscillating waveform, so it can be thought of as the difference between average blood pressure and systolic/diastolic maximum/minimum blood pressures. These are plotted as error bars in **Figure 24**, **Figure 25**, and **Figure 26**, which show that pressure

remains constant over 20 minutes of flow and the pressure and flow rate drops over 20 minutes remain constant for all trials of particulate injections.

Table 4 Parameters recorded during particle control test. Data was taken before the test and after 20 minutes of flow. 2 trials were used for each microsphere injection, and 3 were used for the PPODA-QT tests.

		Proximal Pressure (mmHg)		Distal Pressure (mmHg)			
Trial	Time	Mean	Deviation	Mean	Deviation	Flow Rate (mL/min)	Temperature (°C)
0 Spheres	Before	133	40	22	11	222	37-40
	After	154	19	29	18	214	
1500 Spheres	Before	136	19	29	11	235	
	After	152	11	24	3	222	
3000 Spheres	Before	136	31	27	12	231	
	After	150	44	30	10	222	
4500 Spheres	Before	138	50	31	12	235	
	After	130	42	18	12	226	
PPODA-QT	Before	118	57	26	12	119	
	After	125	56	28	14	113	

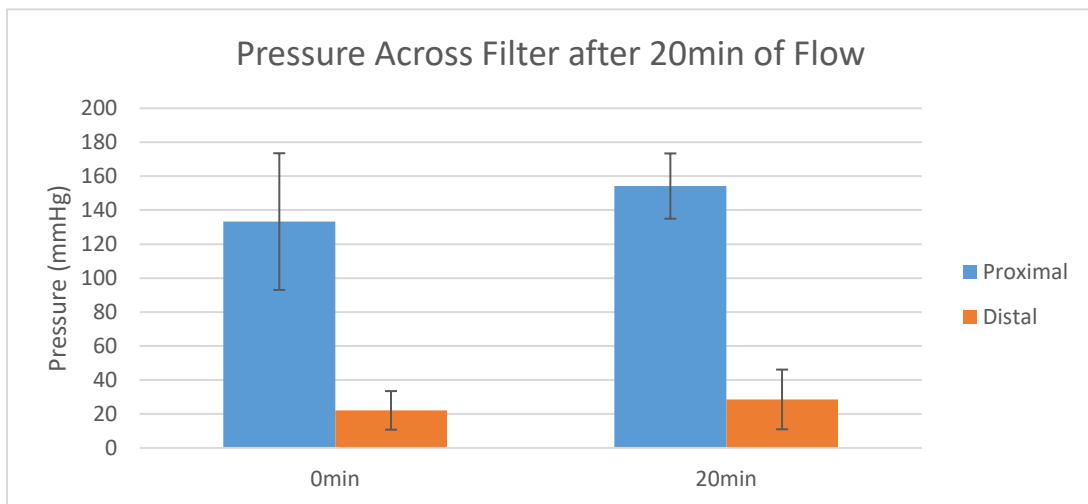


Figure 24 The pressure on both sides of the filter after injecting DI water containing 0 particles.

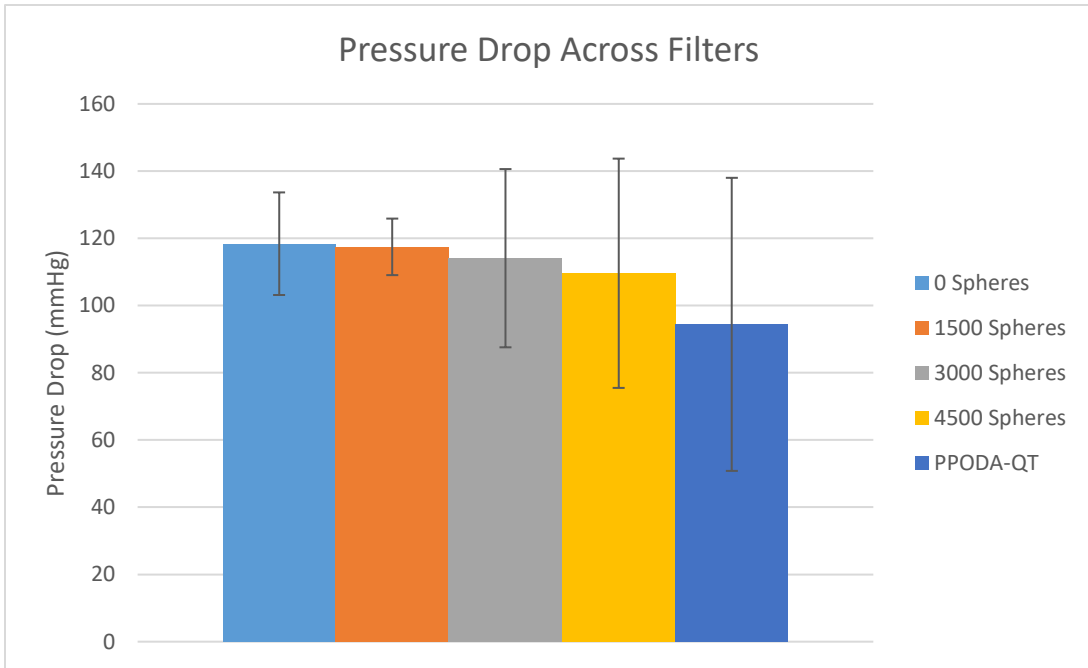


Figure 25 The pressure change from proximal to distal the filter for all trial configurations.

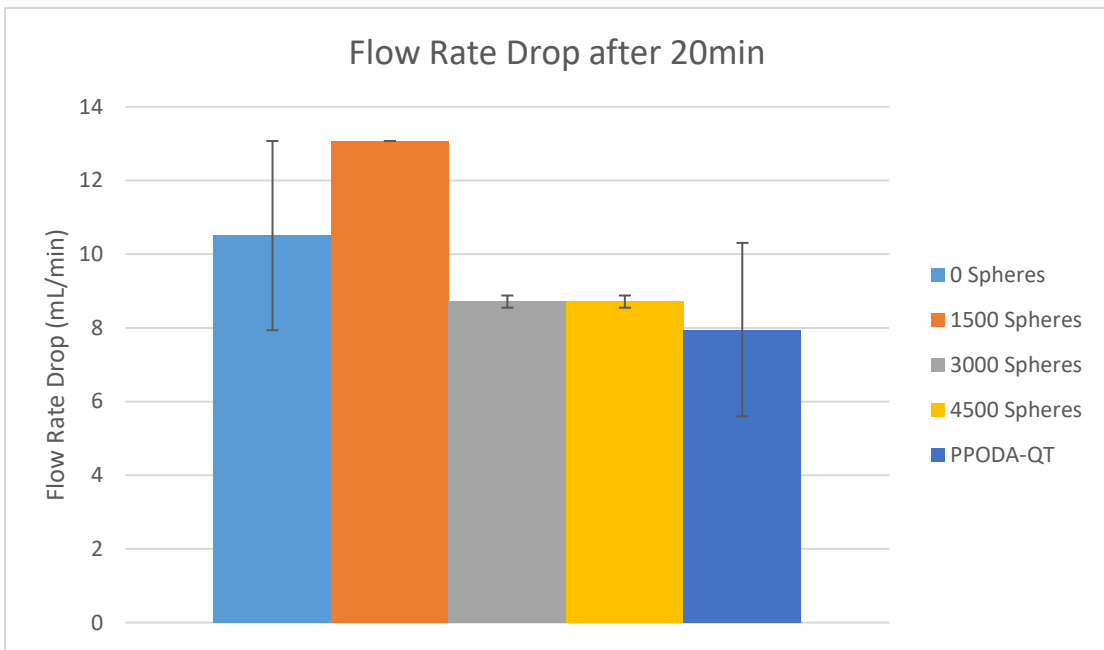


Figure 26 The change in flow rate across each filter for each trial configuration.

Discussion

The *in vitro* flow loop was built such that surgical scenarios can be mimicked accurately for both training purposes as well as device development. With a combinations of the components

outlined earlier, all of the design considerations laid out in the **In Vitro Model System Key Requirements** section have been met. Physiologically relevant pressures, temperatures, and flow rates have been achieved with 5.0 μ m filters, which can be removed for later analysis counting. The other physical requirements such as size and radiopacity have been met, and this model can be used for accurate surgical practice. Other aneurysm shapes and sizes can be made to span the ranges of potential disease states.

Over the course of 20 minute non-particulate trials, no significant difference was observed in pressures, indicating that the system is stable and sufficiently contamination-free for reliable use with the filters without clogging. In addition, even with 4500 injected 10 μ m spheres (well above the USP <788> standard), the system is still stable. This indicates that this system can be used for particulate analysis and understanding even beyond the scope of human use. Furthermore, flow rate drops from the beginning of the test stayed statistically constant for all of these levels of particulates. Furthermore, no difference in pressure or flow rate drop between PPODA-QT and the microspheres was observed, indicating that it may not pose a human particulation hazard. This will be explored further in **CHAPTER 3**.

As the digital flow meter presented problems related to sampling rate and measurement accuracy necessitating manual measurement during all tests, a different flow meter should be acquired. An analog flow meter could be incorporated into the system with an op-amp system similar to the pressure transducers and thermocouples. This would enable the BDL to record all data at lower sampling rates and keep hands-on work minimal.

In addition to the flow meter upgrade, a new USB data acquisition system could simplify the process. The sampling rate on the USB-6009 system is limited by the number of channels being used. By upgrading this system to one containing the common NI 9201 and NI 9213 (National

Instruments, Austin, Texas) for pressure transducer/flow meter and thermocouple acquisition, respectively, the limited sampling frequency and need for the custom signal amplification developed here would be eliminated. This would add to the usability of the system and allow for faster design iterations and upgrades.

The culmination of this work is that the lab now has a documented, modifiable model for testing endovascular devices. This will allow the laboratory to further expand laboratory scope, test more mechanically-accurate blood vessel mimics, and practice procedures for new and existing methods.

Aim 1 is now complete, as an in vitro model has been developed that simulates human physiological and anatomical conditions. **CHAPTER 3** will use this model to develop a method for confirming adherence to USP <788> as outlined in Hypothesis 1.

CHAPTER 3

AIM 2 - PARTICLE COUNTING AND CHARACTERIZATION

Background

Any medical procedure contains inherent risk. When medical professionals treat a given disorder, the aim is to treat it quickly, effectively, and reduce the possibility of causing other issues. While some of these hazards may be small, many of the dangers present during neuroendovascular procedures are exceptionally high. Any mistakes made during neurosurgery can have immediate life-changing consequences. Therefore, devices designed for treating neural disorders must be designed with the highest standards in mind. In the case of treating cerebral aneurysms, these standards guide engineers to design products that minimize the risk for aneurysm rupture, accelerate procedure times, and have minimal potential for downstream embolism.

Many of these issues have already been resolved for PPODA-QT and other liquid embolics. As it is delivered as a liquid, the risk for aneurysm perforation is negligible in comparison to coils. Rupture due to over-pressurization remains a concern if the balloon seal is too tight, but previous studies have shown successful embolizations in canine and porcine animal models.^{6,39} PPODA-QT can be delivered rapidly to reduce surgical risk, as balloon occlusion time longer than 5 minutes has been associated with increased complications.^{6,38} Onyx®, a current liquid embolic can only be injected slowly to reduce negative effects of the solvent DMSO, resulting in multiple balloon inflation cycles and injections. One study found an average Onyx® procedure time of 95 minutes, which furthers the risk of surgical complications.²⁵ These effects include vasospasm and

cytotoxicity, which can be eliminated with the faster and DMSO-free procedure that PPODA-QT provides.^{6,17,21–24,27,46}

Downstream embolic risks due to particulation from PPODA-QT are currently unknown. The focus of this project is to develop methods to test downstream particulation so these methods can be applied to PPODA-QT and other materials. To deliver nutrients to different regions of the body, arteries taper to arterioles and eventually capillaries. This allows for diffusion and other transport processes to act at a sustainable rate. These capillaries often reach diameters as small as 3µm, meaning that the 6-8µm red blood cells must often fold themselves in order to pass through.^{57,58} These tiny blood vessels are redundant, so neighboring vessels can provide sufficient nutrients to feed tissues in the case that some were embolized. However, ischemia occurs if enough vessels are blocked that the surrounding tissue is not delivered essential nutrients, a process that eventually causes tissue death. USP <788> sets limits on the microscopic particles shed during liquid injections so that ischemia risks are lowered.⁴² In order to verify that liquid embolics such as PPODA-QT can meet the requirements of USP <788> under simulated human conditions, this chapter focuses on the developed *in vitro* model, along with multiple imaging techniques, to assess injection particulates for USP <788> compliance in the following aim and hypothesis:

Hypothesis 1 – An *in vitro* system that mimics human physiological and anatomical conditions can be built to test liquid embolic conformation to the USP <788>

Aim 2 – Use the aforementioned *in vitro* model and different microscopy techniques to characterize the shape and number of liquid embolic particles released during aneurysm embolization

Methods

Two distinct materials were compared in this study: PPODA-QT cured in solution as well as a 10.0 μ m polypropylene sphere particle counting standard. PPODA-QT was analyzed via SEM, and both were used in filter analysis via DIC microscopy. An automated counting program was developed for this analysis. Finally, digital inline holography feasibility was performed with the 10.0 μ m sphere standard.

PPODA-QT Preparation

PPODA-QT was prepared similarly for all tests. 1.080g of PPODA (average molecular weight ~800, Sigma-Aldrich, St. Louis, MO) was mixed with 0.330g of QT (Sigma-Aldrich, St. Louis, MO) via two 3mL polypropylene syringes connected with two female-female luers and one male-male luer to increase mixing (**Figure 27**). These are mixed via a series of 30 strokes, and each stroke is completed in under 1 second. Then 0.37mL of Conray-60[®] contrast agent (Villegint, France) diluted to 11.0pH with NaOH, was added and the entire solution was mixed for 1 minute at the rate above. It was then injected through a needle into a liquid solution, or through a mock catheter made of 0.025" inner diameter polyimide tubing attached to 18 gauge EFD dispenser tips (Nordson Medical, East Providence RI) into the aneurysm model.



Figure 27 Syringe-Fitting configuration for PPODA-QT mixing

Scanning Electron Microscopy

Scanning Electron Microscopy (SEM) was used to perform initial tests and characterization. As SEM only highlights surface features and is a delicate instrument requiring specific coatings and other preparation techniques, it was only used for visual characterizations of PPODA-QT particle visualization and counting for USP <788>. Samples of PPODA-QT were prepared as outlined above and injected into beakers filled with water or saline. They were then allowed to cure and the aqueous solution was filtered through EMD Millipore 0.4 μ m polycarbonate filters. Filters were dried, mounted to aluminum studs, and then coated with Gold-Palladium for SEM analysis.

USP <788>

As outlined in **CHAPTER 1**, USP <788> governs the allowable particles shed during injection. **Table 2** details the requirements laid out by the standard. In addition to those outlined above, a requirement of test cleanliness is laid out: no more than 20 particles $\geq 10\mu$ m or 5 particles $\geq 25\mu$ m are allowed. This cleanliness can be accomplished by using a particulate hood, ultrapure water, and other precautions. As the BDL does not currently have all of these capabilities, samples were covered and protected from dust during all storage. Samples of 10.0 μ m polystyrene spheres (EZY-CALTM Particle Size Standards, Thermo Scientific) were diluted to varying concentrations between 0-4500 parts/mL with ultrapure water in a laminar flow hood. All items were washed with soap, isopropyl alcohol, and then rinsed in a sonicator filled with ultrapure water.

In-Line Digital Holography

A digital holography setup (outlined in **CHAPTER 2**) was designed to image particles flowing downstream of the injection site in the *in vitro* model. A Helium-Neon laser (HeNe) (633nm wavelength) was passed through a 40x objective and 25 μ m spacial filter to improve the beam

quality. A 26mm diameter x 106mm focal length lens collected the diverging light and collimated it to pass through the sample and on to the CMOS camera. The sample consisted of water containing 2000 particles/mL of the 10.0 μ m standard clamped between two glass slides.

Differential Interference Contrast Microscopy

Optical microscopy was also used because it is faster and requires less up-front cost than either of the methods shown above. 10.0 μ m particles were injected into a mock aneurysm and flow was maintained for 20 minutes. PPODA-QT was injected into a mock aneurysm under Fogarty balloon (Edwards Lifesciences, Irvine, CA) protection and allowed to cure for 10min. The balloon was then deflated but remained in place for another 20 minutes. 5.0 μ m polycarbonate filters were used to capture particles downstream during this time. They were then placed on glass slides and imaged using a Leica DMI8 confocal microscope at the Imaging and Histology Core Facility at NAU. Images were taken using DIC microscopy, a special type of microscopy with which augments slight changes in refractive index of transparent samples. This technique highlights relatively transparent objects such as the bead standard and PPODA-QT particles on the polycarbonate filters (**Figure 29**). The edges of the filter were identified and the microscope was set to automatically take and stitch together images across a square on the x-y plane that covered the entire filter. For a 25mm diameter filter, this is a total of 600-700 images at 10x magnification, equating to a square with roughly 25-26 images per side. It also did this at multiple z heights to focus across small variations on the filter surface (**Figure 28**).⁵⁹ Any images that contained the edge of the filter or outside were discarded during analysis to reduce edge effects such as the forceps scratches on the top of the DIC image in **Figure 29**.

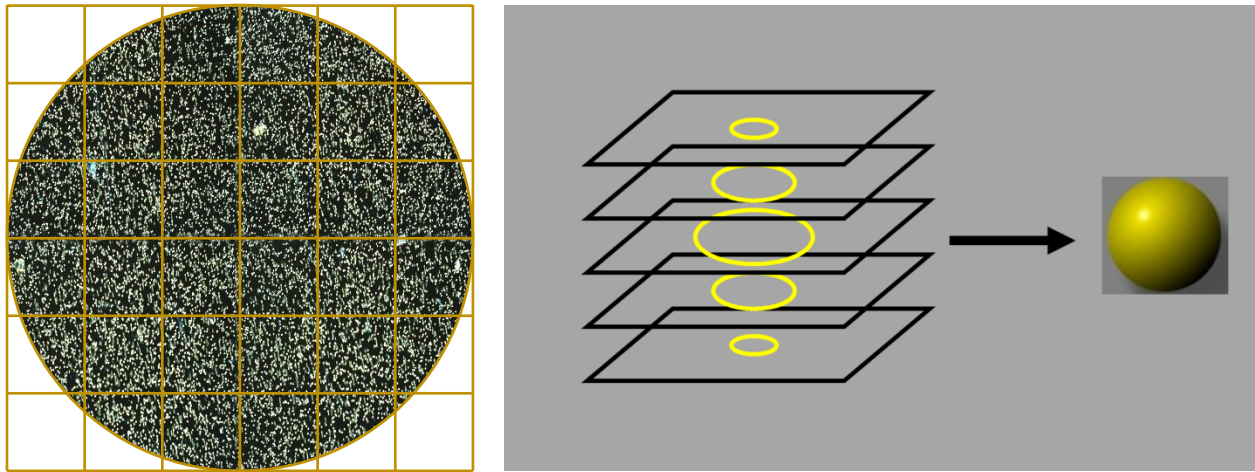


Figure 28 Example of the x-y grid of pictures taken (L), and an example of a sphere taken at various focus depths to illustrate the use of a z stack (R) (Northwestern University)

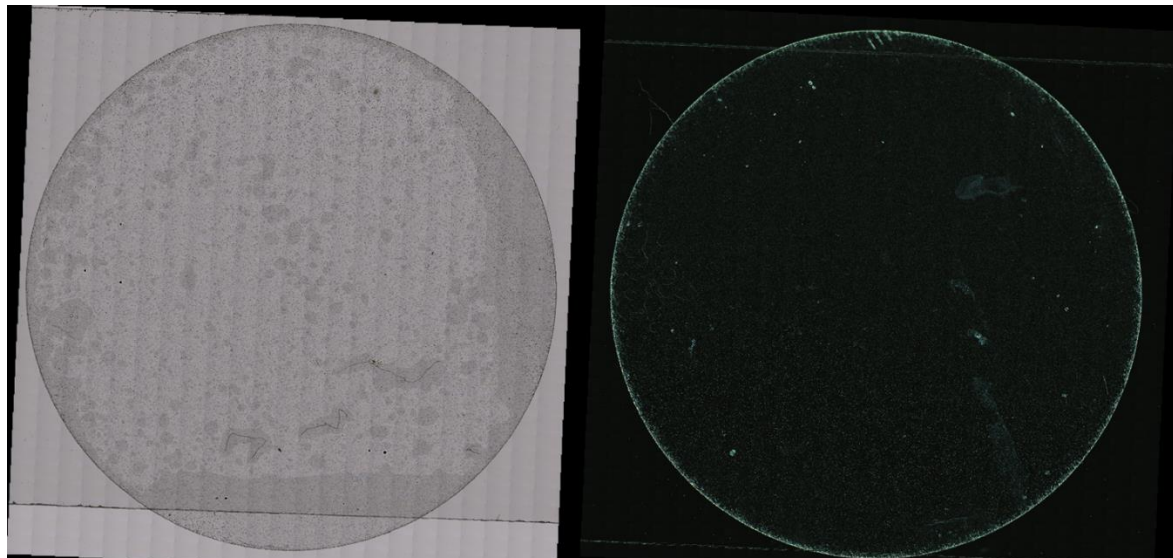


Figure 29 Example of a filter analyzed under normal bright field (BF) light microscopy (L) and Differential Interference (DIC) microscopy (R)

Counting Methods

The particles were analyzed via a combination of ImageJ (National Institutes of Health, Bethesda, MD) and MATLAB (MathWorks, Natick, MA) software. A MATLAB program was used to open the images in ImageJ. The user then set the intensity threshold to filter aberrations in the image. The 5.0 μm pores were used for reference for size. Then the MATLAB program automatically subtracted all of the images at different focus levels for a given x-y position (one

z-stack). This reduces glare and other intensity issues and makes particles on the surface of the filter even more distinct. ImageJ was then set to detect and count any image larger than $79\mu\text{m}^2$, which would ignore distinct pores but identify any particles larger than $10\mu\text{m}$ in diameter. These particles were then counted for all images. They are outputted and sorted by area, semi-major, and semi-minor diameters. A flow chart for this process is shown in **Figure 30**, and the code for this program is shown in **APPENDIX B**.

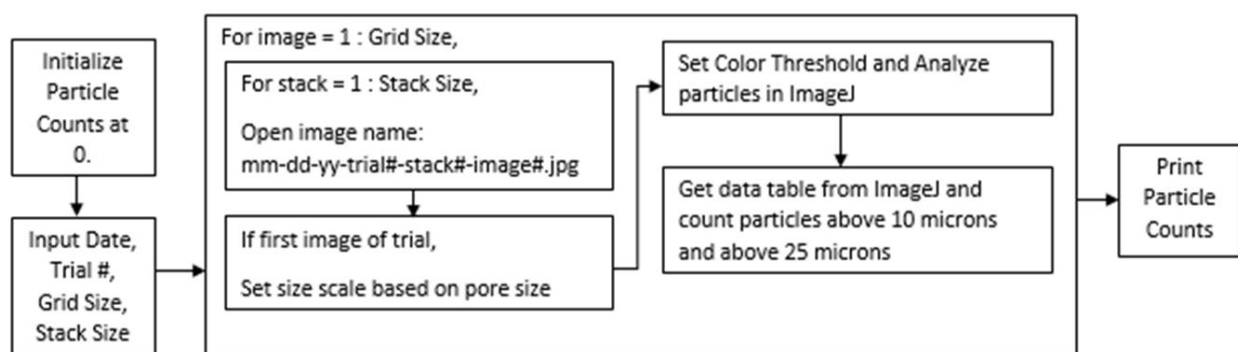


Figure 30 Flow chart illustrating the process of the coupled Matlab and ImageJ automated particle counting analysis.

Results

USP <788>

All methods used to characterize the system and PPODA-QT for USP <788> are outlined in their respective sections below.

Scanning Electron Microscopy

Images of PPODA-QT showed distinct morphology depending on how the particles were generated. Some pieces of PPODA-QT were spherical, whereas others had jagged edges (**Figure 31**). These shapes can be used to categorize the particles. SEM was not used to characterize PPODA-QT for USP <788>.

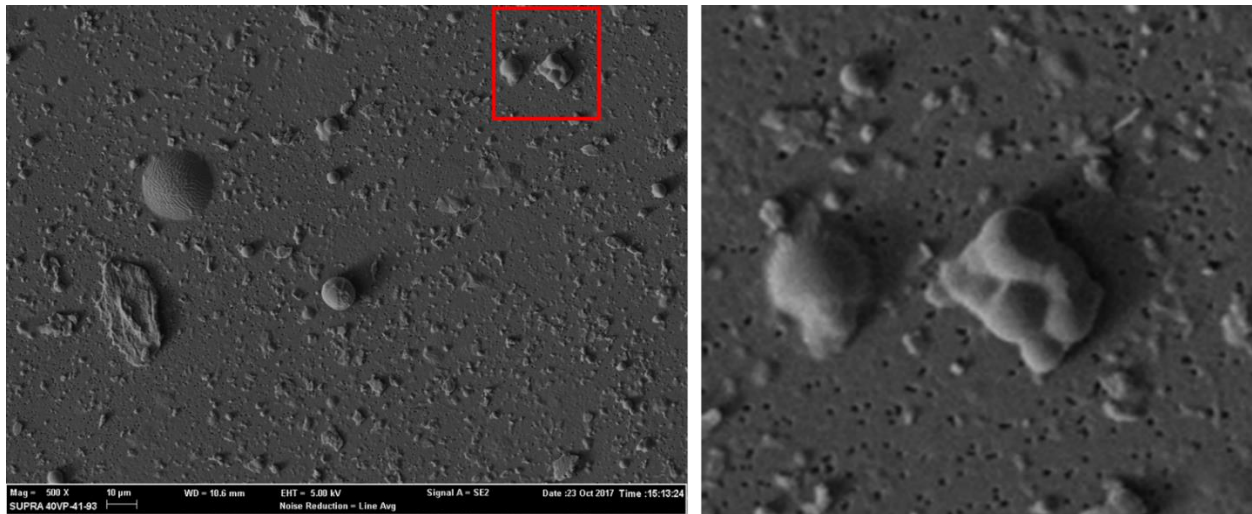


Figure 31 SEM image taken of various PPODA-QT morphologies. On the left is a 500x image with multiple particles of PPODA-QT. This sample was generated with little concern for contamination (such as the bubble and large flake on the left), but still shows multiple types of PPODA-QT shapes. In the center is a $\sim 10\mu\text{m}$ PPODA-QT sphere, and smaller PPODA-QT spheres are scattered throughout the image. In the top right, expanded in the image on the right, are different small particles, including spherical and jagged PPODA-QT.

Figure 32 shows the smooth surface texture of PPODA-QT that was injected through microcatheters into DI water and allowed to cure in situ. The smooth surface features support the categorization discussed above and shown in **Figure 29**.

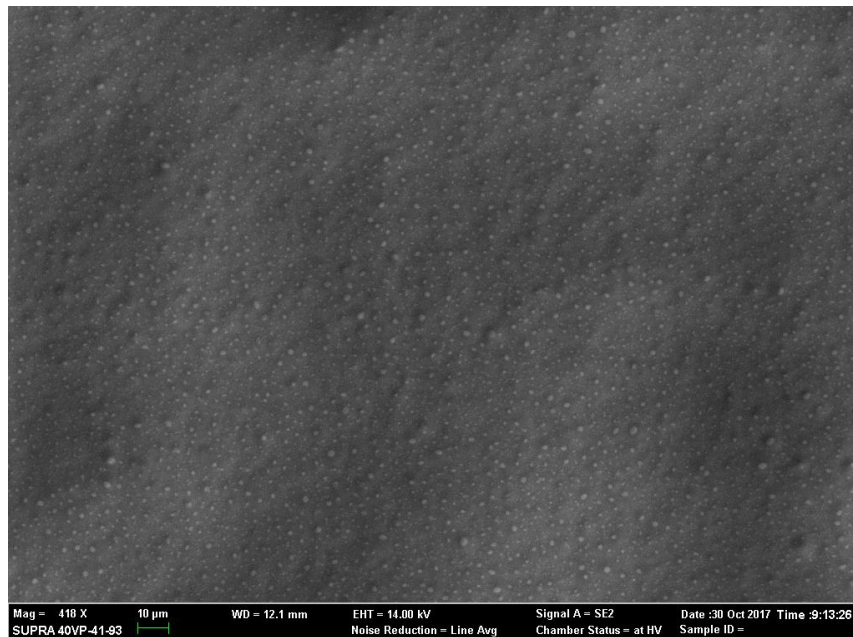


Figure 32 A 418x image of the surface of PPODA-QT when formed in DI water.

Digital Holography

Initial feasibility of the inline digital holography counting method was proven. Images of the sample showing a strong diffraction pattern due to either the 10.0 μm particles or microscopic surface contamination. Further refinements are necessary for full holographic resolution, but proof of concept images are shown in **Figure 33**.

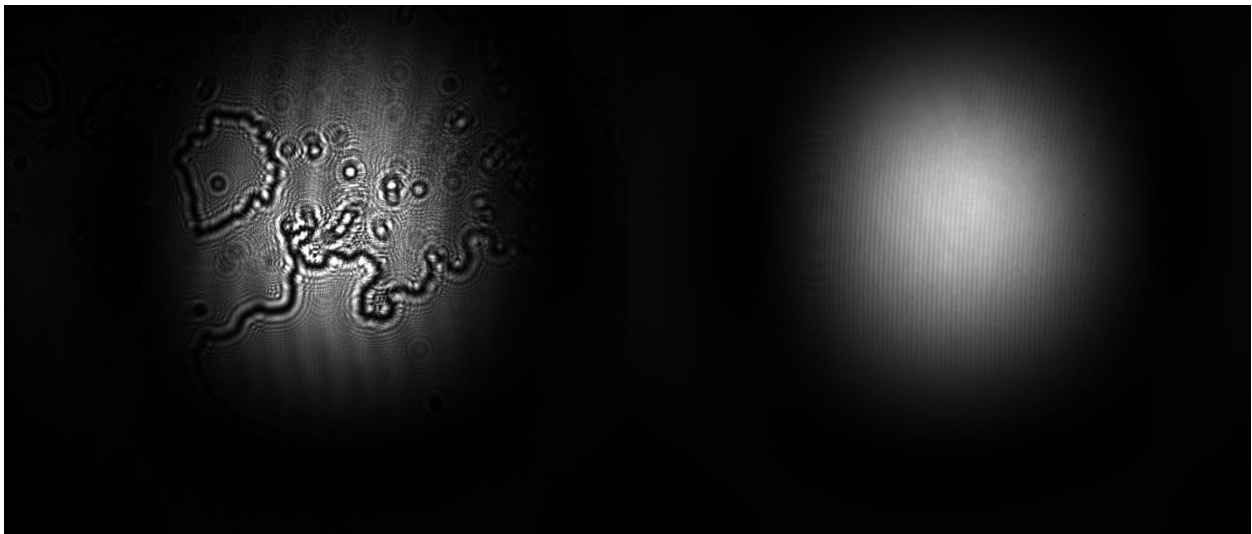


Figure 33 Images showing the edges of air bubbles as well as small particles and their associated diffraction patterns (L) as well as an image showing the base diffraction pattern of the CMOS camera detector cover (R)

Differential Interference Contrast Microscopy

DIC microscopy was the method used to count particles for USP <788> compliance. **Figure 34** shows the steps in the counting process. a) shows the original image used for processing at a given x-y location. The entire 8 image z-stack (10.0 μm spacing) at this location was analyzed via MATLAB and ImageJ, and the minimum intensity at each pixel was used to create image b). Then it was converted to black and white and the intensity threshold was increased so that many of the pores would be removed, as seen in c). Finally, c) was analyzed so that the particles above 79 μm^2 (10 μm diameter) were identified in d), and the output particle sizes are shown in the table.

This process must be set once for every image, and then it will automatically apply the same process to the rest of the images in the sample.

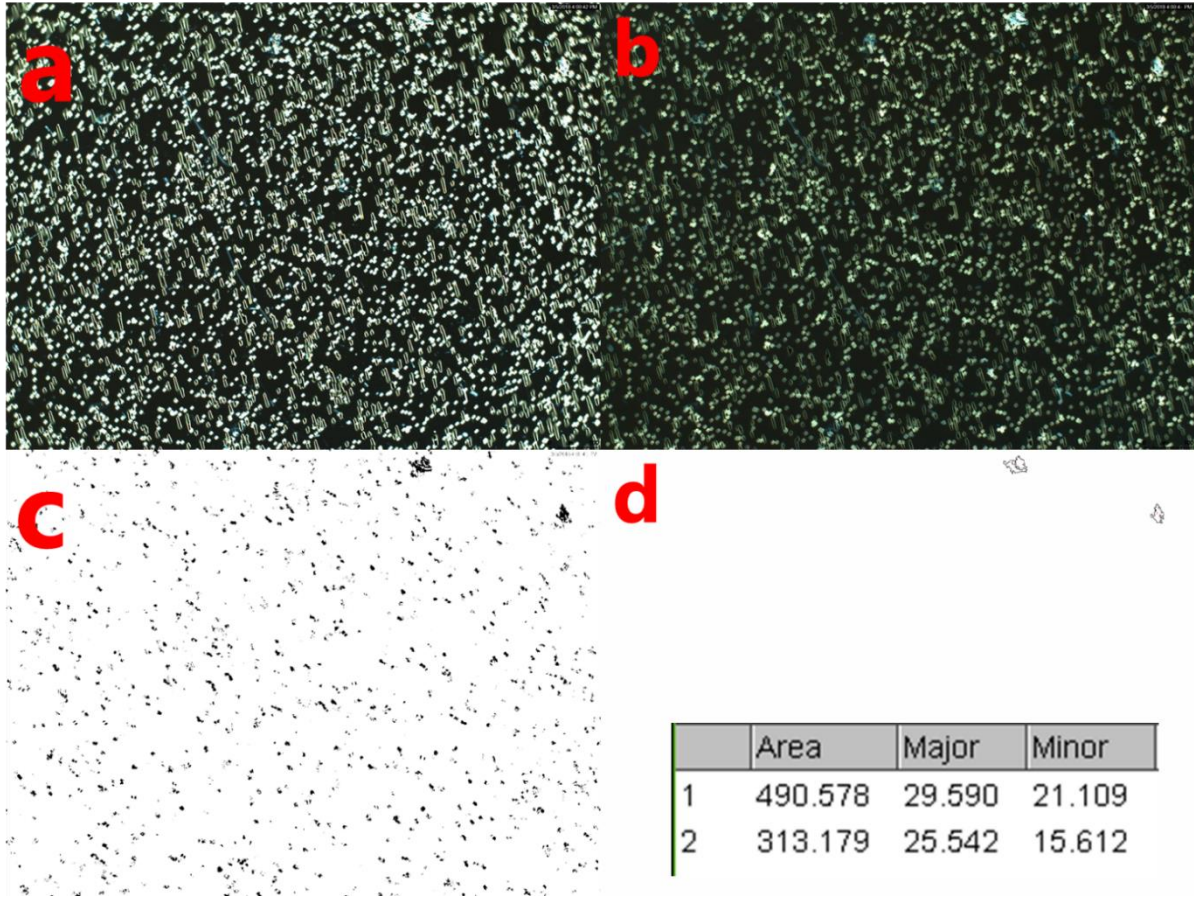


Figure 34 The various stages of particle counting via DIC microscopy, MATLAB, and ImageJ. a) shows the most in focus image in a given z-stack. b) shows the same location, but with each pixel corresponding to the minimum intensity across the 5 image z-stack (10.0 μ m spacing). c) shows this image once it has been converted to black and white and the intensity threshold was increased to remove many of the pores and small objects. d) shows the 2 particles detected, as well as the output of their area and major and minor diameter.

This was repeated for 8 samples to generate a calibration curve ranging from 0 to 4500 input 10.0 μ m beads. The number of particles counted by the automated method was orders of magnitude from the expected value, as well as inconsistent between tests. Trial 2 with 3000 particles was ignored as an outlier (Table 5 and Figure 35).

After this, PPODA-QT was injected into an aneurysm in the model as described in the methods above. The aneurysm dimensions of 10 x 8 x 4mm (H x W x Neck), making it a small, small-necked aneurysm with a volume of ~0.35mL. Each sample released 1 large (~1mm) particle, and similarly-sized particles stuck to the catheter and balloon was observed in all 3 samples (**Figure 36**). This has not been observed by the BDL animal models or in models using new, FDA approved neuroendovascular balloons and microcatheters, so future tests should incorporate those devices instead of the substitutes used here. The automated particle counting is shown in **Table 5** and **Figure 35**.

Table 5 The number of injected sphere standards and PPODA-QT injected into the model and the number of particles counted by the automated counting program. The 3000 Sphere Trial 2 was ignored as an outlier because it at least one orders of magnitude different than the other trials. More explanation below.

Material	Trial	10-25µm Particles	>25 µm Particles
0 Spheres	1	1	0
	2	5	3
1500 Spheres	1	64	2
	2	85	3
3000 Spheres	1	4	6
	2*	670*	162*
4500 Spheres	1	10	0
	2	13	4
PPODA-QT	1	11	2
	2	16	7
	3	13	3

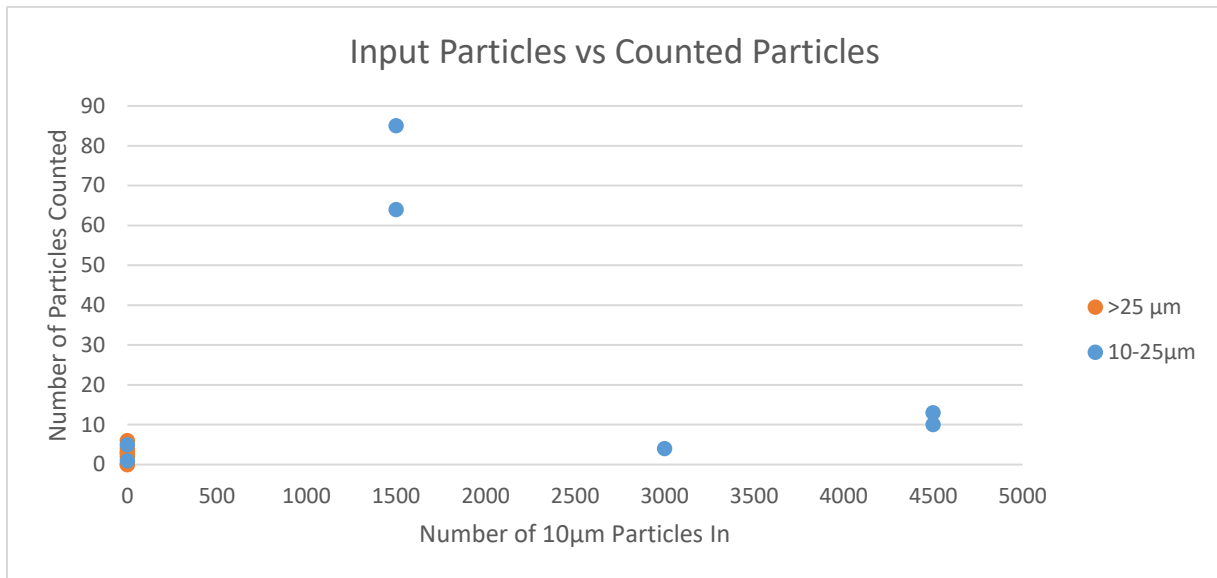


Figure 35 Particles counted by the automated particle counting method vs the number of particles put into the system.

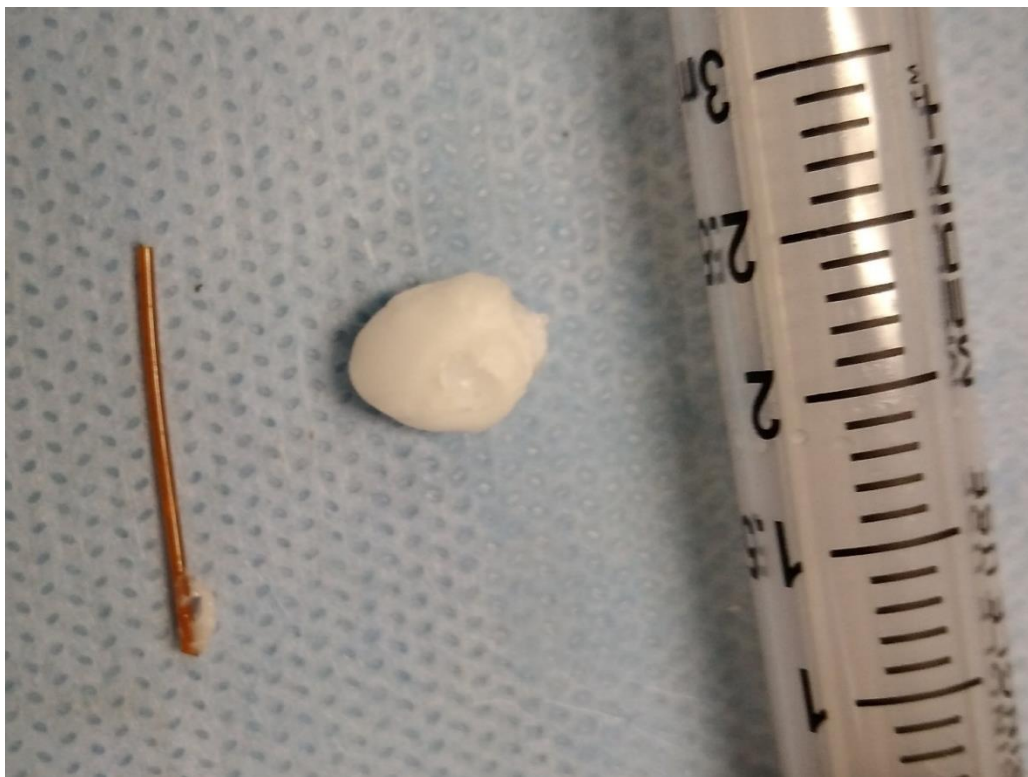


Figure 36 Image showing a mock catheter with PPODA-QT stuck to the tip (L), the explanted PPODA-QT embolic (C), and a 3mL syringe for reference (R)

Discussion

Scanning Electron Microscopy

SEM has been established as a method for understanding surface features and other particulate characterization of liquid embolics such as PPODA-QT. Particles cured as individuals and those broken off larger pieces can be distinguished. While it was not explored here, this could potentially prove to be a reliable method of determining specifically how PPODA-QT particulates over the duration of an injection and in long-term studies. Individual spherical polymer particles formed independently are likely the lowest-risk shape from a clinical perspective. While they do not form the smallest possible cross-section in a certain direction, they are consistent in all directions and therefore the symmetry means that they only pose embolic risk in situations with vessels of a smaller diameter. In addition, it appears that individual particles can form on the order of single microns (**Figure 31**) meaning that many of the particles shed from this procedure could pose no embolic risk. However, cytotoxic and genotoxic risks of these microscopic particles have not been investigated and would be addressed during FDA-mandated ISO 10993 testing, which is beyond the scope of this project.

Digital Holography

Holography has been established as a completely novel method to image PPODA-QT and other liquid embolics. It can be used to gain 3D information regarding the polymer as well as measure its particulation characterization. Further analysis will need to be done in order to bring its full potential to USP <788> and other particle characterization applications, but this remains a promising use of this technology.

Differential Interference Contrast Microscopy

DIC microscopy has been applied to obtain large quantities of data quickly in a form that is simple to analyze. Through the development of MATLAB and ImageJ analysis programs, it now can be used to rapidly analyze filters used to capture downstream particles. Now that this analysis method is set up, it can be used for this and other applications where many pictures must be analyzed for particulate or other object detection.

However, this counting method still needs further development. Particle counts were far from expected values, indicating that procedural modifications must be made. This could include further validation of input particle quantities, as well as further analysis to find any locations in the model where particles could be trapped before they reach the filter.

Furthermore, the 3000 Sphere Trial 2 had an order of magnitude greater number of particles counted than the other trials, including $>25\mu\text{m}$ particles (of which there should be none). Due to analysis delays, the image was taken a week after the filter system, and it appears that hundreds of contaminating particles were deposited on the filter in this time. This, combined with the fact that the particle counts are orders of magnitude larger than any other trials, justifies it being removed as an outlier in **Figure 35**. Notably, the 1 Sphere Trial 1 had the same analysis delay but did not show the same level of contamination. This highlights the high variability present in the filter method due to handling.

USP <788>

Because the counting methods are still under development and more tests must be run to determine their accuracy, USP <788> compliance has not yet been established. In addition, contamination greater than the requirement of than 20 particles $\geq 10\mu\text{m}$ or 5 particles $\geq 25\mu\text{m}$ remains outstanding.

Conclusion

While the framework for two test methods has been developed, further work must still be done in order to bring both the DIC microscopy and inline digital holography to full USP <788> compliance. More controls should be run in order to determine whether the test methods successfully capture and count all particles put into the system. As discussed earlier, this would include using the proper neuroendovascular devices to prevent sticking, as well as potential investigations into ways that particles are trapped on surfaces in the flow loop other than the filter surface. Steps should be taken to decrease contamination, such as performing the test in a laminar flow hood or a cleanroom. Due to a combination of lack of success with DIC microscopy analysis as well as the time-intensiveness, invasiveness, and resulting variability of the test, future studies should focus on holography as the primary method of particle counting. It is non-invasive and live, meaning that it will likely give more accurate, cheaper, and faster results.

Some issues with final particle counting can be attributed to the large amount of filtering and automated analysis of the DIC images. Using filters that will generate clearer images, finding methods to make surface particles more distinct, and minimizing contamination will make this image processing more accurate and precise. If an automated counting process such as that presented here is to be used in the future, further steps must be made to ensure the images being used more clearly show particles before they are analyzed.

Once this has been done, PPODA-QT and other materials can be fully tested and assessed for USP <788> compliance (Aim 2). An *in vitro* system that mimics human physiological and anatomical conditions has been built, but it is not yet fully ready to test for USP <788>

conformation (Hypothesis 1). Therefore, Hypothesis 1 remains inconclusive until the test methods are finalized.

CHAPTER 4

AIM 3 - IN VIVO MODEL

Introduction

Despite the controls and standards placed upon the *in vitro* testing of medical devices by various regulatory bodies, the final test of practical device safety is often *in vivo* testing. Depending on the specific disease state and method being tested, different models can be used. As discussed in **CHAPTER 1**, previous studies using saccular aneurysms were surgically created in canine models (**Figure 9**). While this model presents an excellent initial feasibility test for the filling capabilities of PPODA-QT, it does not provide an accurate picture of the human aneurysm position and healing response. The surgical creation, which includes stitching of a jugular vein pouch on the carotid artery to form an aneurysm, is limited to side-wall aneurysms of small and medium sizes.¹⁸

The leporine (rabbit) elastase model used here improves upon the surgical canine model in that it minimizes trauma at the vessel neck, reducing the inherent healing response to the aneurysm formation surgery. This means that, in theory, all histological and inflammatory response is due to the embolization procedure used to treat the aneurysm, rather than both the aneurysm creation and embolization procedures. This model has been growing in popularity and modifications of it have been used by many different research groups.^{30,60-62}

The first step of the procedure is to access the right common carotid (RCC) artery. After access is gained, a balloon catheter is inserted to occlude the beginning of the RCC where it branches from the right subclavian (RS) artery. The neck can also be occluded with a surgical clip. The

occluded RCC is then filled with elastase, which breaks down the elastin present in the blood vessel. This weakens it and allows it to expand. Finally, the top of the RCC is tied off so that the weakened vessel can slowly grow over the course of a month. Then the aneurysm is ready for treatment. This entire process is detailed in **Figure 37**.⁶³

When the aneurysm has fully developed, it can be treated with various treatments. This procedure is outlined in **CHAPTER 1** and below. Afterwards, the animals can be monitored for any negative results of the procedure, which may include stroke-like symptoms, right side – left side movement inconsistencies, and other neurological defects.

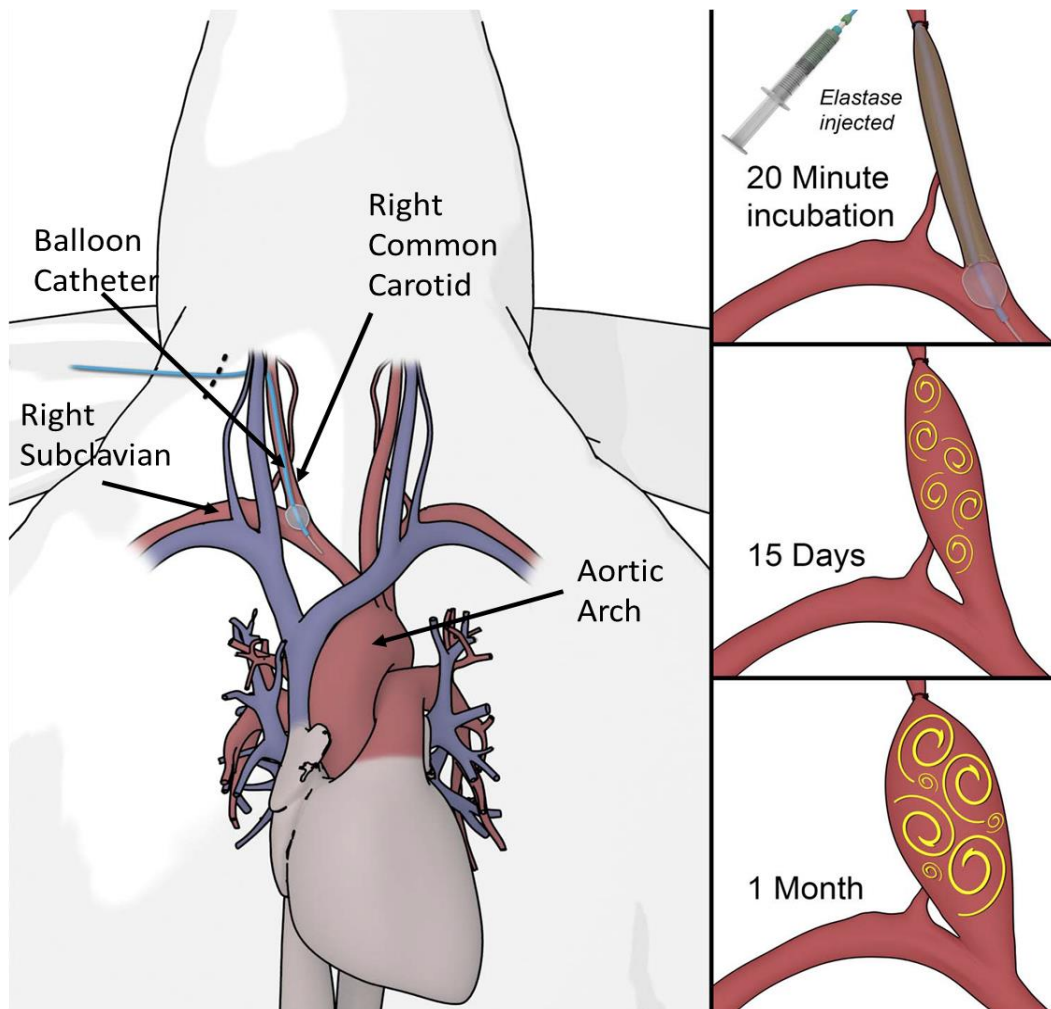


Figure 37 Diagram showing the initial creation procedure and progression of the rabbit elastase aneurysm model (Brinjikji et. al 2016).

The development of this model is Aim 3 in addressing Hypothesis 2:

Hypothesis 2 – An *in vivo* aneurysm model can be developed to evaluate liquid embolic without observed negative embolic effects

Aim 3 – Develop an *in vivo* rabbit aneurysm model that can eventually be used to evaluate liquid embolic efficacy and safety

Materials and Methods

The progression of the rabbit model can be divided into three sections: the aneurysm creation surgery, embolization procedure, and post-mortem analysis. The three are outlined below:

Aneurysm Creation Surgery

New Zealand rabbits were used for this procedure (materials list in **APPENDIX C**). Multiple blood-thinning regimens were adopted in order to prevent clotting of the aneurysm during the procedure. At the end of the study, a combination of Plavix (Clopidogrel) (15mg/kg) and aspirin (acetylsalicylic acid) (10mg/kg) were administered orally, daily from 3 days before the aneurysm creation surgery, and maintained until embolization. They were sedated with Ketamine/Xylazine/Acepromazine (60/6/1 mg/kg) and anesthesia was maintained with isoflurine (1-1.5% in O₂ at ~1 L/min). Sterile technique was used to access and isolate the RCC. Access to the vessel was gained with a 24G IV catheter or a modified microcatheter, and the RCC branch off of the RS was occluded with a surgical clip. At the end of the study, the decision was made to use a 3F Fogarty balloon catheter in a 5F introducer to occlude the RCC endovascularly under fluoroscopic guidance for all future animals.

A suture was used to seal the vessel around the catheter. 80U of porcine elastase was suspended in saline or 9pH PBS and injected into the blood vessel, where it incubated for 20 minutes (longer if appropriate if the full volume of elastase did not fit in the vessel or leaked out). The clip was then removed, and the RCC was flushed and tied off 2-3cm distal to the RS. The surgical site was repaired and the rabbit was monitored for 21 days until the aneurysm development was complete.

Embolization Procedure

The materials used for this procedure are documented in **APPENDIX C**. After sedation as outlined above, access to the right femoral artery was gained and a 5F introducer was inserted into the vessel. Fluoroscopic guidance was used to bring a 5F angiocatheter up to the RS to image the aneurysm. After confirmation of the aneurysm size and shape (calculated using **Equation (2)**), a microcatheter was inserted into the aneurysm and a balloon catheter was placed over the neck. PPODA-QT was filtered for sterility and then prepared as outlined in **CHAPTER 3**. The balloon was inflated with contrast, and the subtraction setting on the fluoroscope was used to view the PPODA-QT as it was injected into the aneurysm with a high pressure injection catheter. The catheter tip was slowly withdrawn to keep it out of the bolus of the PPODA-QT filling the aneurysm. The catheter was left in place until ~5min post-mixing, and the balloon was deflated at 6-10min post-mixing. Aneurysm embolization was confirmed via fluoroscopy. All surgical tools were removed, the right femoral artery was tied off, and the access site was closed.

$$\text{Ellipsoid: } V = \frac{\pi * \text{Width} * \text{Depth} * \text{Height}}{6} \quad (2)$$

(Depth = Width for 2D images)

Necropsy

Animals were euthanized per the Institutional Animal Care and Use Committee (IACUC) approved methods appropriate for rabbits and the American Veterinary Medical Association (AVMA) guidelines or died from surgical complications. The aneurysms were excised, imaged, and stored in formalin for histological analysis. If neurological symptoms were observed, a craniotomy was performed to look for stroke signs in the brain.

Results

Aneurysm creations and embolizations have been performed on a total of 8 animals so far. This thesis covers the initial steps to create the model. Future studies by the BDL will improve and expand upon the *in vivo* aneurysm creation and PPODA-QT embolization.

Aneurysm Creation Surgery

Aneurysms were created, but they did not accurately represent large saccular aneurysms as hoped. Most of them were found to be roughly the same diameter as the original RCC, indicating that the elastase digestion did little to nothing to weaken the vessel. Large clots were observed occluding the distal section of the vessel, filling nearly half the length of the aneurysm. These clots have been observed previously.⁶⁰ Further studies must be done to improve the aneurysms and make the shape more indicative of the natural aneurysm disease state. The new endovascular procedure, using a balloon catheter for occlusion, microcatheter for injection, and elastase mixed with contrast, shows promise. An angiogram of the area (top) and an example vessel that is sealed and filled with radiopaque elastase (bottom) during the elastase incubation is shown in **Figure 38**.

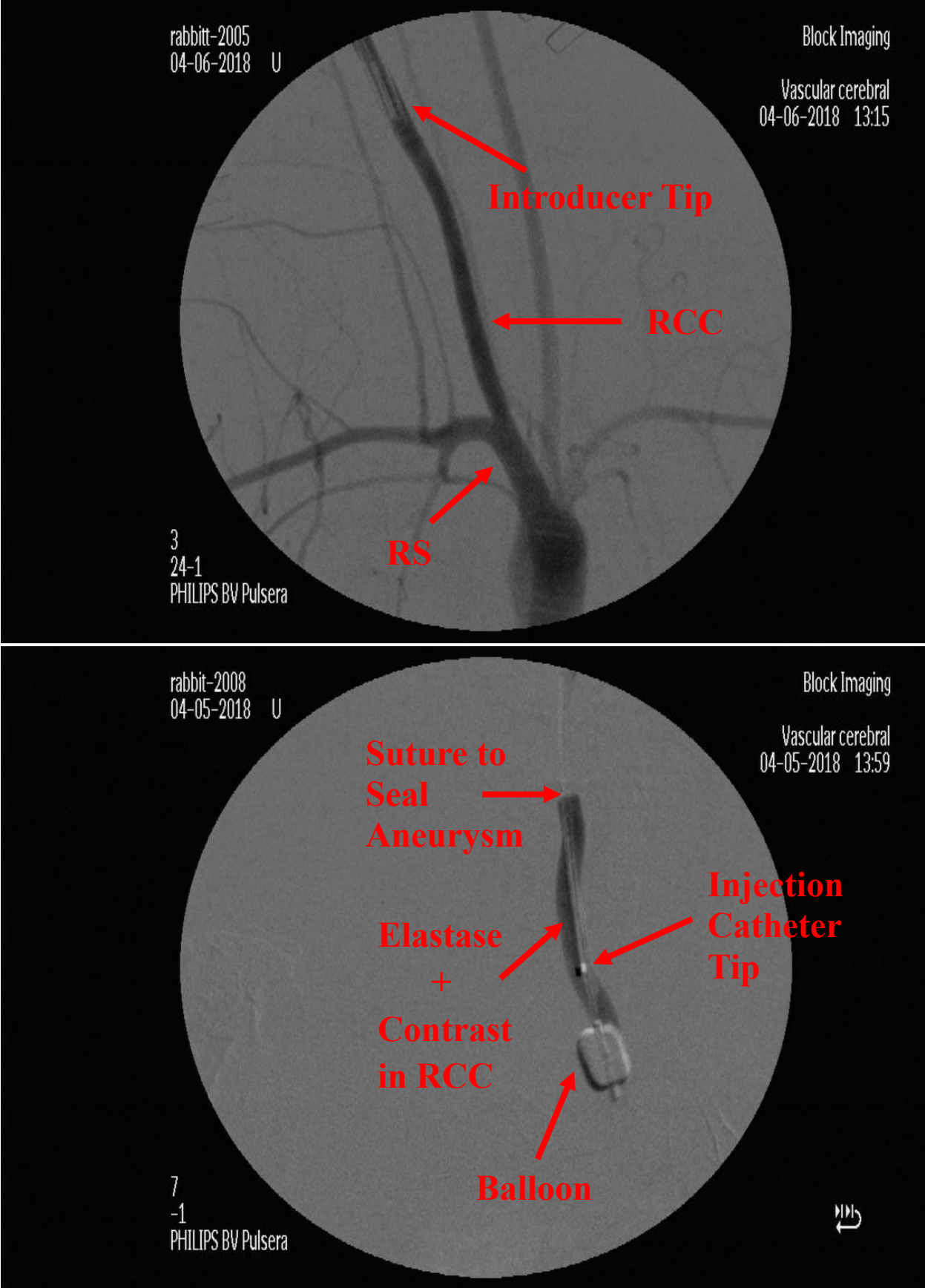


Figure 38 The full surgical vessel area (top) and the sealed RCC during the elastase incubation under fluoroscopy (bottom).

Embolization Procedure

Aneurysm sizes of ~0.1mL were filled. These aneurysms were not saccular, however, and they had neck sizes roughly equal to the vessel lumen. Complications occurred during injection because the radiopacity of PPODA-QT was tuned for visibility in larger aneurysms. Because the aneurysmal volume was so small, it was very difficult to view the PPODA-QT filling the aneurysm. A close-up view of a “tent-like” aneurysm with the largest width at the neck than aneurysm width is shown on the left in **Figure 39**. This aneurysm is very difficult to treat with PPODA-QT as its non-adhesive properties mean it may dislodge from the aneurysm over time (**Figure 41**). This would likely be a contraindication for the use of PPODA-QT and many other aneurysm treatment devices.

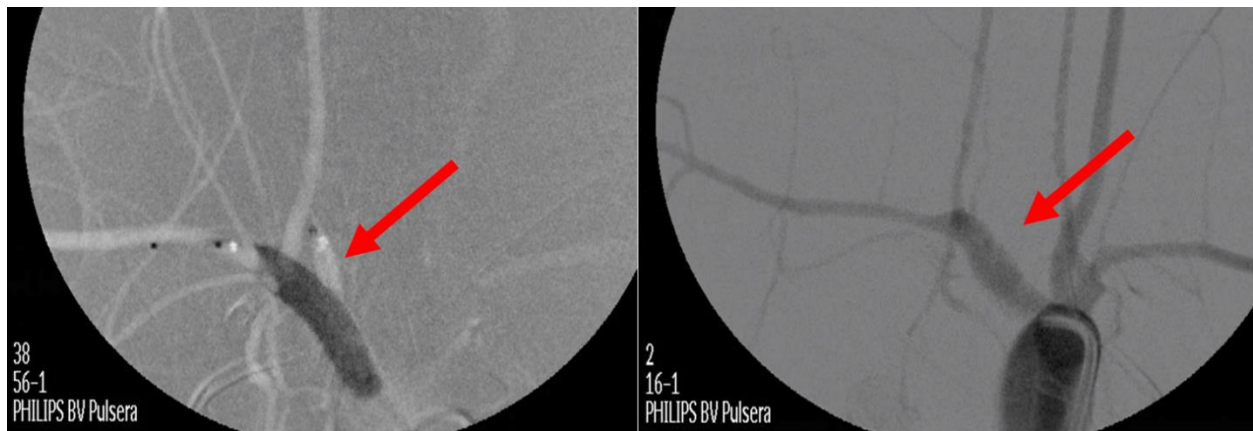


Figure 39 Aneurysm filling procedure. Left shows the aneurysm in white. A microcatheter sits inside it, and a balloon filled with contrast occludes the neck. Right shows the vessel after the procedure with the aneurysm fully occluded and therefore not visible.

Necropsy

Necropsies were performed and the aneurysm site was extracted for analysis. Visual analysis was initially performed, and then the sample was stored in formalin for later histological work, which is not discussed here.

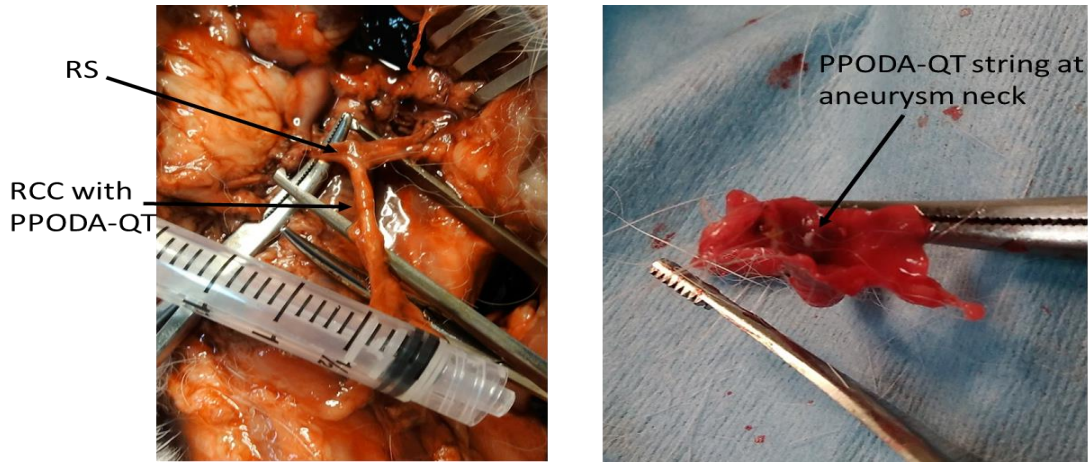


Figure 40 Rabbit 9073. The images show the vessel before excision (L) and PPODA-QT visible at the neck of the aneurysm (R)

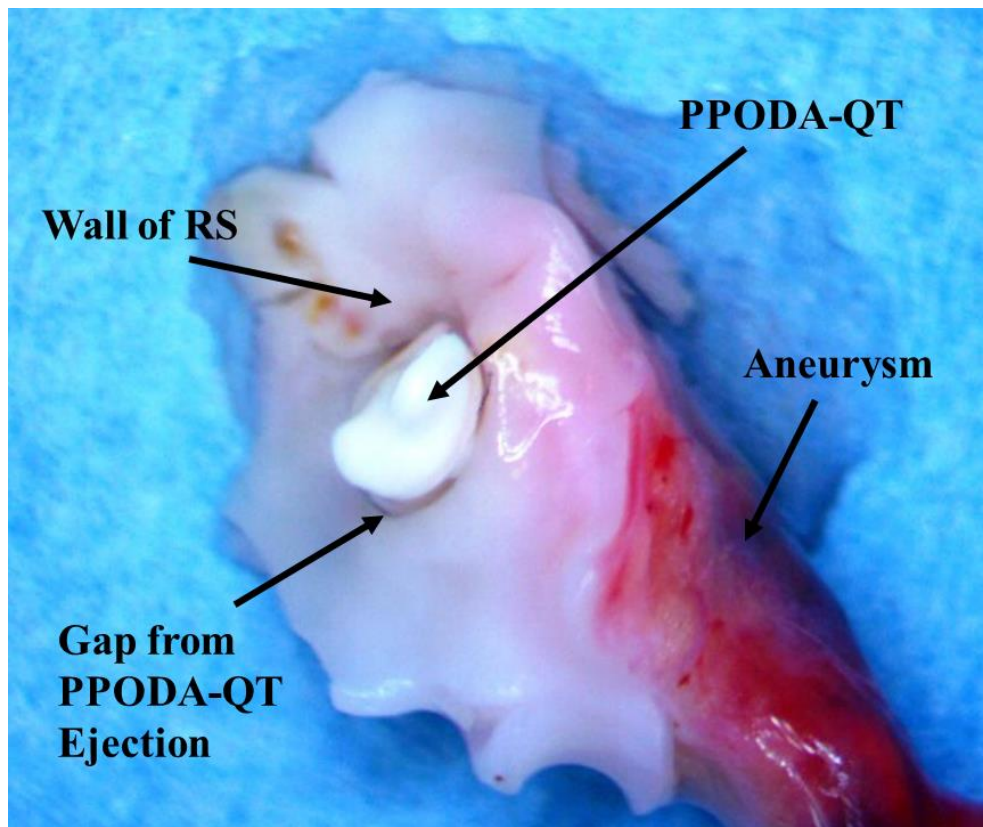


Figure 41 Image of PPODA-QT that has been ejected from the aneurysm and would disrupt the RS blood flow.

Table 6 Summary of the rabbit embolization surgeries

Rabbit Embolization Results				
Rabbit ID	Date of Surgery	Date of Embolization	Date Euthanized	Notes
9071	10/31/2017	12/4/2017	12/4/2017	Died of surgical complications post-embolization
9073	10/31/2017	12/7/2017	1/12/2018	PPODA-QT found occluding RS
9078	10/31/2017	12/5/2017	1/21/2018	Termed from degloving complications, potential downstream migration of PPODA-QT that could also be related to trauma during necropsy
519	12/19/2017	1/9/2018	NA	None
520	1/15/2018	2/7/2018	2/7/2018	Died of surgical complications post-embolization
524	12/19/2017	1/12/2018	NA	Died of surgical complications post-embolization
525	1/15/2018	2/6/2018	2/13/2018	Clot observed on surface of PPODA-QT. Will be confirmed via histology
527	12/19/2017	1/8/2018	1/8/2018	Died of surgical complications post-embolization

Discussion

Inconsistent aneurysm formation was a main cause of concern throughout the model development. Rather than saccular aneurysms, the ones created here had a cylindrical shape, which would likely be a contraindication for such treatments in human patients, as the potential for migration of a liquid embolic is present. Because PPODA-QT is non-adhesive (but self-adhering), a neck narrower than the total aneurysm width is necessary to prevent migration. Any other shape, such as those shown here, would be considered contraindications of PPODA-QT unless other procedural or device modifications are made.

The aneurysm creation surgery has undergone multiple iterations. After observing large clots in the aneurysm, Plavix and aspirin dosages before and after the procedures were adopted. Due to increased skill and shorter procedural times later on, isoflurine anesthesia was abandoned. After beginning with external surgical clips, balloons were adopted so that traditional neuroendovascular techniques could be continued. Performing this procedure under fluoroscopy meant that it was possible to visualize the seal on the RCC branch during elastase (mixed with contrast) incubation. Elastase was initially suspended in saline, but 9pH PBS proved to be more effective in dissolving it, so that modification has also been made, as well as the addition of contrast for fluoroscopic visualization. Finally, a 5F introducer was adopted as the preferred access method, which meant that the balloon and injection microcatheter could be inserted and removed while maintaining hemostasis. All of these modifications will be essential to further studies in the BDL.

While the *in vivo* model was successfully embolized in several cases, complications due to poor aneurysm formation prevented accurate assessment of PPODA-QT as an effective treatment. Because the aneurysms were very small, it was difficult to see PPODA-QT injected into the aneurysm. Larger aneurysms or more radiopaque PPODA-QT could remedy this problem. However, more radiopaque PPODA-QT would appear too dark in a larger aneurysm more relevant to the disease state, where distinguishing between fill volumes would be very difficult.

In addition, saccular aneurysms are less likely to eject PPODA-QT. Because the aneurysms in this study were essentially cylindrical and PPODA-QT is non-adhesive, PPODA-QT could easily slide out. In a saccular aneurysm with a larger max diameter than neck size, this would not occur, and embolic risks would be minimized. The PPODA-QT would be far better contained. Larger aneurysms, which would enable better PPODA-QT visualization, would also reduce the risk of

overfilling. A string of PPODA-QT reached into the RS of one animal, and a small hole, likely from the injection microcatheter, was observed. This protruding and rough PPODA-QT surface could have had negative effects on the blood flow. The ongoing models will be survived up to 3mo before they are euthanized for analysis.

Conclusion

Initial results of embolism with PPODA-QT are promising, but further work must be done to ensure the aneurysm model is accurate to truly test PPODA-QT under real world conditions. The primary step will be to identify root causes of the lack of aneurysm growth. Different elastase compounds, elastase mixtures, longer digestion times, and external application could all be investigated to determine how to create better and larger aneurysms. This will likely address many of the problems described above. This will also provide further opportunity to optimize the process with various catheters, procedural times, and other parts of the process.

The cylindrical aneurysms described here have the potential to be a new model. Wide-necked aneurysms are often contraindications for various treatments, so these could be used for developing devices that are effective in treating these disease states. For example, these aneurysms could be used to test the effectiveness of coils or liquid embolics in conjunction with stents or flow diverters. The flow diverters could prevent the ejection of the device inside of the aneurysm, effectively treating the aneurysm with multiple complementary devices. Further work will need to be performed to determine applicability of the model for this use.

CHAPTER 5

CONCLUSIONS

This project shows the process of building up research capabilities regarding liquid embolic use and particulate characterization. It covers the design of an *in vitro* flow model, multiple methods of counting and analyzing microscopic particles, and the development of an *in vivo* model to test liquid embolics and other aneurysm treatment devices. A variety of different techniques have been used that encompass the fields of physics, engineering, and biology. This has clarified the level of embolic risk from PPODA-QT from both an engineering and medical approach. A summary of the findings from each aim and its implication in answering the hypotheses are discussed below:

Aim 1 - Develop an *in vitro* model that mimics human physiological and anatomical conditions

An *in vitro* model was successfully created to practice and imitate endovascular surgery. It can successfully simulate physiologically-relevant vascular pressures, temperatures, and flow rates, and customizable inserts can be used to recreate various anatomies for different disease states.

This model was used primarily with models designed for straightforward access and anatomically-relevant aneurysms so that rapid testing of PPODA-QT and other neuroendovascular devices could be performed. It contains a filter system that can be used to capture downstream particles and assess devices for embolic risk.

Further studies will incorporate more sophisticated monitoring sensors and data acquisition hardware, which will make the physiological condition monitoring more accurate and user-

friendly. In addition, new anatomies and model types can be incorporated into the model to test in various disease states.

Aim 2 - Use the aforementioned in vitro model and different microscopy techniques to characterize the shape and number of liquid embolic particles released during aneurysm embolization

Microscopic techniques were developed to assess downstream particulation during endovascular procedures. SEM was initially used to understand basic distinguishing characteristics of various PPODA-QT particles so that differences between independently-formed and broken particles could be distinguished. Then a method of DIC microscopy, MATLAB, and ImageJ analysis was developed to count total particle sizes and numbers to confirm USP <788> conformation for various materials. Finally, an inline digital holography setup was created to be used for future non-invasive particle analysis.

Future Work

Further work will be done by the BDL to improve these test methods. Initial studies show that the filters primarily capture contamination, so further preparation, such a cleanroom setup, must be developed to remove contamination from the system. In addition, using off the shelf microcatheters and neurovascular balloon catheters rather than ones made in the lab could reduce issues such as the PPODA-QT sticking that was observed in initial tests.

Aim 3 - Develop an in vivo rabbit aneurysm model that can eventually be used to evaluate liquid embolic efficacy and safety

A rabbit aneurysm model was developed in order to test various treatment methods. While some initial embolizations were attempted, the purpose of this study was primarily to develop the aneurysm itself. Various aneurysm sealing procedures, elastase mixtures, and access routes were used, and an endovascular approach with balloon occlusion and elastase in 9pH PBS was the final iteration. Further studies with this new approach will be used to evaluate PPODA-QT's embolic efficacy.

Future Work

More studies will need to be performed in order to test PPODA-QT as a viable aneurysm treatment device. These tests can begin once saccular aneurysms are created. In addition, elastase concentration and solvents could be varied to test their effects on aneurysm shape and size. Finally, the model still has the potential to be used in other disease states, such as wide-necked aneurysm treatment.

Hypothesis 1 - An in vitro system that mimics human physiological and anatomical conditions can be built to test liquid embolic conformation to the USP <788>

Initial results show that the model can simulate physiological conditions, and a method has been developed to analyze downstream particulation during procedures. However, the hypothesis must be rejected for now because further studies must be performed in order to finalize the counting method in either DIC microscopy or inline digital holography. After this is done, USP <788> testing can commence for PPODA-QT and other devices.

Hypothesis 2 - An in vivo aneurysm model can be developed to evaluate liquid embolic without observed negative embolic effects

This hypothesis must also be rejected because liquid embolic treatment of physiologically-accurate aneurysms has not yet been performed. The model has been developed and ongoing studies hope to successfully create an accurate aneurysm that can simulate a naturally-occurring saccular aneurysm. Then it can be used to assess PPODA-QT and other treatment options.

However, the model as it stands today could potentially be used for harder to treat wide-necked aneurysms, providing a new model for device testing.

Limitations and Further Research

While this large study covers many aspects of liquid embolic particulation analysis, there are significant limitations and areas for improvement. As outlined above, contamination issues must be remedied to fully adhere to the USP <788> standard. This could be accomplished via a cleanroom setup or performing the full USP <788> characterization with non-invasive inline digital holography. Performing the study non-invasively has the potential to minimize contamination in handling, and it can also be performed live for shorter analysis. Once the *in vivo* model is finalized, the safety confirmed in the *in vitro* model can be verified in a living model. This two-sided approach will present a full understanding of the absolute and practical results of liquid embolic particulation, enabling the lab to create safer, better medical devices.

Final Flow Loop Design and Particle Counting Approach

Over the course of this thesis work, an ideal flow loop system has been conceptualized. To simplify the physiological condition maintenance, more advanced data acquisition systems could be used. A National Instruments Input Module (NI 9201) and Thermocouple Module (NI 9213)

could be housed in a chassis (cDAQ-9174), and the combination of these would eliminate the power supply and signal amplification box. This would also enable the VI to be run at higher sampling frequencies. The same pressure transducers and thermocouples could be used, but a new analog flow meter would address the sampling issues found with the current digital one.

More physiologically-relevant model materials could improve stiffness and endovascular surface properties. Studies to explore new or existing materials that will more closely mimic vascular compliance would be valuable to identify better candidates than the polyurethane resin used here. Further cleaning and smoothing of the model core could also be used to smooth the endovascular surface of the model.

A more advanced programmable pump, such as the Biomedical Device Consultants (BDC) PD-1100, could be used to mimic physiological waveforms more accurately than the current pump.⁶⁴ Housing the entire system in a particulate hood or cleanroom could alleviate contamination issues.

Finally, a non-invasive live counting device would be ideal for USP <788> testing. A light extinction or scattering method such as the Eaton CCM 01 Contamination Control Monitor Set could be incorporated into the system.⁶⁵ This would enable live counting of particles non-invasively, improving accuracy, timeliness, and reliability.

A combination of these improvements has the potential to drastically improve the *in vitro* model and particle counting system. By incorporating these changes, the BDL could drastically improve the speed and accuracy of its testing. This would enable the BDL to develop safer devices even faster, streamlining the way towards helping improve lives around the world.

REFERENCES

1. CDC. Stroke Facts | cdc.gov. CDC. <https://www.cdc.gov/stroke/facts.htm>. Published 2018. Accessed January 23, 2018.
2. Brain Aneurysm - Causes, Symptoms, Warning Signs, Treatment. Health Jade. <https://healthjade.com/brain-aneurysm/>. Accessed February 18, 2018.
3. Brain Aneurysm Foundation. Brain Aneurysm Statistics and Facts – Brain Aneurysm Foundation. Brain Aneurysm Foundation. <http://www.bafound.org/about-brain-aneurysms/brain-aneurysm-basics/brain-aneurysm-statistics-and-facts/>. Published 2017. Accessed May 8, 2017.
4. University of Nebraska - Lincoln. Pressure Vessels. [http://emweb.unl.edu/NEGAHBAN/Em325/18-Pressure-vessels/Pressure vessels.htm](http://emweb.unl.edu/NEGAHBAN/Em325/18-Pressure-vessels/Pressure%20vessels.htm). Accessed February 7, 2018.
5. Johns Hopkins Medicine. Endovascular Coiling | Johns Hopkins Medicine Health Library. https://www.hopkinsmedicine.org/healthlibrary/test_procedures/neurological/endovascular_coiling_92,P08768. Accessed February 14, 2018.
6. Brennecka C, Preul M, Becker T, Vernon B. In vivo embolization of lateral wall aneurysms in canines using the liquid-to-solid gelling PPODA-QT polymer system: 6-month pilot study. *J Neurosurg*. 2013;119(1):228-238. doi:10.3171/2013.3.JNS121865.
7. Cognard C, Weill A, Spelle L, et al. Long-term Angiographic Follow-up of 169 Intracranial Berry Aneurysms Occluded with Detachable Coils. *Radiology*. 1999;212(2):348-356. doi:10.1148/radiology.212.2.r99j147348.
8. Cognard C, Weill A, Castaings L, Rey A, Moret J. Intracranial berry aneurysms: angiographic and clinical results after endovascular treatment. *Radiology*. 1998;206(2):499-510. doi:10.1148/radiology.206.2.9457205.
9. Hayakawa M, Murayama Y, Duckwiler GR, Gobin YP, Guglielmi G, Viñuela F. Natural history of the neck remnant of a cerebral aneurysm treated with the Guglielmi detachable coil system. *J Neurosurg*. 2000;93(4):561-568. doi:10.3171/jns.2000.93.4.0561.
10. Henkes H, Fischer S, Weber W, et al. Endovascular Coil Occlusion of 1811 Intracranial Aneurysms: Early Angiographic and Clinical Results. *Neurosurgery*. 2004;54(2):268-285. doi:10.1227/01.NEU.0000103221.16671.F0.
11. Kurre W, Berkefeld J. Materials and techniques for coiling of cerebral aneurysms: How much scientific evidence do we have? *Neuroradiology*. 2008;50(11):909-927. doi:10.1007/s00234-008-0446-y.
12. Ries T, Groden C. Endovascular Treatment of Intracranial Aneurysms: Long-Term Stability, Risk Factors for Recurrences, Retreatment and Follow-Up*. *Clin Neuroradiol*. 2009;19(1):62-72. doi:10.1007/s00062-009-8032-1.
13. Ayton Hope JK, Byrne J V., Molyneux AJ. Factors influencing successful angiographic occlusion of aneurysms treated by coil embolization. *Am J Neuroradiol*. 1999;20(3):391-399.

14. Murayama Y, Nien YL, Duckwiler G, et al. Guglielmi Detachable Coil embolization of cerebral aneurysms: 11 years' experience. *J Neurosurg.* 2003;98(5):959-966. doi:10.3171/jns.2003.98.5.0959.
15. Sluzewski M, Menovsky T, Van Rooij WJ, Wijnalda D. Coiling of very large or giant cerebral aneurysms: Long-term clinical and serial angiographic results. *Am J Neuroradiol.* 2003;24(2):257-262.
16. Van Rooij WJ, Sluzewski M. Coiling of very large and giant basilar tip aneurysms: Midterm clinical and angiographic results. *Am J Neuroradiol.* 2007;28(7):1405-1408. doi:10.3174/ajnr.A0556.
17. Youn SO, Lee J II, Ko JK, Lee TH, Choi CH. Endovascular treatment of wide-necked intracranial aneurysms using balloon-assisted technique with hyperform balloon. *J Korean Neurosurg Soc.* 2010;48(3):207-212. doi:10.3340/jkns.2010.48.3.207.
18. Becker TA, Preul MC, Bichard WD, Kipke DR, McDougall CG. Preliminary investigation of calcium alginate gel as a biocompatible material for endovascular aneurysm embolization in vivo. *Neurosurgery.* 2007;60(6):1119-1127. doi:10.1227/01.NEU.0000255447.90106.12.
19. Ducruet A, McDougall CG. Neurosurgeon Interviews.
20. Simon SD, Reig a. S, James RF, Reddy P, Mericle R a. Relative cost comparison of embolic materials used for treatment of wide-necked intracranial aneurysms. *J Neurointerv Surg.* 2010;2(2):163-167. doi:10.1136/jnis.2009.001719.
21. Murayama Y, Viñuela F, Ulhoa A, et al. Nonadhesive liquid embolic agent for cerebral arteriovenous malformations: Preliminary histopathological studies in swine rete mirabile. *Neurosurgery.* 1998;43(5):1164-1172. doi:10.1097/00006123-199811000-00081.
22. Deveikis JP. Endovascular therapy of intracranial arteriovenous malformations - Materials and techniques. *Neuroimaging Clin N Am.* 1998;8(2):401+.
23. Johnston SC, Wilson CB, Halbach V V., et al. Endovascular and surgical treatment of unruptured cerebral aneurysms: Comparison of risks. *Ann Neurol.* 2000;48(1):11-19. doi:10.1002/1531-8249(200007)48:1<11::AID-ANA4>3.0.CO;2-V.
24. Matsumaru Y, Hyodo A, Nose T, Hirano T, Ohashi S. Embolic materials for endovascular treatment of cerebral lesions. *J Biomater Sci Ed.* 1997;8(7):555-569.
25. Molyneux AJ, Cekirge S, Saatci I, Gál G. Cerebral Aneurysm Multicenter European Onyx (CAMEO) Trial: Results of a Prospective Observational Study in 20 European Centers. *Am J Neuroradiol.* 2004;25(1):39-51.
26. Piske RL, Kanashiro LH, Paschoal E, Agner C, Lima SS, Aguiar PH. Evaluation of onyx hd-500 embolic system in the treatment of 84 wide-neck intracranial aneurysms. In: *Neurosurgery.* Vol 64. ; 2009. doi:10.1227/01.NEU.0000340977.68347.51.
27. Chaloupka JC, Huddle DC, Alderman J, Fink S, Hammond R, Vinters H V. A reexamination of the angiotoxicity of superselective injection of DMSO in the swine rete embolization model. *Am J Neuroradiol.* 1999;20(3):401-410.
28. Jahan R, Murayama Y, Pierre Gobin Y, Duckwiler GR, Vinters H V., Viñuela F. Embolization of arteriovenous malformations with Onyx: Clinicopathological experience in

- 23 patients. *Neurosurgery*. 2001;48(5):984-997. doi:10.1097/00006123-200212000-00027.
29. Raftopoulos C, Mathurin P, Boscherini D, Billa RF, Boven M Van, Hantson P. Prospective analysis of aneurysm treatment in a series of 103 consecutive patients when endovascular embolization is considered the first option. *J Neurosurg*. 2000;93(2):175-182. doi:10.3171/jns.2000.93.2.0175.
 30. Struffert T, Roth C, Romeike B, Grunwald IO, Reith W. Onyx in an experimental aneurysm model: histological and angiographic results. *J Neurosurg*. 2008;109(1):77-82. doi:10.3171/JNS/2008/109/7/0077.
 31. Jiang B, Paff M, Colby GP, Coon AL, Lin L-M. Cerebral aneurysm treatment: modern neurovascular techniques. *BMJ*. 2016;1(3):93-100. doi:10.1136/svn-2016-000027.
 32. Choi BJ, Lee TH, Kim CW, Choi CH. Endovascular graft-stent placement for treatment of traumatic carotid cavernous fistulas. *J Korean Neurosurg Soc*. 2009;46(6):572-576. doi:10.3340/jkns.2009.46.6.572.
 33. Burrows AM, Cloft H, Kallmes DF, Lanzino G. Periprocedural and mid-term technical and clinical events after flow diversion for intracranial aneurysms. *J Neurointerv Surg*. 2014;1-6. doi:10.1136/neurintsurg-2014-011184.
 34. Fiorella D, Arthur A, Byrne J, et al. Interobserver variability in the assessment of aneurysm occlusion with the WEB aneurysm embolization system. *J Neurointerv Surg*. 2015;7(8):591-595. doi:10.1136/neurintsurg-2014-011251.
 35. Mine B, Pierot L, Lubicz B. Intrasaccular flow-diversion for treatment of intracranial aneurysms: the Woven EndoBridge. *Expert Rev Med Devices*. 2014;11(3):315-325. doi:10.1586/17434440.2014.907741.
 36. Tateshima S, Jones JG, Mayor Basto F, Vinuela F, Duckwiler GR. Aneurysm pressure measurement before and after placement of a Pipeline stent: feasibility study using a 0.014 inch pressure wire for coronary intervention. *J Neurointerv Surg*. 2016;8(6):603-607. doi:10.1136/neurintsurg-2014-011214.
 37. Ding YH, Dai D, Schroeder D, Kadirvel R, Kallmes DF. Experimental testing of the dual-layer Woven EndoBridge device using an elastase-induced aneurysm model in rabbits. In: *Interventional Neuroradiology*. Vol 22. ; 2016:299-303. doi:10.1177/1591019916628202.
 38. Brennecka CR, Preul MC, Vernon BL. In vitro delivery, cytotoxicity, swelling, and degradation behavior of a liquid-to-solid gelling polymer system for cerebral aneurysm embolization. *J Biomed Mater Res - Part B Appl Biomater*. 2012;100 B(5):1298-1309. doi:10.1002/jbm.b.32696.
 39. Brennecka CR, Preul MC, Bichard WD, Vernon BL. In vivo experimental aneurysm embolization in a swine model with a liquid-to-solid gelling polymer system: Initial biocompatibility and delivery strategy analysis. *World Neurosurg*. 2012;78(5):469-480. doi:10.1016/j.wneu.2011.10.029.
 40. McLemore R, Lee BH, Vernon B. Surfactant effects on the kinetics of Michael-type addition reaction in reverse emulsion polymeric systems. *J Biomed Mater Res - Part B Appl Biomater*. 2009;89(1):191-198. doi:10.1002/jbm.b.31205.
 41. Brennecka CR, Preul MC, Becker TA, Vernon BL. In vivo embolization of lateral wall

- aneurysms in canines using the liquid-to-solid gelling PPODA-QT polymer system: 6-month pilot study. *J Neurosurg.* 2013;119(1):228-238. doi:10.3171/2013.3.JNS121865.
42. USP <788> PARTICULATE MATTER IN INJECTIONS. *United States Pharmacopia.* 2012. http://www.usp.org/sites/default/files/usp_pdf/EN/USPNF/revisions/788_particulate_matter_in_injections.pdf. Accessed May 8, 2017.
 43. Bogren HG, Buonocore MH, Gu WZ. Carotid and vertebral artery blood flow in left- and right-handed healthy subjects measured with MR velocity mapping. *J Magn Reson Imaging.* 4(1):37-42. <http://www.ncbi.nlm.nih.gov/pubmed/8148554>. Accessed May 8, 2017.
 44. Napolitano A, Hawkins EG. The Physics Hypertextbook. physics.info. doi:10.6028/jres.068A.042.
 45. Brain Aneurysm Foundation. <https://www.bafound.org/>. Accessed December 29, 2017.
 46. Medtronic. Neurovascular Product Catalog. 2017:14. <https://www.medtronic.com/content/dam/medtronic-com/products/neurological/neurovascular-product-catalog.pdf>. Accessed January 3, 2018.
 47. Utah Medical Products Inc. Blood Pressure Transducer - Deltran Blood Pressure Monitoring. <http://www.utahmed.com/deltran.htm>. Accessed March 2, 2018.
 48. thermocoupleinfo.com. Type K Thermocouple - Type K Thermocouples - K Type Thermocouples - K Type Thermocouple. <https://www.thermocoupleinfo.com/type-k-thermocouple.htm>. Accessed April 15, 2018.
 49. Omega. Low Flow Plastic Turbine - FTB-421. <https://www.omega.com/pptst/FTB-420.html>. Accessed March 2, 2018.
 50. Locke Well & Pump Company. Stenner 170DM5. https://www.lockewell.com/index.php?main_page=product_info&products_id=168. Accessed March 4, 2018.
 51. Sterlitech. Sterlitech PP 25. <https://www.sterlitech.com/polypropylene-in-line-holder-540100.html>. Accessed March 4, 2018.
 52. EMD Millipore Sigma. Isopore™ Membrane Filters - Filter Discs and Membranes. http://www.emdmillipore.com/US/en/product/Isopore-Membrane-Filters,MM_NF-C153#specifications. Accessed March 4, 2018.
 53. Aribisala BS, Morris Z, Eadie E, et al. Blood pressure, internal carotid artery flow parameters, and age-related white matter hyperintensities. *Hypertension.* 2014;63(5):1011-1018. doi:10.1161/HYPERTENSIONAHA.113.02735.
 54. Smooth-On. Clear Flex™ 50 Product Information | Smooth-On, Inc. <https://www.smooth-on.com/products/clear-flex-50/>. Accessed March 8, 2018.
 55. Mann CJ, Yu L, Lo C-M, Kim MK. High-resolution quantitative phase-contrast microscopy by digital holography. *Opt Express.* 2005;13(22):8693. doi:10.1364/OPEX.13.008693.
 56. LabX. 2002 Philips BV Pulsera CArm XRay Fluoroscope Medical | For Sale | LabX Ad LV38158521. <https://www.labx.com/item/2002-philips-bv-pulsera-c-arm-x-ray-fluoroscope-medical/LV38158521>. Accessed March 9, 2018.

57. Paxton S, Peckham M, Adele K, Paxton S, Adele K, Peckham M. The Leeds Histology Guide. 2003. <http://www.histology.leeds.ac.uk/circulatory/capillaries.php>. Accessed March 15, 2018.
58. MediaLab. Red Blood Cell (RBC) Size Variation. https://www.labce.com/spg579126_red_blood_cell_rbc_size_variation.aspx. Accessed March 15, 2018.
59. Northwestern University. Z Stack. Northwestern University Center for Advanced Research. <http://cam.facilities.northwestern.edu/files/2014/07/Picture-17.png>. Accessed April 18, 2018.
60. Altes TA, Cloft HJ, Short JG, et al. Creation of saccular aneurysms in the rabbit: A model suitable for testing endovascular devices. *Am J Roentgenol*. 2000;174(2):349-354. doi:10.2214/ajr.174.2.1740349.
61. Hoh BL, Rabinov JD, Pryor JC, Ogilvy CS. A modified technique for using elastase to create saccular aneurysms in animals that histologically and hemodynamically resemble aneurysms in human. *Acta Neurochir (Wien)*. 2004;146(7):705-711. doi:10.1007/s00701-004-0276-6.
62. Grunwald IQ, Romeike B, Eymann R, Roth C, Struffert T, Reith W. An experimental aneurysm model: a training model for neurointerventionalists. *Interv Neuroradiol*. 2006;12(1):17-24. http://www.pubmedcentral.nih.gov/articlerender.fcgi?artid=3355307&tool=pmcentrez&render_type=abstract.
63. Brinjikji W, Ding YH, Kallmes DF, Kadirvel R. From bench to bedside: Utility of the rabbit elastase aneurysm model in preclinical studies of intracranial aneurysm treatment. *J Neurointerv Surg*. 2016;8(5):521-525. doi:10.1136/neurintsurg-2015-011704.
64. BDC Laboratories. Pulsatile Pump Systems. <http://www.bdclabs.com/testing-equipment/pulsatile-pump-systems/>. Accessed May 2, 2018.
65. Eaton. CCM 01-Set. <http://www.eaton.com/Eaton/ProductsServices/Filtration/HydraulicandLubricationOilFilters/ContaminationMonitoring/InlineMeasuringSystems/CCM01-Set/index.htm>. Accessed May 2, 2018.

APPENDICES

APPENDIX A

IN VITRO MODEL DIAGRAMS

This appendix lays out the sensor specifications, electrical amplification circuits, and software diagrams. First are the specification sheets:

Pressure Transducers⁴⁷

Deltran® Disposable Pressure Transducer	
Continuous Flow Rate (for models with integral flush device)	3cc/hr (+2/-1cc/hr) or 30cc/hr (\pm 10cc/hr) at 300 mmHg
Operating Pressure Range	-50 to +300 mmHg
Sensitivity	5 μ V/V/mmHg, \pm 2% (typically \leq \pm 1%)
Zero Drift With Time	\leq \pm 1.0 mmHg/8 hours after 10 min. warm-up to operating temperature
Leakage Current	<2 μ A @ 115 Vac rms at 60 Hz
Unbalance	\pm 75 mmHg
Overpressure Protection	-400 to +4000 mmHg
Operating Temperature	15° C to 40° C
Excitation Voltage and Frequency	2 to 10 Vdc; or Vac rms to 5 kHz
Operating Life	>500 hours
Storage Temperature	-25° C to +65° C
Defibrillation Withstand	5 discharges/5 minutes of 400 joules @ 50 ohm load
Natural Frequency	>200 Hz in saline
Phase Shift	<5° at 5 kHz
Output Impedance	270 Ohms to 400 Ohms
Input Impedance	270 Ohms to 400 Ohms

Thermocouple (Reference Table for General K-Type Thermocouples)⁴⁸

Type K Thermocouple

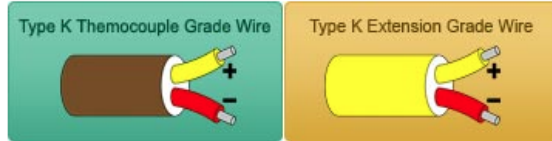
Type K Thermocouple (Nickel-Chromium / Nickel-Alumel): The type K is the most common type of thermocouple. It's inexpensive, accurate, reliable, and has a wide temperature range. The type K is commonly found in nuclear applications because of its relative radiation hardness. Maximum continuous temperature is around 1,100C.

Type K Temperature Range:

- Thermocouple grade wire, -454 to 2,300F (-270 to 1260C)
- Extension wire, 32 to 392F (0 to 200C)

Type K Accuracy (whichever is greater):

- Standard: +/- 2.2C or +/- .75%
- Special Limits of Error: +/- 1.1C or 0.4%




Type of K Thermocouple

- Consideration for bare wire type K thermocouple applications:

Type K Thermocouple Reference Table:

K



ITS-90 Table for Type K Thermocouple (Ref Junction 0°C)

<http://reotemp.com>

K

°C	0	1	2	3	4	5	6	7	8	9	10
Thermoelectric Voltage in mV											
0	0.000	0.039	0.079	0.119	0.158	0.198	0.238	0.277	0.317	0.357	0.397
10	0.397	0.437	0.477	0.517	0.557	0.597	0.637	0.677	0.718	0.758	0.798
20	0.798	0.838	0.879	0.919	0.960	1.000	1.041	1.081	1.122	1.163	1.203
30	1.203	1.244	1.285	1.326	1.366	1.407	1.448	1.489	1.530	1.571	1.612
40	1.612	1.653	1.694	1.735	1.776	1.817	1.858	1.899	1.941	1.982	2.023

LOW FLOW PLASTIC TURBINE



FTB-420 Series



- ✓ Low Flow Rates 0.1 to 2.5 LPM
- ✓ High Accuracy $\pm 3\%$ of Reading
- ✓ Lightweight Turbine Ensures Fast Startup
- ✓ Mounts in Any Orientation

OMEGA's FTB-420 Series features proven turbine technology in a small package for low flow applications. The turbine technology provides a highly repeatable sensor ideally suited for measurement of either volume dispensing and/or flow rate applications. The small turbine reacts quickly to on/off dispensing applications. Each sensor is 100% tested, ensuring long service life.



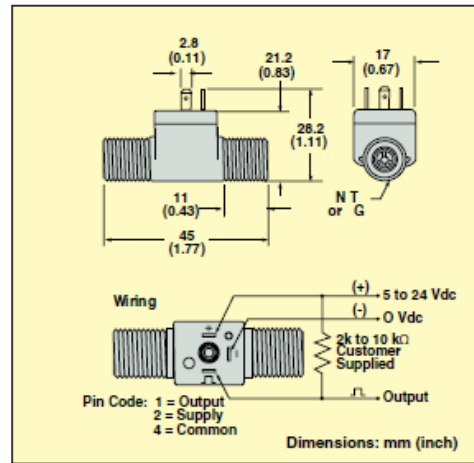
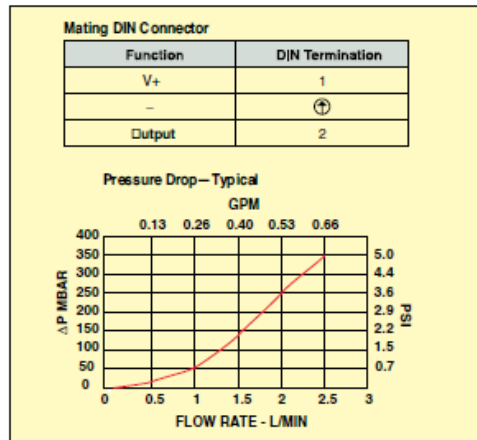
FTB-421 shown actual size.

SPECIFICATIONS

Wetted Materials:

- Body: Nylon 12 (FTB-421)
- Turbine: Nylon 12 (FTB-421)
- Bearings: PTFE/15% graphite
- Operating Pressure: 24 bar (350 psi)
- Burst Pressure: 97 bar (1400 psi)
- Flow Range: 0.026 to 0.65 GPM (0.1 to 2.5 LPM)
- Pulses: 83,200 per gallon (22,000 per liter)
- Frequency Output: 36.6 to 917 Hz
- Operating Temperature: -20 to 100°C (-4 to 212°F)
- Viscosity: 32 to 70 SSU (0.8 to 16 centistokes)
- Filter: <50 Microns
- Input Power: 5 to 24 Vdc
- Output (Hz): NPN sinking open collector @ 20 mA maximum leakage

- Current: 10 μ A (3 to 30K pull up resistor required)
- Accuracy: $\pm 3\%$ of reading
- Repeatability: 0.5% of full scale
- Electrical Connection: 9.4 mm spacing 3-pole DIN connector (1" high)
- Inlet/Outlet Ports: 1/4 NPT or 1/4 G male



To Order	
Model No.	Description
FTB-421	Low flow nylon turbine 1/4 NPT
FTB-421G	Low flow nylon turbine 1/4 G thread

Comes complete with DIN connector and operator's manual.
Ordering Example: FTB-421, low flow nylon turbine 1/4 NPT.

Next are the signal amplification circuits that are housed in the Signal Amplification Box:

Pressure Transducers, Thermocouples, and Flow Meters (respectively):

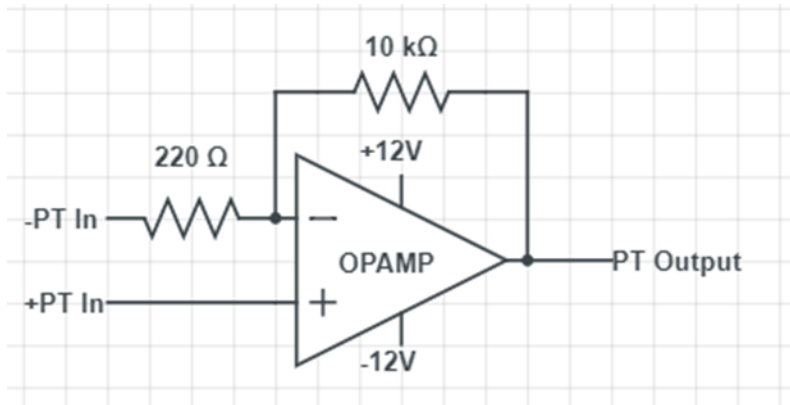


Figure A- 1 22x gain inverting circuit for the pressure transducer

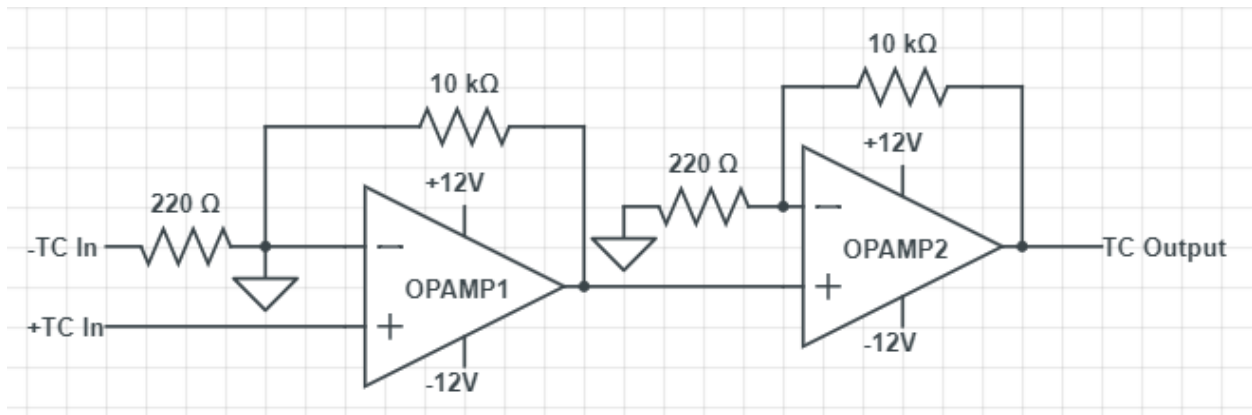


Figure A- 2 484x gain inverting circuit for the thermocouple

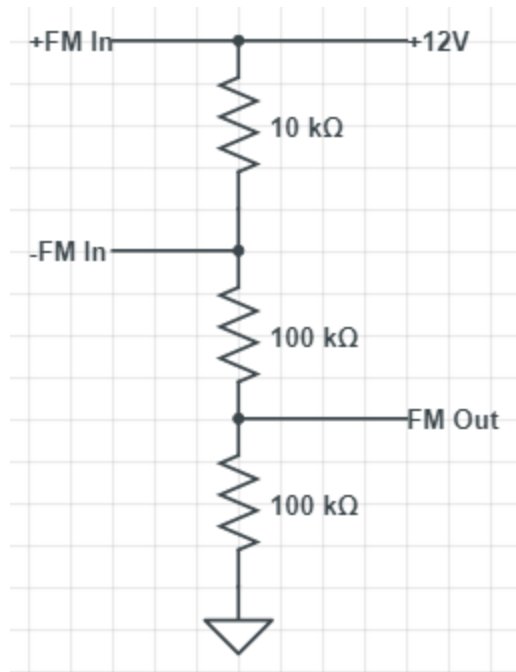


Figure A- 3 Voltage splitting circuit for the flow meter

Here is the Signal Amplification Box bill of materials as well as images of the setup:

Table A- 1 Components used in the Signal Amplification Box

Signal Amplification Box Component List				
Sub-Assembly	Component Name	Source	P/N	Quantity per Circuit
Pressure Transducer Amplification (4 Circuits)	220Ω, 1/4W Resistor	Digi-Key	CF14JT220RCT-ND	1
	10kΩ, 1/4W Resistor	Digi-Key	CF14JT10kOCT-ND	1
	LM741CN Op-amp	Digi-Key	LM741CNNS/NOPD-ND	1
	8-Pin Holder	Digi-Key	AE9986-ND	1
Thermocouple Amplification (2 Circuits)	220Ω, 1/4W Resistor	Digi-Key	CF14JT220RCT-ND	2
	10kΩ, 1/4W Resistor	Digi-Key	CF14JT10kOCT-ND	2
	LM741CN Op-amp	Digi-Key	LM741CNNS/NOPD-ND	2
	8-Pin Holder	Digi-Key	AE9986-ND	2
Flow Meter Amplification (2 Circuits)	100kΩ, 1/4W Resistor	EE Shop	Unsure	2
	10kΩ, 1/4W Resistor	Digi-Key	CF14JT10kOCT-ND	1
Signal Amplification Box	4 Position Wire Terminal Block	Digi-Key	ED2877-ND	8
	Female Banana Plug	Digi-Key	J150-ND (White), J151-ND (Red), J152-ND (Black), J153-ND (Green)	1 of each
	4-40, 1-1/2" Machine Screw	McMaster-Carr	91781A119	4
	4-40 Nut	McMaster-Carr	91841A005	4
	Solderable Breadboard	Ebay	SB404	2
	Box Bottom	MakerLab	NA	1
	Box Top	MakerLab	NA	1

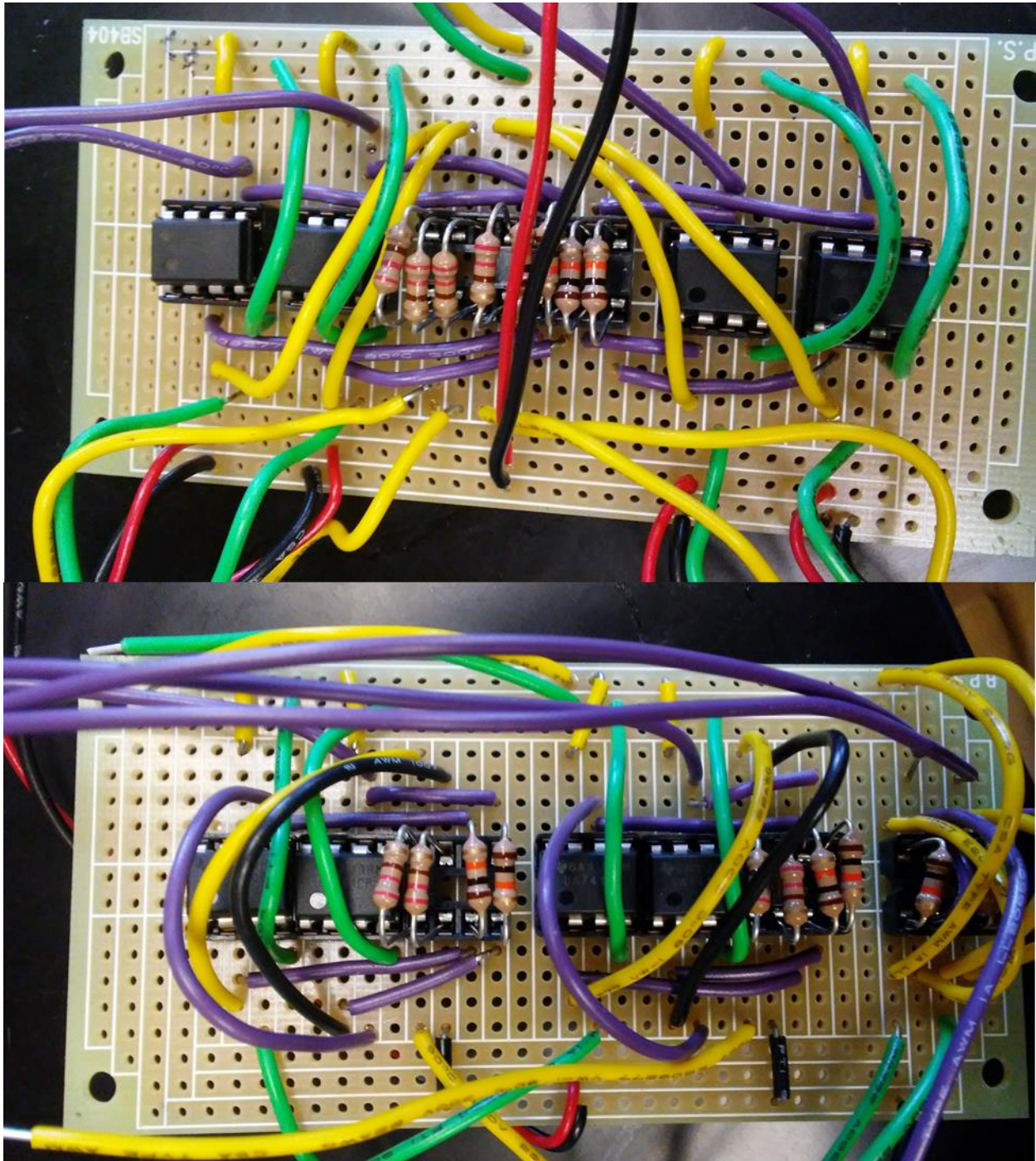


Figure A- 4 Breadboards used inside the Signal Amplification Box. The top image shows the 4 pressure transducer circuits (Figure A- 1), and the bottom shows the 2 thermocouple amplification circuits in the left and middle (Figure A- 2), as well as the flow meter circuit on the right (Figure A- 3)

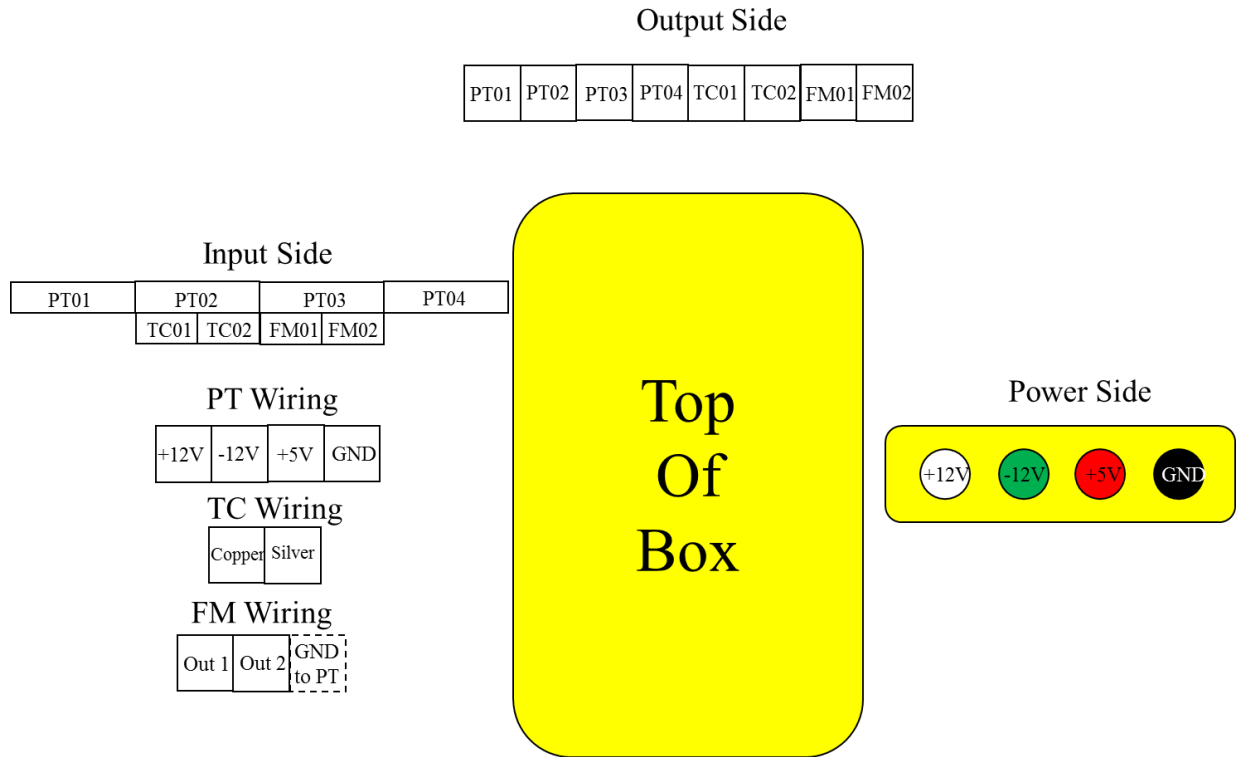


Figure A- 5 Wiring diagram for the signal amplification box. The Power Side uses female banana plug inputs, and the other sides use wire screw block terminals

Here are screenshots of the LabVIEW program Block Diagram that controls the in vitro flow model parameters:

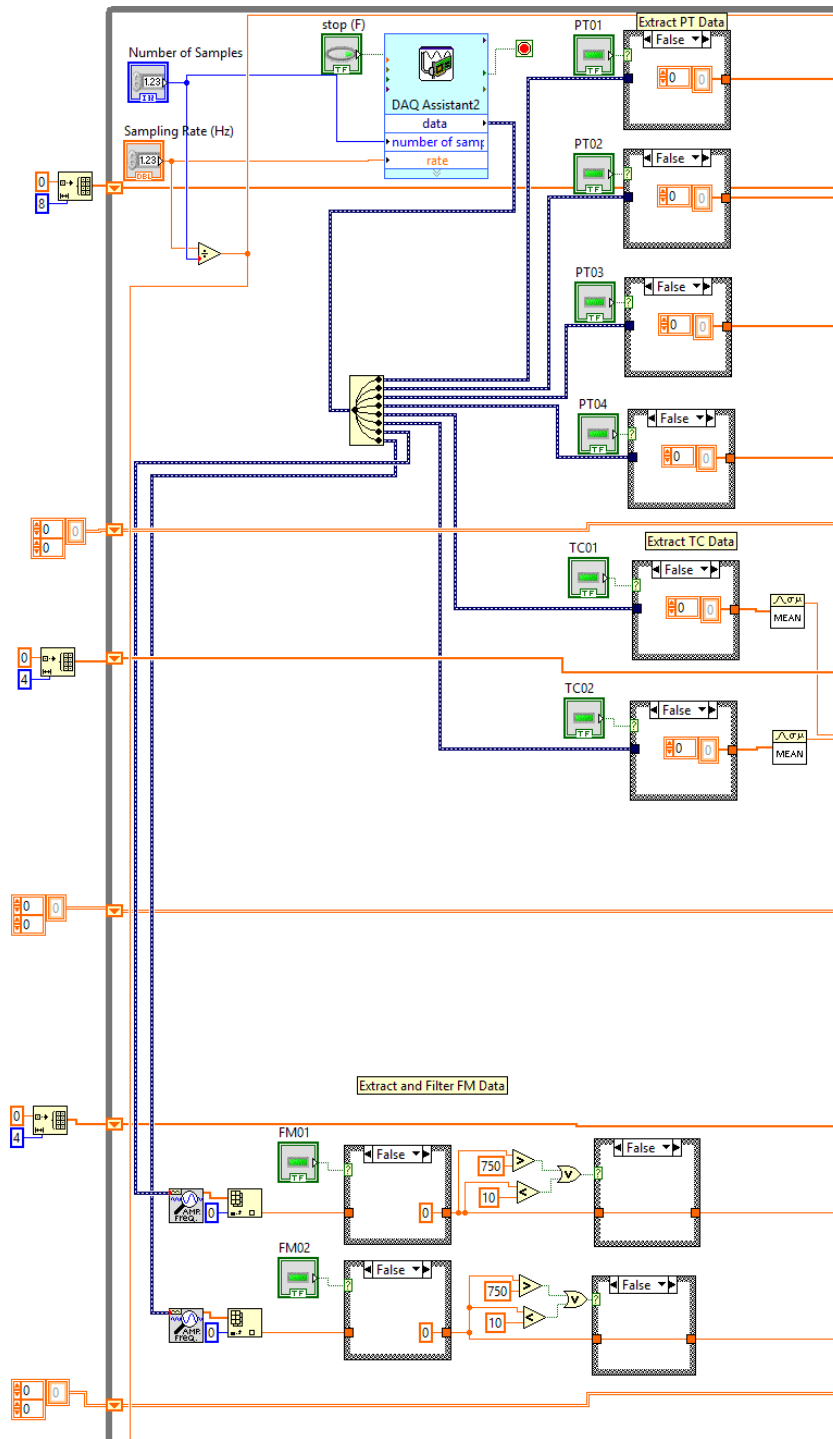


Figure A- 6 Part 1 of 3 of Flow Loop Monitor VI block diagram. This is where channels are activated or closed, data is collected, and some initial filtering of outliers is done for the flow meters.

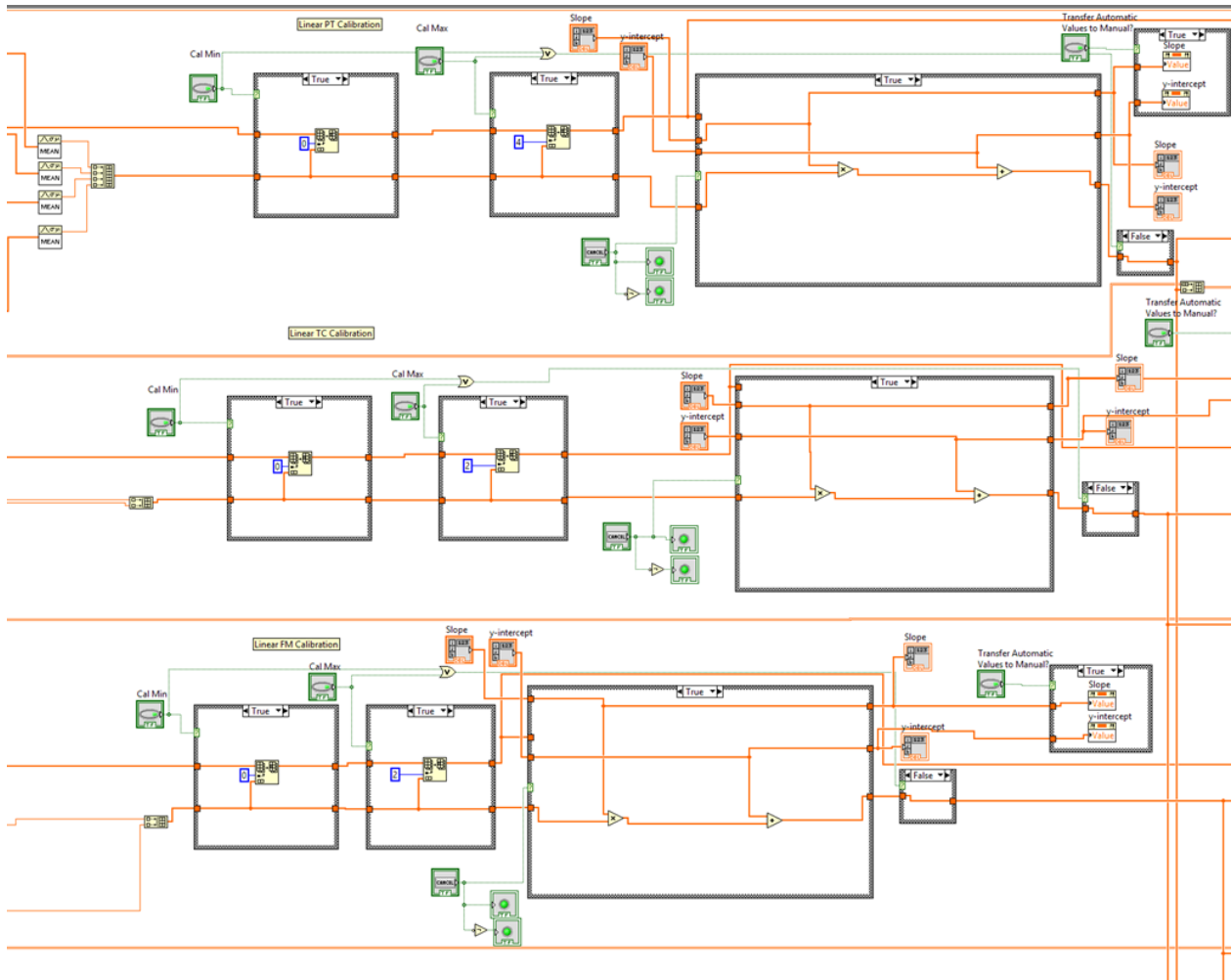


Figure A-7 Part 2 of 3 of Flow Loop Monitor VI block diagram. This is where the automatic calibration structures are located, calibration lines are calculated, and the option is given to transfer the automatic calibration values to manual calibration mode.

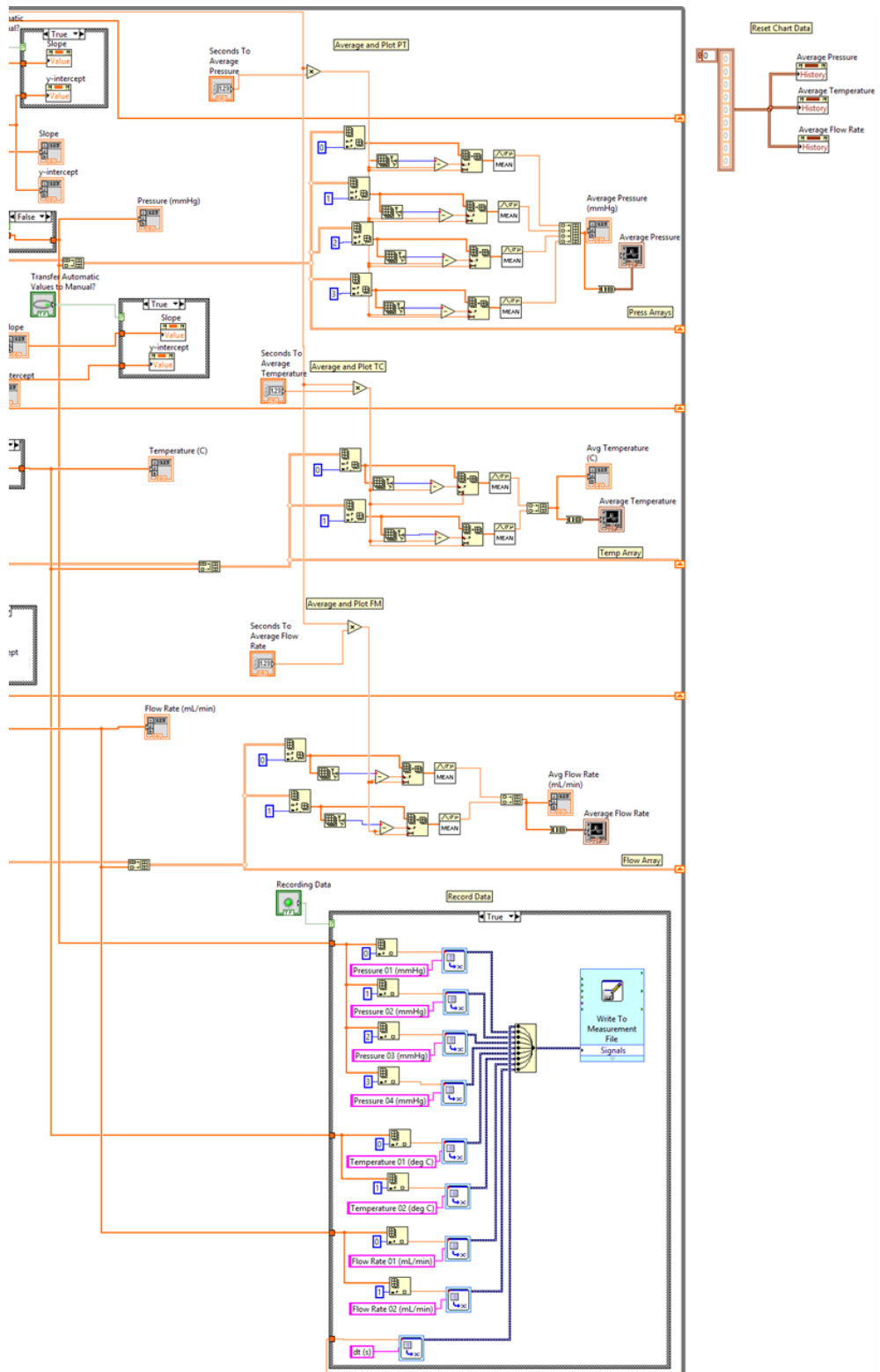


Figure A- 8 Part 3 of 3 of Flow Loop Monitor VI block diagram. This is where the values are averaged for graphing and display on the charts. The bottom structure is where data is recorded to a .csv file.

Table A- 2 All data taken during 5µm filter trials with polypropylene standard spheres as well as PPODA-QT

				Proximal Pressure (mmHg)				Distal Pressure (mmHg)					
Material	Number of Spheres	Trial	Time (min)	Min	Max	Mean	Deviation	Min	Max	Mean	Deviation	Flow Rate (mL/min)	Temp (°C)
Poly propylene Spheres	0	1	0	69	199	140	65	12	42	26	15	222	37-40
			20	140	182	160	21	-1	53	30	27	214	
		2	0	110	141	127	15	9	24	18	8	235	37-40
			20	130	165	148	18	19	35	27	8	222	
Poly propylene Spheres	1500	1	0	119	152	138	16	21	38	30	8	235	37-40
			20	133	167	152	17	27	33	29	3	222	
		2	0	113	156	134	22	13	40	29	14	235	37-40
			20	146	157	152	5	18	21	19	2	222	
Poly propylene Spheres	3000	1	0	114	147	132	16	13	32	21	10	231	37-40
			20	94	187	150	46	23	45	33	11	222	
		2	0	86	177	139	45	17	46	33	14	235	37-40
			20	100	181	149	41	18	35	28	8	226	
Poly propylene Spheres	4500	1	0	82	185	139	51	18	45	32	13	235	37-40
			20	77	177	131	50	5	32	17	13	226	
		2	0	81	179	137	49	18	40	29	11	231	37-40
			20	89	159	130	35	8	29	20	11	222	
PPODA-QT	NA	1	0	54	154	113	50	14	36	26	11	119	37-40
			20	62	166	123	52	11	38	27	13	113	
		2	0	59	172	122	56	15	33	25	9	117	37-40
			20	59	188	126	64	14	44	29	15	106	
		3	0	46	173	118	63	10	38	26	14	113	37-40
			20	64	171	125	53	10	40	28	15	105	

APPENDIX B

IMAGEJ AND MATLAB COUNTING PROGRAM

This appendix and code explanation was written by Kevin LoGrande.

```
%Automated Particle Analysis
%Author: Kevin A LoGrande
%Last Updated: 04-21-2018

%This code is used for the automated particle analysis of z-stacks in ImageJ.
%The user inputs basic information about the trial and sets a scale, then
%the code automatically opens images, stacks them, and counts the particles.
%The code outputs the number of particles over 10 and over 25 microns.

%Notes:
%1. All images must be named as follows: mm-dd-yy-trial#-stack#-image#.tif
%   (e.g. 03-03-18-trial2-stack1-image5.tif)
%2. The miji.m script must be ran first to ensure interfacing between
%   imageJ and MATLAB

%first, we initialize the particle counts at zero
micron25=0;
micron10=0;

%user inputs date, trial number, number of stacks, and stack size
date = input('Input the date in the format mm-dd-yy\n','s');
trial = input('Input the trial number.\n');
StackSize = input('Input the number of z heights.\n');
GridSize = input('Enter the number of images in the grid.\n');

%image analysis for various stacks
for image = 0:GridSize

    %automatically opens the images to be analyzed if they follow the
    %naming convention
    for stack = 0:StackSize
        MIJ.run('Open...',sprintf('path=[%s-trial%i-stack%i-image%i.jpg]',
date, trial, stack, image))
    end

    %uses ImageJ to stack the images and project them to a single image
    MIJ.run('Images to Stack')
    MIJ.run('Z Project...', 'projection=[Min Intensity]')

    %on the first stack, the user sets a known scale to be applied to the
    %rest of the stacks
    if image == 0
        scale = input('Draw a line of known length in ImageJ, then press
enter.\n');
        MIJ.run('Set Scale...')
    end
end
```

```

%Sets a threshold that eliminates filter pores, but includes particles
MIJ.run('8-bit')
MIJ.setThreshold(100,255);
MIJ.run('Make Binary')

%ImageJ analyzes particles, then passes the results to MATLAB to count
%particles over 10 microns and over 25 microns.
MIJ.run('Analyze Particles...', 'size=80.0-Infinity circularity=0.0-1.0
show=[Nothing] display clear include')

data=MIJ.getResultsTable;
[rows,columns]=size(data);

for i=1:rows
    if data(i,2)>=25
        if data(i,2)/data(i,3)>2

            micron25=micron25+1;

        elseif data(i,2)>=10

            micron10=micron10+1;

        end
    end

%close images after counting particles to save memory space
MIJ.run('Close All')
End

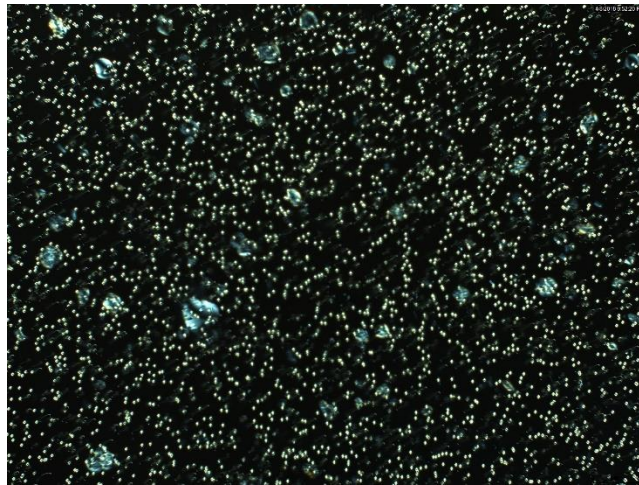
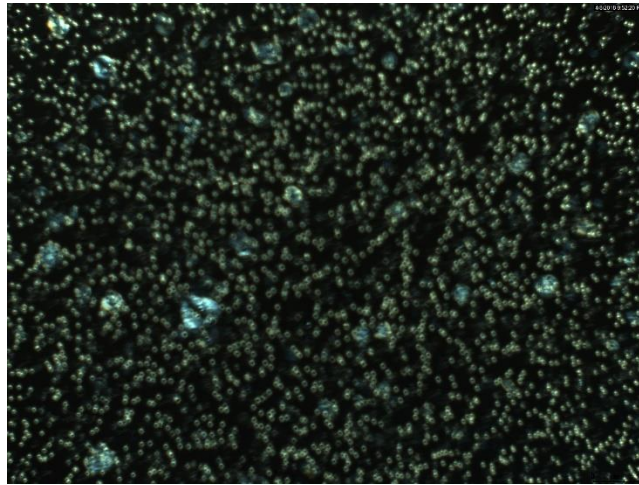
%Printng analysis results.
fprintf('There are %i particles larger than 10 microns and %i particles
larger than 25 microns\n',micron10,micron25)

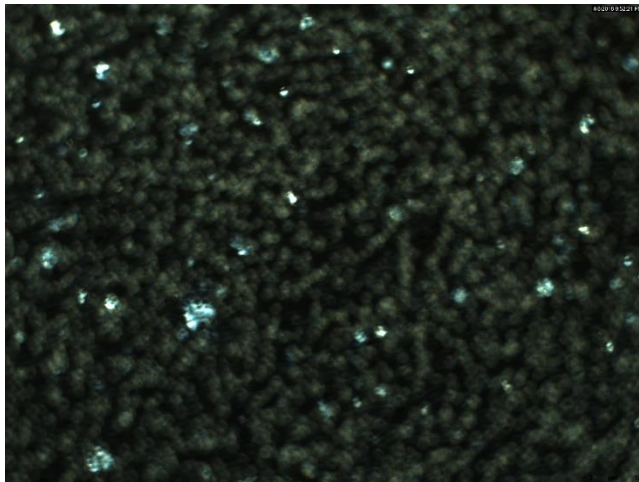
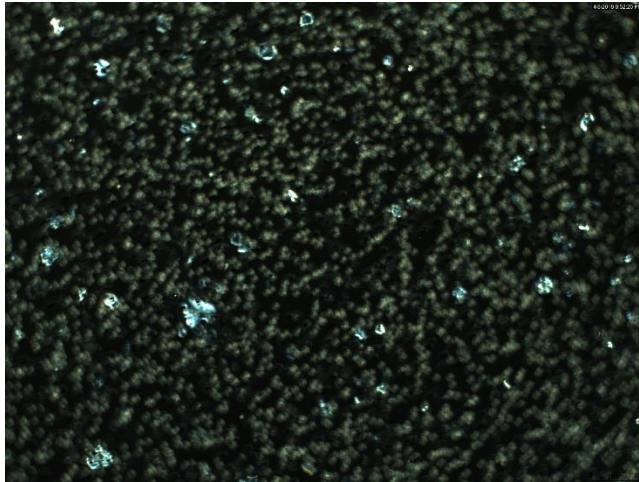
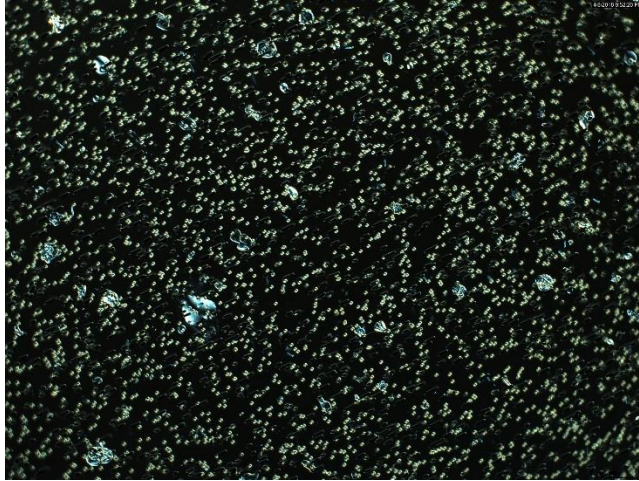
```

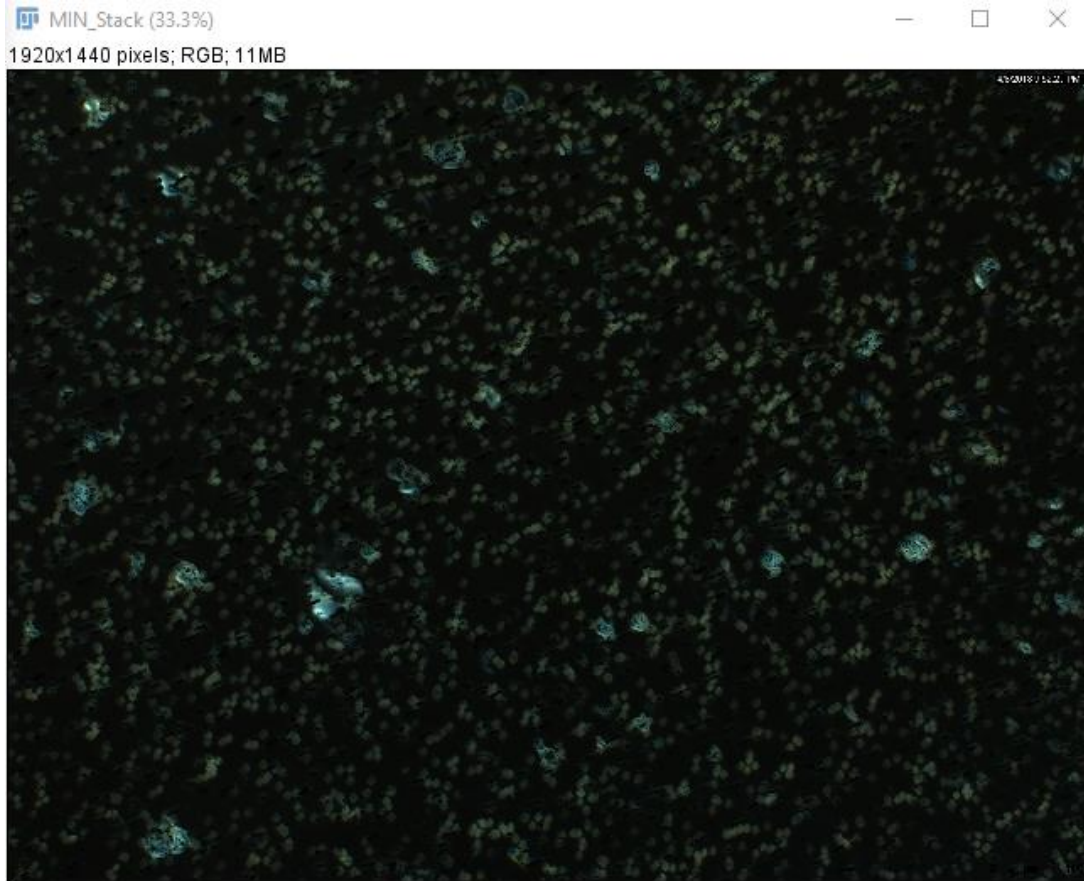
Some of the commands are explained below.

```
MIJ.run('Z Project...', 'projection=[Min Intensity]')
```

After the images are open and stacked, this function projects a single image based on the minimum intensity of light at each pixel. This makes the pores dimmer than the particles. The original images, as well as the result are shown below.





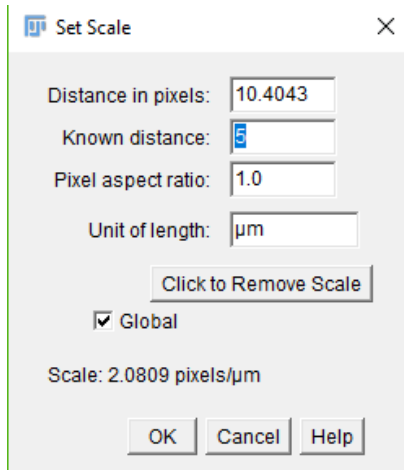


```
if image == 0
    scale = input('Draw a line of known length in ImageJ, then press
enter.\n');
    MIJ.run('Set Scale...')
end
```

The MATLAB variable “scale” is not important and isn’t used. This just acts as a delay, telling the user to draw a line using the ImageJ command window. I have been using the non-blurred axis of a pore as the line of known length. I zoom in and draw a line across the pore. A visual is shown below.



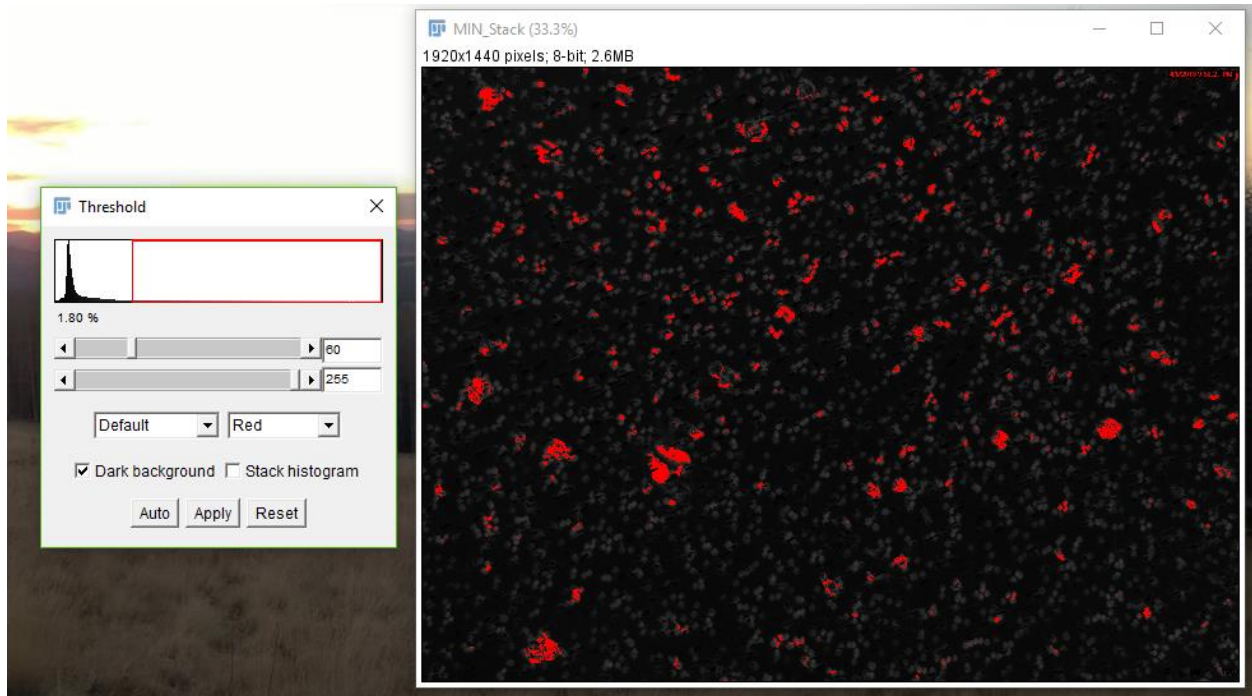
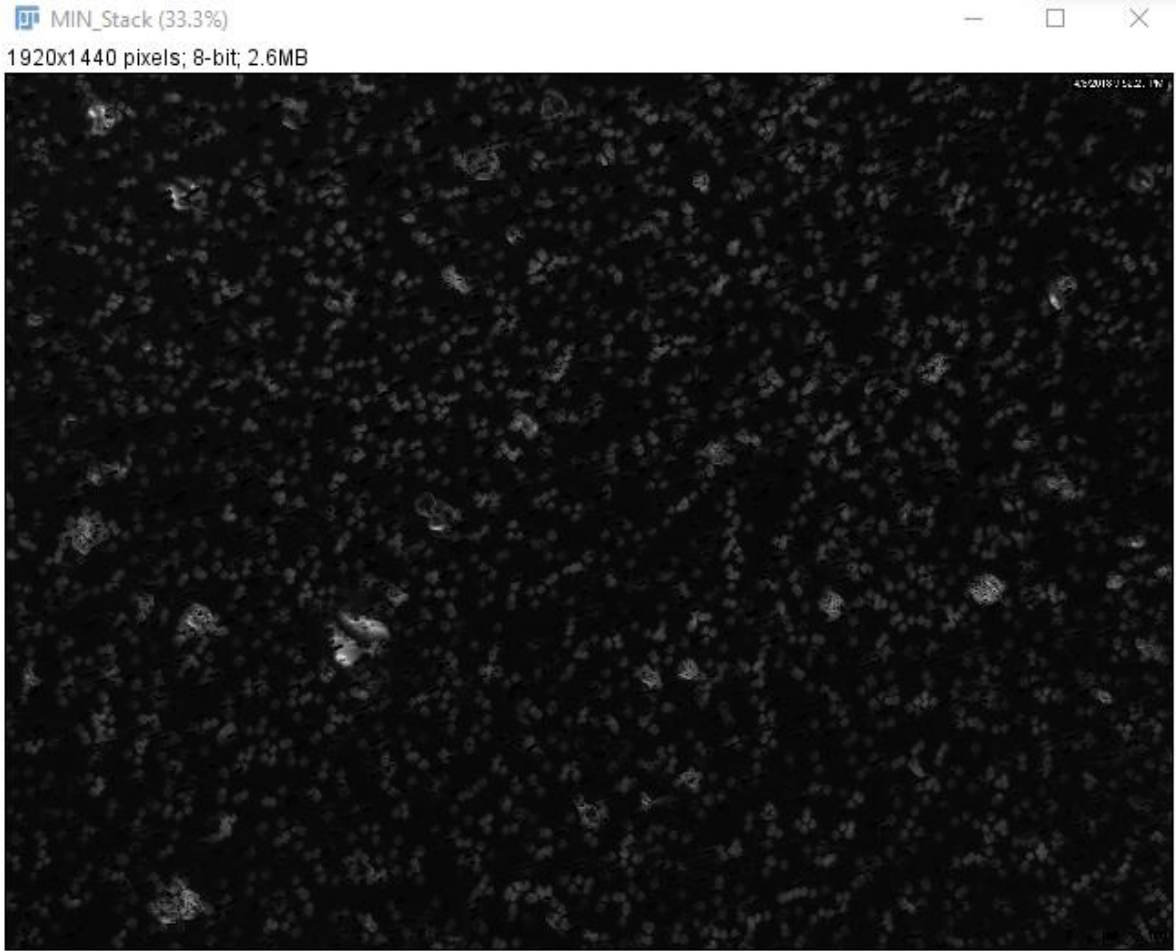
After the line is drawn, as per the instructions of the code, you press enter. (Note: this will store a zero in to the variable “scale”, but again this is not a used variable.) Now that a line is drawn the set scale command opens the dialog box shown below.

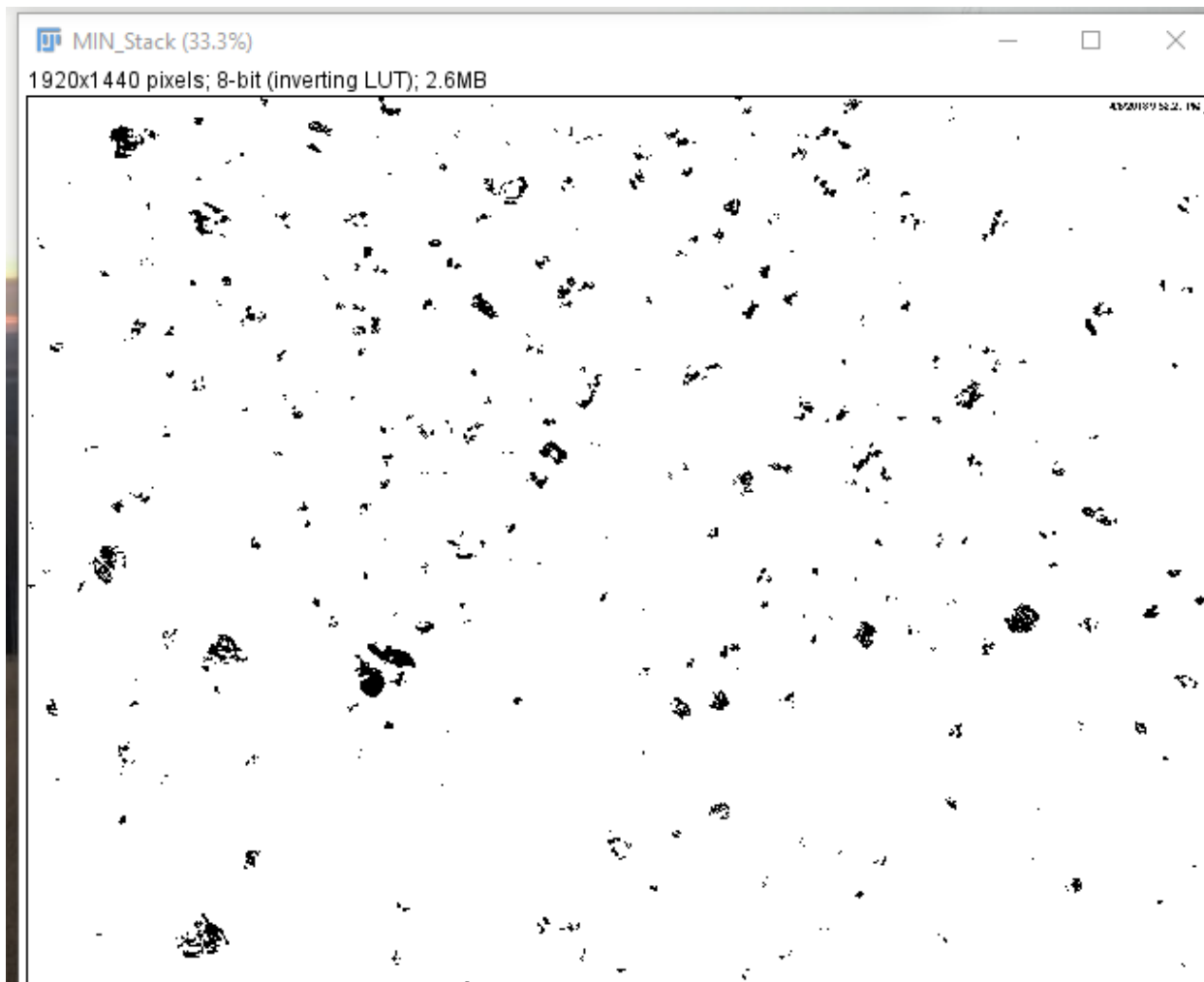


The distance in pixels is automatically filled from the line we drew. We know this distance is 5 microns. I make sure to click the “global” check box to ensure this scale is applied to every subsequent image.

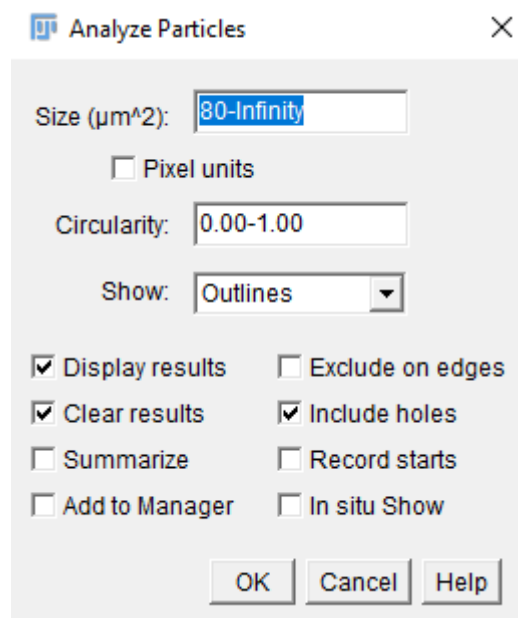
```
MIJ.run('8-bit')
MIJ.setThreshold(60,255);
MIJ.run('Make Binary')
```

This set of commands converts the image to an 8-bit gray scale image, then sets a threshold and converts to binary (black and white). Visuals for this process are shown below.

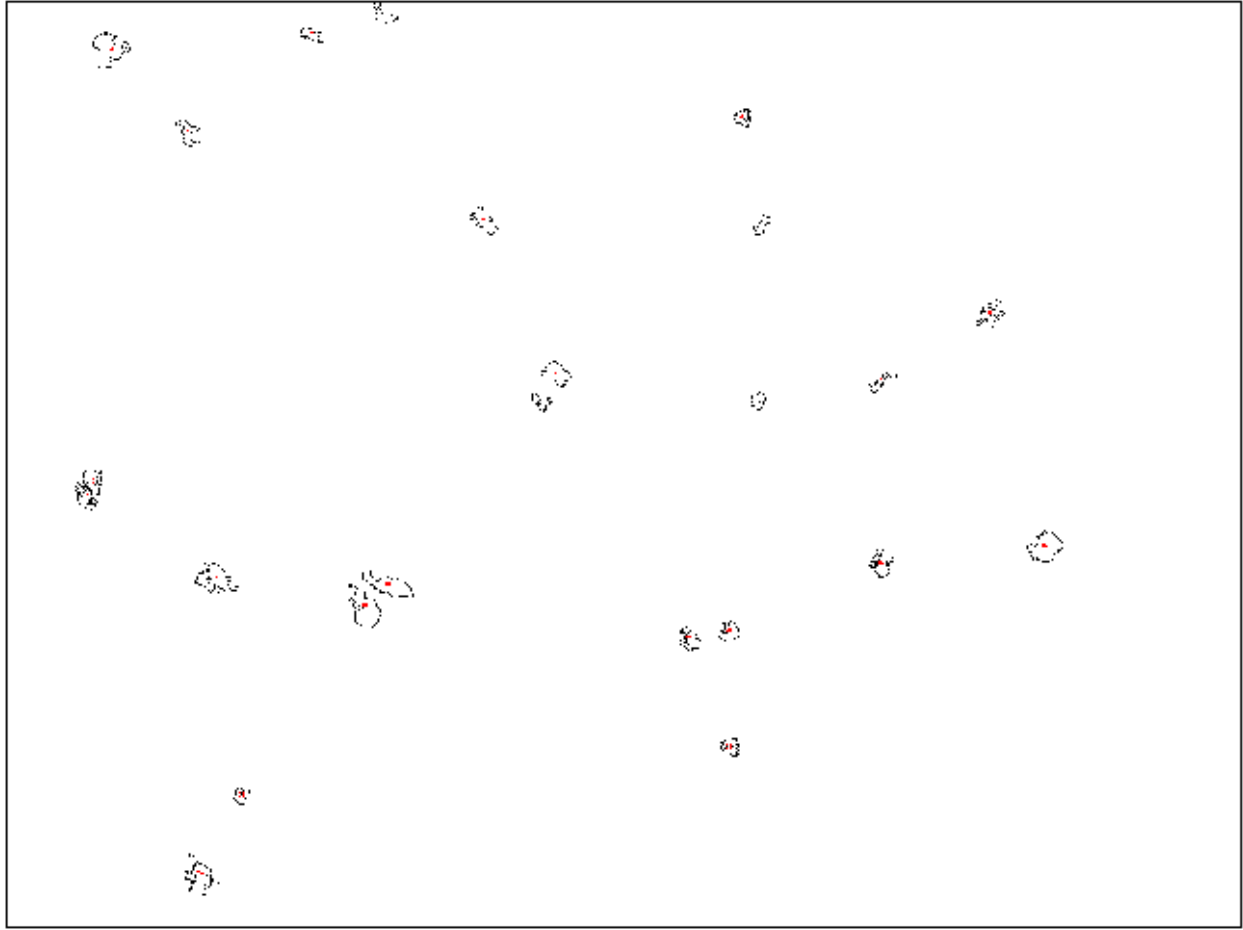




```
MIJ.run('Analyze Particles...','size=80.0-Infinity circularity=0.0-1.0  
show=[Nothing] display clear include')
```



× The “analyze particles” command would generally open the dialog box shown, but by defining all keys in the code, the dialog box is automatically filled in. Note that in this image I have “show: outlines.” This is not the case in the code, but for purposes of visualizing results, I have included it here. The image of the outlined particles as well as the results table is shown below.



Results

	Area	Major	Minor	Angle
1	99.769	16.573	7.665	147.253
2	89.145	15.631	7.261	157.345
3	393.072	23.088	21.676	113.201
4	94.226	11.214	10.698	139.919
5	146.189	18.974	9.810	113.551
6	190.762	23.947	10.143	134.312
7	80.600	15.629	6.566	51.939
8	166.744	18.711	11.347	62.712
9	220.785	20.951	13.417	148.249
10	110.624	24.926	5.651	35.669
11	88.222	11.163	10.063	76.312
12	84.988	13.564	7.978	148.821
13	157.275	17.533	11.421	106.786
14	145.266	19.068	9.700	122.977
15	379.215	24.843	19.435	33.181
16	191.917	18.779	13.012	81.268
17	327.945	23.674	17.637	155.325
18	371.363	38.159	12.391	161.011
19	402.309	29.676	17.261	114.169
20	140.647	14.963	11.968	64.702
21	137.182	15.727	11.106	119.435
22	96.536	12.628	9.733	150.141
23	85.912	12.800	8.546	65.005
24	307.852	23.582	16.621	103.055

```
data=MIJ.getResultsTable;
```

This command passes the data table shown on the left to a MATLAB array (I named the array “data”). Only the actual data is passed, not the number of the particle. Therefore the MATLAB array is 24x4 in size with the first column being “area.” The remaining code just manipulates the data array and adds to the particle counts.

APPENDIX C

RABBIT PROCEDURE MATERIALS

Rabbit Elastase Aneurysm Creation Procedure Materials

- Ketamine/Xylazine/Acepromazine at 60/6/1 mg/kg
- Isoflurine (1-1.5% in O₂ at ~1 L/min)
- 1x Clippers
- Blunt dissection/access tools
- 1x Surgical Clip
- Sutures
- 5F introducer
- 3F Fogarty balloon catheter
- 1x shortened microcatheter
- 1x Sterile Filter
- 80U Elastase (Worthington Biochemical Corporation, Lakewood, NJ)
- 9pH PBS
- 1x 1mL syringe

PPODA-QT Aneurysm Embolization Procedure Materials

Surgical Materials

- Ketamine/Xylazine/Acepromazine at 60/6/1 mg/kg
- Heparin
- Lidocaine
- Isoflurine (1-1.5% in O₂ at ~1 l/min)
- Surgical drape
- Iodine
- Alcohol wipes
- Blunt Dissection/access tools
- Catheter lidocaine lube
- 1x 5F introducer
- Scissors
- Saline
- 1x Introducer stabilization suture
- 1x 5F angiocatheter
- 2x Y-Tuohy Borst
- Contrast (Isovue)
- 1x ~20.5G needle
- Fluoroscope ruler or micrometer
- 1x Guidewire ~0.010"

- 1x Scepter Balloon Catheter ~3.0-4.0mm OD
- 3x 1mL Polycarbonate syringes
- 1x 3mL Polypropylene syringes
- 1x Microcatheter (Codman Prowler and Velocity Penumbra were used)
- Blood vessel repair kit
- Closure sutures
- Wound closure adhesive
- 4x 3-way Stopcocks

PPODA-QT Preparation Materials

- 1x 3mL PP syringe with 1.080g + Dead Volume PPODA
- 1x 3mL PP syringe with 0.330g +Dead Volume QT
- 11.00pH Conray
- 1x 1mL PC syringe (for 0.46mL Conray)
- 1x ~22.75G needle for Conray
- 2x Female-Male 0.2 μ m syringe filter
- 2x Female-female connector
- 2x 3mL PP syringe
- 1x Male-male connector
- 1x Injection syringe
- 1x Injection wings